The Role of Hydrogen in Selected Oxysalt Minerals

by Sasha Herwig

A Thesis submitted to the Faculty of Graduate Studies
of

The University of Manitoba

in partial fulfilment of the requirements of the degree of

MASTER OF SCIENCE

Department of Geological Sciences

University of Manitoba

Winnipeg, Manitoba

Canada

THE UNIVERSITY OF MANITOBA

FACULTY OF GRADUATE STUDIES
*****
COPYRIGHT PERMISSION

The Role of Hydrogen in Selected Oxysalt Minerals

BY

Sasha Herwig

A Thesis/Practicum submitted to the Faculty of Graduate Studies of The University of

Manitoba in partial fulfillment of the requirement of the degree

Of

MASTER OF SCIENCE

Sasha Herwig © 2009

ABSTRACT

It is imperative to try and develop a better understanding of the critical role of hydrogen in oxysalt minerals and the solutions they crystallize from; this will be accomplished using the experimental technique of single-crystal x-ray diffraction and the application of bond-valence theory. The main themes are (a) the arrangements of interstitial hydrogen bonds (b) the effect of hydrogen on structure topology and (c) how hydrogen, as a function of pH, affects speciation in aqueous solutions (specifically borate solutions) which in turn determines (in part) the minerals that crystallize from those solutions.

Interstitial hydrogen bonding is examined in the minerals with the general formula $X_2 M(TO_4)_2(H_2O)_2$, where X=Ca, Na; M = Mg, Fe^{2+}, Mn^{2+}, Co^{2+}, Ni, Cu^{2+}; T = P, As^{5+}, S^{6+}. Minerals of $X_2 M(TO_4)_2(H_2O)_2$ general composition show three distinct structure-types with subtle yet significant differences in bond topology of the interstitial species. It is interstitial bonds that control the stability of minerals, as these weak bonds are more easily broken with changing conditions than the stronger bonds of the structural unit.

The effect of hydrogen on structure topology is examined in minerals of the $MgSO_4(H_2O)_n$ series, where n=0-7. These minerals are extremely sensitive to changes in the environment (presence of H_2O, humidity); this is reflected in structural modifications to accommodate dehydration and rehydration.

The link between minerals and solutions is examined with respect to low-temperature hydrated borate minerals. It has been suggested that borate minerals crystallizing out of solutions utilize aqueous borate complexes to build their structural

units, and that mineral structures may then be an indicator of the pH of the environment

in which they form.

ACKNOWLEDGEMENTS

LIST OF TABLES

LIST OF FIGURES

TABLE OF CONTENTS

CHAPTER 1

1. Introduction

In minerals, H in the form of H_2O and OH^- is often a major constituent required by stoichiometry (on the order of several wt %), or as a trace component (on the order of a few ppm by weight). Even the presence of small concentrations of hydrogen can profoundly affect the physical, chemical and thermodynamic properties of minerals, which determines bulk properties of the rocks in which they are found. In turn, H is a major influence on many important geologic processes such as metamorphic reactions, deformation and weathering.

Hydrogen plays a significant role in contributing to the great structural and chemical diversity of minerals. Deep in the Earth's mantle where there is little H (as compared to the Earth's surface and near-surface environment), there are only five different minerals that are nominally anhydrous and relatively chemically and structurally simple. However, at shallow depths in the Earth's crust, the Earth's surface and near-surface environment, H is quite abundant and there are approximately four thousand known minerals, most of which have hydrous components, and most of which are chemically and structurally complex. Of course, H concentration is not the only difference between mantle and crust composition and is not solely responsible for the observed distribution of minerals within the Earth, but it does have a significant contribution in this regard.

The nature and speciation of aqueous solutions (below the critical temperature of water) is determined by the activity of hydrogen, or the pH of the solution. This has important geologic and environmental implications as pH is a dominant factor controlling the dissolution and precipitation of minerals.

A crystal structure may be represented by two components, the structural unit and the interstitial complex, where the structural unit may be defined as the strongly bonded part of the structure and the interstitial complex may be defined as the interstitial species (usually large, low valence cations and H_2O groups) that are much more weakly bonded, and link the structural units together (Hawthorne, 1992). Hydrogen bonding has a major influence on the stability of minerals, especially when hydrogen is a component of the interstitial complex of a crystal structure. These hydrogen bonds are much weaker than the bonds of the structural unit component of a crystal structure, and are more easily broken with changing environmental conditions.

Hydrogen is the lightest element; it has only one electron in a $1s^1$ configuration and it can either "gain" an electron to become H^- or "lose" an electron to become H^+ (Kotz & Triechel, 1996). Hydrides are compounds of hydrogen with a more electropositive element (or group). In this case, hydrogen behaves similarly to a halogen and accepts an electron to fill its 1s-orbital. Hydrates and oxyhydroxy (hydrated) compounds are those where hydrogen bonds with a more electronegative element such as oxygen. In these compounds, it covalently shares its only electron. It cannot completely give up its electron, which gives rise to unequal charge distribution as the oxidizing element "pulls" the electron toward itself, forming a covalent bond with hydrogen. The result is a polar molecule (OH or H_2O) that has a partial positive charge on the hydrogen side (because of the "unshielded" proton- the electron density is centered around the oxygen) and a partial negative charge on the oxygen (lone pair) side. This is what makes hydrogen so important: It forms "multi-purpose" molecular groups that can act as a cation on one end and can also act as an anion on the other end. The hydrogen bond is the

"attraction" between the positively charged hydrogen and the negatively charged lone pair electrons.

Hydrogen bonding is a donor-acceptor interaction that involves hydrogen atoms (Jeffrey, 1997). It is important to note that the term hydrogen bond refers not just to a single bond but to the entire group of atoms (usually three) involved in the interaction. The arrangement of the atoms involved can be written as $O_D - H \ldots O_A$, where O_D is the strongly bonded donor atom and O_A is the weakly bonded acceptor atom. $H \ldots O_A$ is referred to as the hydrogen bond, and $O_D - H$ is referred to as the hydroxyl bond.

1.2 Static role of hydrogen in minerals

Hydrogen, and more specifically, the bonds that it is capable of forming, are important factors in determining the crystal structures of minerals in which it is found. Hydrogen exerts structural control by preventing polymerization and by propagating bonds through space. It also leads to diversity in mineral structures by introducing flexibility in the way that structures can link together.

The reason that H can do all of these things has to do with the asymmetry of its bonding interactions; as OH and H_2O, it can behave as both a cation and an anion and it is capable of forming very strong bonds and very weak bonds simultaneously.

1.3 Dynamic role of hydrogen in minerals

An important dynamic role of H in minerals is its ability to be a catalyst in solid-state chemical reactions; a good example of this is the influence of H on Si-Al order-disorder reactions in feldspars. Some previous work involving the dynamics of H in minerals will be discussed in section 5.2.

3

1.4 Role of hydrogen in liquids

Hydrogen bonds are responsible for the unique properties of water. Hydrogen bonds give structure and cohesion to water and other liquids and impart physical properties such as surface tension, hydrophobic effect, and its nearly universal solvent capability. Functioning as a solvent, the H atoms attract negative charges, and the oxygen attracts positive charges, breaking bonds and effectively pulling things apart and "rearranging" them. Water's solvent ability increases with decreasing pH, or increasing activity of H ions; the higher the concentration of H ions, the more effective the bond-breaking capacity. This has important geologic and environmental implications as pH is a dominant factor controlling the dissolution and precipitation of minerals.

pH and the activity of H_2O affect polymerization of structural units. With increasing activity of H_2O, structural units trend from frameworks to sheets to chains to clusters to isolated polyhedra i.e., they become less polymerized. This is similar to silicate melts, where an increase in the activity of H_2O tends to depolymerize the melt through an increase in the ratio of network modifiers to network formers. With increasing H content, atoms are more isolated and weakly bonded. In addition, H_2O and OH, when bonded to a structural unit, can prevent any other tetrahedra or octahedra from linking to it, therefore exercising structural control. At lower pH, there are no framework structures.

CHAPTER 2

EXPERIMENTAL TECHNIQUES

2.1 Introduction

The most important analytical techniques used in data collection for this thesis are single-crystal x-ray diffraction and electron micro-probe analysis.

2.2 Single-crystal X-ray diffraction

Single-crystal x-ray diffraction is a tool to obtain three-dimensional information on chemical compounds. The information is in the form of electron density maxima and their position in the unit cell, hence atom positions.

The ability of an atom to scatter or diffract x-rays is proportional to its atomic number, and therefore very light atoms, such as hydrogen, scatter x-rays very little. However, analysis of difference-Fourier maps can yield approximate hydrogen-atom positions. When hydrogen is bonded to anotherr atom, its electron density is pulled toward the other, 'heavier' atom which results in the centre of electron density being shifted toward the heavier atom. Because x-ray diffraction data locates the centre of electron density, rather than the actual position of the atomic nucleus, the resulting interatomic distances are systematically too short.

2.3 Electron microprobe analysis

In electron microprobe analysis (EMPA) an electron beam is focused on the surface of a sample using electromagnetic lenses, and the accelerated high energy electrons produce characteristic x-rays within a small volume of the sample. The characteristic x-rays emitted by the sample are identified using their wavelengths to determine the composition of the sample, and their intensities are measured to determine

concentrations. All elements (except hydrogen, helium, and lithium) can be detected because each element has a specific set of x-rays that it emits.

An electron microprobe is equipped with an energy-dispersive (ED) spectrometer, which electronically sorts and measures x-rays with respect to their energies. Electron microprobes also have several wavelength-dispersive (WD) spectrometers, which use diffraction to sort x-rays by their wavelengths.

Because the electron beam interacts with only a small volume of the sample, EMPA allows collection of localized compositional data and examination of samples too small to be studied with other analytical techniques. In addition, it allows for the determination of the chemical variability of a sample. EMPA is, therefore, well suited to the in-situ study of heterogeneous or zoned samples, allowing the textural relations of the phases to remain visible.

2.4 Experimental Protocol

2.5 Collection of X-ray intensity data

The unit-cell dimensions were determined using a Bruker $P4$ automated four-circle single-crystal X-ray diffractometer equipped with a serial detector and a Mo$K\alpha$ X-ray source. SHELXTL PC Plus (Sheldrick, G) software was used for data reduction and least-squares refinement. More detailed information is discussed in Chapter 5.

2.6 Crystal-structure refinement

All calculations were done with the SHELTXL PC Plus software package. Crystal-structure refinements of brandtite, collinsite and fairfieldite were initiated with the atom coordinates of roselite (Hawthorne & Ferguson, 1977), collinsite (Brotherton *et al.,* 1974) and fairfieldite (Fanfani *et al.,* 1970), respectively. Hydrogen positions were

located using difference Fourier maps, and a restraint was imposed on the refinements such that the O-H distance should be close to 0.98 Å by adding extra weighted observational equations to the least-squares matrix. This procedure results in a more realistic geometry for the hydrogen bonds

2.7 Collection of Electron-Microprobe data

All crystals used for x-ray data collection were mounted in epoxy on 2.5 cm diameter Perspex discs, ground, polished, carbon-coated and analyzed with a Cameca SX-100 electron microprobe operating under the following conditions in wavelength-dispersion mode: excitation voltage: 15 kV, specimen current: 20 nA, beam size: 5 μm, peak count-time: 20 s, background count-time: 10 s. Five points on each crystal were analyzed. Back-scattered-electron images of each crystal show no sign of compositional zoning. Detailed information is given in Chapter 5.

CHAPTER 3
THEORETICAL TECHNIQUES: BOND VALENCE METHOD

3.1. Introduction

Bond-valence theory is an approach to chemical bonding in inorganic structures developed by Brown (1981, 2002) and O'Keefe (1989, 1990) and in terms of bond topology and minerals by Hawthorne (1983, 1992, 1994, 1997).

3.2. Basic concepts

A crystal structure consists of a network of atoms, cations and anions that are connected to each other by chemical bonds. Each atom possesses a valence, which is a measure of an atom's bonding power, and its value (or set of values) is characteristic for a given atom. The number of bonds formed by an atom is its coordination number. A bond valence can be assigned to each bond such that the *sum of bond valences at each atom is equal to the atomic valence*; this is the *valence-sum rule*.

3.3. Correlations with experimental observations

Bond-valence theory correlates well with experimental observations. Brown & Shannon (1973) showed that the sum of bond valences around many cations, including H, (when determined by neutron diffraction) are within 0.04 valence units (vu) of the atomic valence in oxides.

Bond-valences can be calculated quite accurately via:

$$(1) \quad s = \exp[(R - r_{ij})/B]$$

where R is a constant specific for a cation-anion pair, B is a constant (0.37), and r_{ij} is the observed bond length (Brown & Altermatt, 1985). Bond-valence is usually calculated from bond length; it is a measure of the covalence or the degree of electron density shared between

bonding atoms; short bonds have higher bond-valences and vice versa. Bond-valences for a specific cation lie within 20% of their mean value and as such, are characteristic for that cation. If there is more than one type of coordination for a cation, the mean bond-valence is equal to the weighted mean of bond valences in all its given structures. The mean bond-valence correlates with electronegativity. Electronegativity, or electron-accepting capacity, is a measure of the Lewis acid strength; Lewis base strength can be measured for anions.

3.4. The valence-matching principle

Bond-valence theory can deal with complex minerals, many of which contain structural OH^- or H_2O, through the valence-matching principle which can be stated: *the most stable structures will form when the Lewis acidity of the cation (or interstitial complex) closely matches the Lewis basicity of the anion (or structural unit)* (Brown, 2002). We can define a Lewis basicity for a structural unit and a Lewis acidity for an interstitial complex and use the valence- matching principle to make predictions about structures. This is important as it allows us to take an *a priori* (non-experimental) approach to examine a structure; we can predict which compounds will or will not be stable without experimental data.

CHAPTER 4

ROLES OF HYDROGEN IN MINERALS

4.1. Hydrogen and hydrogen bonding

Hydrogen bonding is a donor-acceptor interaction that involves both hydrogen and oxygen atoms.
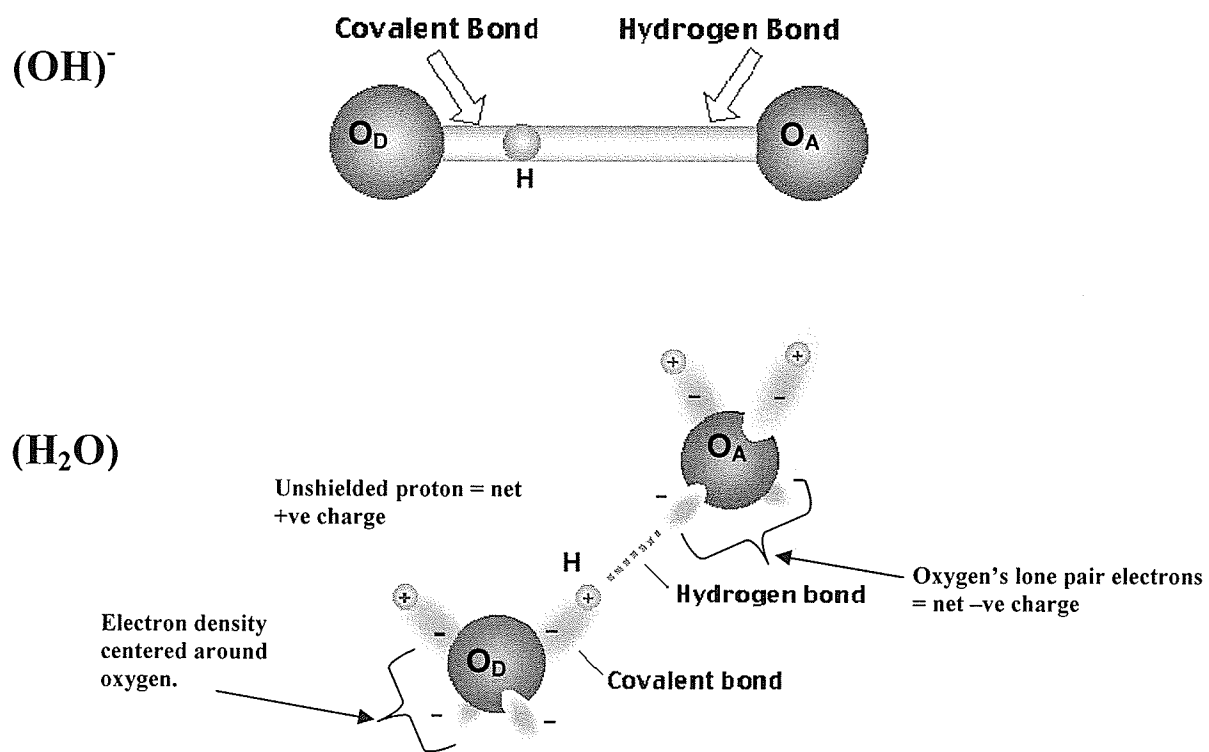
Figure 4.1. Bonding in (OH)⁻ and (H₂O) groups.

The arrangement of the atoms involved can be written as $O_D - H \ldots O_A$, where O_D is the strongly bonded donor anion and O_A is the weakly bonded acceptor anion. $H \ldots O_A$ is referred to as the hydrogen bond, and $O_D - H$ is referred to as the hydroxyl bond (Figure 4.1).

4.2. The effect of hydrogen on structural polymerization

The activity of H_2O and pH affect polymerization of structural units. With increasing activity of H_2O, structural units trend from frameworks to sheets to chains to clusters to isolated polyhedra i.e., they become less polymerized. This is similar to silicate melts, where an increase in the activity of H_2O tends to depolymerize the melt through an increase in the ratio of network modifiers to network formers. With increasing H content, atoms are more isolated and weakly bonded. In addition, H_2O and OH, when bonded to a structural unit, can prevent any other tetrahedra or octahedra from linking to it, therefore exercising structural control. At lower pH, there are no framework structures.

4.3. Role of OH and H_2O in crystal structures

Hawthorne (1992) examined the roles of OH and H_2O in oxide and oxysalt minerals by using bond-valence theory to determine how they influence the interaction of the structural unit and the interstitial complex of crystal structures. In a crystal structure, the structural unit (SU) is the strongly bonded (anionic) array that is charge balanced by the interstital complex, usually large, low valence cations; the interaction between them can be evaluated using the valence-matching principle (Brown, 1981).

As part of the structural unit in minerals, OH and H_2O limit the polymerization of the structural unit. OH and H_2O groups can prevent other polyhedra from linking onto a structure, thereby exercising structural control.

11

As an interstitial component, H_2O can play three different roles (Hawthorne, 1992):

(1) It can bond to an interstitial cation, forming a complex cation; it may do this to

(a) *satisfy* bond-valence requirements of the interstitial cation where there are insufficient neighbouring anions, (b) *transport* bond valence to a distant unsatisfied anion by hydrogen bonding, and (c) *transform* bond-valence so that the interstitial complex and the structural unit may link ie H_2O takes one stronger bond and splits it into two weaker bonds so that the valence matching principle may be satisfied.

(2) Interstitial H_2O not bonded to interstitial cations can occupy individual atomic positions forming a stable hydrogen-bonded network in the interstitial regions between structural units. The purpose of this type of H_2O is to satisfy the bond-valence requirements of H atoms that are part of the structural unit, propagating the bonding across the interstitial space to other parts of the structural unit and bridging cations and anions that would normally be too far apart to bond, yet require additional coordination. (3) Occluded H_2O is not bonded to interstitial cations and is not involved in a H-bond network, however it still affects the physical properties of the mineral.

Hydroxyl groups can also be interstitial species, but this usually only occurs where trivalent cations coordinate OH (Hawthorne, 1992). [6]-coordinated and greater monovalent cations have bond-valences < 0.17 vu. An OH group would have to receive 1 / 0.17 = 6 bonds from monovalent cations to satisfy its bond-valence requirements, which is too large a coordination number for the OH group. [8]-coordinated divalent cations have bond-valences < 0.27 vu.

An OH group would have to receive 1 / 0.27 = 4 bonds from divalent cations to satisfy its bond-valence requirements; this is not too large for a coordination number for

the OH group, but it is too large for the interstitial region of a crystal structure. Trivalent cations have bond-valences ~0.5 vu. An OH group would have to receive 1 / 0.5 = 2 bonds from trivalent cations to satisfy its bond-valence requirements; this is not is too large for a coordination number for the OH group, and it is not too large for the interstitial region of a crystal structure.

CHAPTER 5

HYDROGEN BONDING IN MINERALS WITH THE GENERAL FORMULA
$A_2M(TO_4)_2(H_2O)_2$

5.1. Introduction

Minerals with the general formula $X_2 M(TO_4)_2(H_2O)_2$ are numerous and occur

widely as minor or trace constituents in environments affected by hydrothermal

alteration. They show a wide variety of octahedrally and tetrahedrally coordinated cations

(M = Mg, Fe^{2+}, Mn^{2+}, Co^{2+}, Ni, Cu^{2+}; T = P, As^{5+}, S^{6+}), and yet the interstitial X cation is

almost always Ca, the one exception being kröhnkite, $Na_2Cu^{2+}(SO_4)_2(H_2O)_2$, in which the

interstitial cation is monovalent (Na^+) in order to maintain electroneutrality. Minerals of

$X_2 M(TO_4)_2(H_2O)_2$ general composition show three distinct structure-types (Table 5.1.):

the monoclinic *kröhnkite* group and the triclinic *talmessite* and *fairfieldite* groups. The

crystal structure of kröhnkite was solved by Dahlman (1951) and refined by Hawthorne

& Ferguson (1977). The crystal structure of collinsite was solved by Brotherton *et al.*

(1974), and the structure of the isostructural talmessite was refined by Catti *et al.* (1977),

who showed that the three distinct structure-types can be distinguished on the basis of

cell parameters alone. The crystal structure of fairfieldite was solved by Fanfani *et al.*

(1970). The structures of several other minerals of this type have since been refined

(Table 5.1). Recently, there has been extensive work on the synthesis and structural

characterization of synthetic analogues of these minerals, together with many other

synthetic phases containing the $[M(TO_4)_2(H_2O)_2]$ chain (Fleck *et al.* 2002a,b, 2003,

Kolitsch & Fleck 2005) (Table 5.1). In particular, Fleck *et al.* (2002b) introduced a

classification of these structures based on the space-group symmetry and geometrical

relations between the chains and between the layers of chains and interstitial cations.

Table 5.1. Minerals of the brandtite, collinsite and fairfieldite groups.

Mineral	Formula (end-member)	a (Å)	b (Å)	c (Å)	α (°)	β (°)	γ (°)	Sp. gr.	Ref.
kröhnkite	$Na_2 Cu^{2+} (SO_4)_2 (H_2O)_2$	5.807	12.656	5.517	90	108.32	90	$P2_1/c$	(12)
brandtite	$Ca_2 Mn^{2+} (AsO_4)_2 (H_2O)_2$	5.877	12.957	5.675	90	108	90	$P2_1/c$	(13,14)
roselite	$Ca_2 Co (AsO_4)_2 (H_2O)_2$	5.801	12.989	5.617	90	107.42	90	$P2_1/c$	(15)
wendwilsonite	$Ca_2 Mg (AsO_4)_2 (H_2O)_2$	5.806	12.912	5.623	90	107.4	90	$P2_1/c$	(16)
zincroselite	$Ca_2 Zn (AsO_4)_2 (H_2O)_2$	5.827	12.899	5.646	90	107.69	90	$P2_1/c$	(17)
cassidyite	$Ca_2 Ni (PO_4)_2 (H_2O)_2$	5.729	6.43	5.41	96.8	107.3	104.6	$P\text{-}1$	(18)
collinsite	$Ca_2 Mg (PO_4)_2 (H_2O)_2$	5.729	6.778	5.444	97.31	108.56	107.25	$P\text{-}1$	(13,18)
talmessite	$Ca_2 Mg (AsO_4)_2 (H_2O)_2$	5.874	6.943	5.537	97.3	108.7	108.1	$P\text{-}1$	(19,25)
gaitite	$Ca_2 Zn (AsO_4)_2 (H_2O)_2$	5.899	6.978	5.755	97.41	109.08	108.09	$P\text{-}1$	(20)
beta-roselite	$Ca_2 Co (AsO_4)_2 (H_2O)_2$	5.89	7.69	5.56	112.6	70.8	119.4	$P\text{-}1$	(21,25)
parabrandtite	$Ca_2 Mn^{2+} (AsO_4)_2 (H_2O)_2$	5.89	7.03	5.64	96.77	109.32	108.47	$P\text{-}1$	(22)
hillite	$Ca_2 Zn (PO_4)_2 (H_2O)_2$	5.736	6.767	5.462	97.41	108.59	107.19	$P\text{-}1$	(23)
fairfieldite	$Ca_2 Mn^{2+} (PO_4)_2 (H_2O)_2$	5.795	6.576	5.496	102.39	108.63	90.29	$P\text{-}1$	(13,24)
messelite	$Ca_2 Fe^{2+} (PO_4)_2 (H_2O)_2$	5.95	6.52	5.45	102.3	107.5	90.8	$P\text{-}1$	(21)

15

There has been much work in the last twenty years on developing structural hierarchies or classifications of oxysalt minerals (Hawthorne 1984, 1985, 1986, 1990, 1992, 1994, 1997, Sabelli & Trosti-Ferroni 1985, Liebau 1985, Hawthorne *et al.* 1996, 2000, Hawthorne & Huminicki 2002, Huminicki & Hawthorne 2002, Burns 1999, Burns *et al.* 1996), focusing on the bond topology of the more strongly bonded cations (Hawthorne 1983). With much of this work now in place, it is important to focus on the bond topology of the interstitial species. It is these bonds that control the stability of minerals, as these weak bonds are more easily broken with changing conditions than the stronger bonds of the structural unit. As far as we are aware, these types of interactions have not been examined in terms of (1) the topology of the overall bond arrangements, and (2) the geometry of the local interactions. Here, we examine this issue with regard to the structures of the minerals of the brandtite, collinsite and fairfieldite groups.

5.2. Sample provenance

The crystals used in this work come from the following sources: brandtite: Harstig mine, Harstigen, Sweden; collinsite: Rapid Creek, Yukon Territory, Canada; fairfieldite: Foote mine, North Carolina, U.S.A. Crystal sizes are given in Table 5.2.

Table 5.2. Miscellaneous single-crystal x-ray diffraction data collection and refinement information.

	brandtite	collinsite	fairfieldite
a (Å)	5.877(1)	5.729(1)	5.795(1)
b	12.957(2)	6.778(1)	6.576(1)
c	5.675(1)	5.444(1)	5.496(1)
α (°)	90	97.31(3)	102.39(3)
β	108.00(3)	108.56(3)	108.63(3)
γ	90	107.25(3)	90.29(3)
V (Å^3)	411.06	185.6	193.25
Space group	$P2_1/c$	P-1	P-1
Z	2	1	1
Rad/Mon	MoKα/Gr	MoKα/Gr	MoKα/Gr
Total no. of intensities	1365	2178	2274
No. of unique reflections	1200	1089	1137
R(merge) %	2.7	1.1	1.3
R %	2.6	1.5	1.7
$wR^2(F^2)$	6.5	4.1	4.7
GoF	0.939	0.932	0.943

$R = \Sigma(*F_o*-*F_c*) / \Sigma*F_o*$

$wR = [\Sigma w(*F_o*-*F_c*)^2 / \Sigma F_o^2]$, w = (1 / $\sigma^2(F)$ + 0.0005 F^2)

5.3 Collection of X-ray intensity data

The unit-cell dimensions were determined using a Bruker *P*4 automated four-circle single-crystal X-ray diffractometer equipped with a serial detector and a Mo$K\alpha$ X-ray source. For brandtite, 25 reflections between 10 and 30° 2θ were centered, and a constrained monoclinic cell was determined from the setting angles and refined using least squares. For collinsite and fairfieldite, 25 reflections between 10 and 30° 2θ were centered and a triclinic cell was determined and refined in the same manner. Miscellaneous information on data-collection and structure refinement is given in Table 5.2. We measured single-crystal intensity data from 4 to 60° 2θ with a scan range of 1.2° and scan speeds from 2.0 to 29°/min. Psi-scan data were measured on 20 reflections out to 60° 2θ at 5° increments for absorption corrections modeling each crystal as a triaxial ellipsoid. Intensities were subsequently corrected for Lorentz, polarization and background effects.

5.4 Electron-microprobe analysis

The crystals used for X-ray data collection were mounted in epoxy on 2.5 cm diameter Perspex discs, ground, polished, carbon-coated and analyzed with a Cameca SX-100 electron microprobe operating under the following conditions in wavelength-dispersion mode: excitation voltage: 15 kV, specimen current: 20 nA, beam size: 5 μm, peak count-time: 20 s, background count-time: 10 s. We used the following standards and crystals for $K\alpha$ X-ray lines: Mg: forsterite; Fe: fayalite; Mn: spessartine; Co: $CoNb_2O_6$; Ni: NiSi; Zn: gahnite; P: apatite; As: cobaltite; S: chalcopyrite, Ca: diopside. Five points on each crystal were analyzed. Back-scattered-electron images of each crystal show no

sign of compositional zoning. The chemical formulae were calculated on the basis of ten anions with (OH) = 4 *apfu* (atoms per formula unit). Chemical compositions and unit formulae are given in Table 5.3.

5.5 Crystal-structure refinement

Crystal-structure refinements of brandtite, collinsite and fairfieldite were initiated with the atom coordinates of roselite (Hawthorne & Ferguson 1977), collinsite (Brotherton *et al.* 1974) and fairfieldite (Fanfani *et al.* 1970), respectively. Refinement converged to R-indices of 2.6, 1.5 and 1.7%, respectively. Final positional and displacement parameters are given in Table 5.4., selected interatomic distances are listed in Table 5.5., refined site-scattering values (Hawthorne *et al.* 1995) are given in Table 5.6., and bond valences are given in Table 5.7. Observed and calculated structure-factors are located at The Depository of Unpublished Data, CISTI, National Research Council, Ottawa, Ontario K1A 0S2.

Table 5.3. Chemical composition (wt.%) and unit formulae* (*apfu*)

	Brandtite	Collinsite	Fairfieldite	
P_2O_5	-	42.13	39.34	
As_2O_5	49.58	-	-	
CaO	23.15	33.54	30.60	
MgO	0.86	11.07	0.06	
MnO	13.36	0.15	14.26	
FeO	0.08	1.31	4.49	
PbO	2.48	-	-	
H_2O**	7.68	10.71	9.89	
Total***	97.19	98.91	98.64	
X: Ca	1.94	2	2	
Pb^{2+}	0.05	-	-	
Y: Mg	0.10	0.92	0.01	
Mn	0.88	0.01	0.73	
Fe	0.01	0.06	0.23	
ΣY	0.99	0.99	0.97	
T: P	-	2	2	
As	2	-	-	

*Formulae normalized to 10 anions;
**H_2O calculated by stoichiometry;
*** No other elements were above detection limits.

Table 5.4 Atom coordinates and anisotropic displacement parameters.

(a) brandtite

Site	x	y	z	Ueq	U11	U22	U33	U23	U13	U12
X=Ca	0.56763(11)	0.11965(5)	0.24347(11)	0.0095(2)	0.0095(3)	0.0091(3)	0.0101(3)	-0.0012(2)	0.0034(2)	-0.0011(2)
M=Mn	0	0	0	0.0094(2)	0.0096(4)	0.0089(4)	0.0093(4)	-0.0041(3)	0.0023(3)	-0.0009(3)
T=As	0.22243(5)	0.12174(2)	0.53783(6)	0.00639(11)	0.00747(16)	0.00533(16)	0.00581(16)	0.00021(12)	0.00123(11)	0.00010(11)
O(1)	0.2445(4)	0.03619(19)	0.3558(5)	0.0119(5)	0.0128(11)	0.0120(12)	0.0111(11)	-0.0061(9)	0.0040(9)	-0.0019(9)
O(2)	0.2883(4)	0.05599(19)	0.8451(4)	0.0094(4)	0.0096(10)	0.0090(11)	0.0077(10)	0.0034(9)	0.0000(8)	-0.0000(8)
O(3)	0.9499(4)	0.17265(19)	0.5022(5)	0.0110(5)	0.0084(10)	0.0092(11)	0.0139(12)	0.0005(9)	0.0013(9)	0.0034(8)
O(4)	0.4404(4)	0.20712(19)	0.5795(4)	0.0099(4)	0.0098(10)	0.0084(11)	0.0112(11)	-0.0010(9)	0.0028(8)	-0.0038(8)
OW	0.8087(4)	0.14270(19)	0.9719(4)	0.0099(5)	0.0132(11)	0.0089(11)	0.0067(10)	0.0005(9)	0.0018(8)	-0.0020(8)
H(1)	0.685(6)	0.150(4)	0.811(4)	0.037(15)						
H(2)	0.907(6)	0.205(2)	0.987(9)	0.028(13)						

(b) collinsite

Site	x	y	z	U_{eq}	$U11$	$U22$	$U33$	$U23$	$U13$	$U12$
X=Ca	0.30332(5)	0.75897(4)	0.65422(5)	0.00910(8)	0.00765(12)	0.01038(12)	0.00879(12)	0.00116(8)	0.00351(9)	0.00259(9)
M=Mg	0	0	0	0.00636(18)	0.0058(3)	0.0098(3)	0.0064(3)	0.00095(18)	0.00196(19)	.00258(19)
T=P	0.33308(6)	0.24382(5)	0.66329(6)	0.00577(8)	0.00513(14)	0.00637(14)	0.00578(14)	0.00174(10)	0.00175(10)	0.00225(10)
O(1)	0.25585(18)	0.07243(15)	0.40377(18)	0.00989(18)	0.0098(4)	0.0102(4)	0.0078(4)	-0.0007(3)	0.0019(3)	0.0037(3)
O(2)	0.33308(18)	0.12722(15)	0.89146(18)	0.00899(17)	0.0088(4)	0.0109(4)	0.0089(4)	0.0055(3)	0.0037(3)	0.0040(3)
O(3)	0.15488(18)	0.37340(14)	0.63328(18)	0.00907(17)	0.0091(4)	0.0098(4)	0.0104(4)	0.0036(3)	0.0036(3)	0.0058(3)
O(4)	0.61936(17)	0.38661(14)	0.72049(18)	0.00948(17)	0.0064(4)	0.0100(4)	0.0100(4)	0.0024(3)	0.0025(3)	0.0007(3)
OW	0.94947(18)	0.27786(14)	0.06803(18)	0.00884(17)	0.0084(4)	0.0084(4)	0.0088(4)	0.0024(3)	0.0023(3)	0.0025(3)
H(1)	0.838(4)	0.316(4)	0.077(4)	0.039(7)						
H(2)	1.117(3)	0.392(3)	0.144(5)	0.050(8)						

(c) fairfieldite

Site	x	y	z	Ueq	U11	U22	U33	U23	U13	U12
X=Ca	0.6010(1)	0.2337(1)	0.3329(1)	0.0091(1)	0.0093(2)	0.0090(2)	0.0086(2)	0.0012(1)	0.0030(1)	0.0002(1)
M=Mn	0	0	0	0.0095(1)	0.0095(2)	0.0105(2)	0.0071(2)	-0.0001(1)	0.0020(1)	0.0005(1)
T=P	0.2452(1)	0.2324(1)	0.6475(1)	0.0070(1)	0.0083(2)	0.0065(2)	0.0059(2)	0.0018(1)	0.0017(1)	0.0004(1)
O(1)	0.2451(2)	0.0693(2)	0.3961(2)	0.0111(2)	0.0129(5)	0.0108(4)	0.0078(4)	-0.0007(3)	0.0030(4)	-0.0004(4)
O(2)	0.3050(2)	0.1179(2)	0.8781(2)	0.0101(2)	0.0117(4)	0.0105(4)	0.0086(4)	0.0048(3)	0.0024(3)	0.0009(3)
O(3)	0.0021(2)	0.3271(2)	0.6145(1)	0.0106(2)	0.0097(4)	0.0103(4)	0.0114(4)	0.0032(3)	0.0024(3)	0.0020(3)
O(4)	0.4545(2)	0.3994(2)	0.6957(2)	0.0100(2)	0.0106(4)	0.0081(4)	0.0110(4)	0.0021(3)	0.0034(3)	-0.0007(3)
OW	-0.1529(2)	0.2999(2)	0.0674(2)	0.0119(2)	0.0154(5)	0.0102(4)	0.0090(4)	0.0015(4)	0.0029(4)	0.0011(4)
H(1)	-0.277(4)	0.346(5)	-0.071(5)	0.052(9)						
H(2)	-0.072(5)	0.432(3)	0.181(5)	0.054(9)						

Table 5.5. Selected interatomic distances (Å)

	brandtite			collinsite			fairfieldite	
Ca-O(1)		2.435(3)	Ca-O(1)h		2.583(1)	Ca-O(1)		2.478(1)
Ca-O(1)a		2.986(3)	Ca-O(1)l		2.700(1)	Ca-O(1)a		2.725(1)
Ca-O(2)c		2.489(3)	Ca-O(2)j		2.517(2)	Ca-O(2)c		2.490(1)
Ca-O(2)e		2.533(3)	Ca-O(2)l		2.591(1)	Ca-O(2)a		2.501(1)
Ca-O(3)		2.374(3)	Ca-O(3)		2.472(1)	Ca-O(3)n		2.336(1)
Ca-O(4)		2.522(3)	Ca-O(3)k		2.403(1)	Ca-O(4)		2.458(1)
Ca-O(4)b		2.453(3)	Ca-O(4)h		2.378(1)	Ca-O(4)h		2.467(1)
Ca-OWc		2.413(3)	Ca-OWh		2.392(1)	Ca-OWn		2.439(1)
$<Ca$-O>		2.526	$<Ca$-O>		2.505	$<Ca$-O>		2.487
M-O(1)	x2	2.138(2)	M-O(1)d	x2	2.114(1)	M-O(1)d	x2	2.136(1)
M-O(2)c,e	x2	2.256(2)	M-O(2)c,e	x2	2.146(1)	M-O(2)c,e	x2	2.268(1)
M-OWf,a	x2	2.144(2)	M-OWl,m	x2	1.996(1)	M-OWd	x2	2.174(1)
$<M$-O>		2.179	$<M$-O>		2.085	$<M$-O>		2.193
T-O(1)		1.696(2)	T-O(1)		1.556(1)	T-O(1)		1.557(1)
T-O(2)		1.696(2)	T-O(2)		1.555(1)	T-O(2)		1.557(1)
T-O(3)g		1.662(2)	T-O(3)		1.517(1)	T-O(3)		1.516(1)
T-O(4)		1.685(2)	T-O(4)		1.543(1)	T-O(4)		1.551(1)
$<T$-O>		1.685	$<T$-O>		1.543	$<T$-O>		1.545

Symmetry operators: a = $-x+1, -y, -z+1$; b = $x, -y+., z-.$; c = $x, y, z-1$; d = $-x, -y, -z$; e = $x-1, y, z-1$; f = $x-1, y, z+1$; g = $x-1, -y+., z+.$; h = $-x+1, -y+1, -z+1$; i = $x, y+1, z$; j = $-x+1, -y+1, -z+2$; k = $-x, -y+1, -z+1$; l = $x-1, y, z$; m = $-x+1, -y, -z$; n = $x+1, y, z$.

Table 5.6. Refined and assigned site-scattering values (*epfu**)
for selected sites

	X-site refined**	X-site assigned***	Y-site refined**	Y-site assigned
brandtite	40.6(1)	42.9	23.56(1)	23.5
collinsite	40	40.2	13.12(5)	12.9
fairfieldite	40	40.6	25.08(5)	24.7

*electrons per formula unit
** all X-sites refined as Ca; brandtite and fairfieldite
Y-site refined as Mn, collinsite Y-site refined as Mg;
*** assigned from chemical formula.

Table 5.7. Selected donor (D) oxygen-hydrogen-acceptor (A) oxygen interatomic distances (Å) and angles (°)

	D-H(1)	D-H(2)	H(1)...A(1)*	H(2)...A(2)*	D-A(1)	D-A(2)	‹DHA(1)	‹DHA(2)	‹H(1)-D-H(2)
brandtite	0.98(1)	0.98(1)	1.78(2)	1.61(2)	2.712(3)	2.521(4)	157(5)	153(4)	105(4)
collinsite	0.98(1)	0.98(1)	1.604(6)	1.633(6)	2.5699(16)	2.6060(19)	168(2)	171(3)	107(2)
fairfieldite	0.98(1)	0.98(1)	1.753(7)	1.685(8)	2.720(2)	2.646(2)	168(3)	166(3)	101(3)

* brandtite: A(1) = O(4); A(2) = O(3)

*collinsite: A(1) = O(4); A(2) = O(4)

*fairfieldite: A(1) = O(4); A(2) = (3)

Table 5.8. Bond-valence (vu)* tables

	Ca	M^{2+}	T^{5+}	H(1)	H(2)	Σ
			brandtite			
O(1)	0.28 0.07	$0.39^{x2}\downarrow$	1.21			1.95
O(2)	0.24 0.21	$0.28^{x2}\downarrow$	1.21			1.94
O(3)	0.33		1.33		0.30	1.96
O(4)	0.22 0.27		1.25	0.30		2.04
OW	0.30	$0.38^{x2}\downarrow$		0.70	0.70	2.08
Sum	1.92	2.10	5.00	1.00	1.00	
			collinsite			
O(1)	0.19 0.14	$0.32^{x2}\downarrow$	1.18			1.83
O(2)	0.23 0.19	$0.29^{x2}\downarrow$	1.18			1.89
O(3)	0.26 0.31		1.31			1.88
O(4)	0.33		1.22	0.30	0.30	2.15
OW	0.32	$0.44^{x2}\downarrow$		0.70	0.70	2.16
Sum	1.97	2.10	4.89	1.00	1.00	
			fairfieldite			
O(1)	0.25 0.13	$0.39^{x2}\downarrow$	1.18			1.95
O(2)	0.24 0.24	$0.28^{x2}\downarrow$	1.18			1.94
O(3)	0.37		1.31		0.30	1.98
O(4)	0.27 0.26		1.19	0.30		2.02
OW	0.28	$0.35^{x2}\downarrow$		0.70	0.70	2.03
Sum	2.04	2.04	4.86	1.00	1.00	

* calculated with the parameters of Brown & Altermatt (1985)

27

5.6 Description of the structures

The T-site atoms are normally As^{5+} and P^{5+}, and are surrounded by a regular tetrahedral arrangement of O atoms. The M-site atoms are normally divalent and are surrounded by an octahedral arrangement of four O atoms and two (H_2O) groups. The X-site atoms are commonly Ca and are surrounded by an irregular [8]-coordinated polyhedral arrangement of seven O atoms and one (H_2O) group. All three structure-types are based on infinite $[M(TO_4)_2(H_2O)_2]$ chains that extend in the c direction with a repeat distance of ~ 5.55 Å. These chains are linked into continuous structures by interstitial Ca atoms and by hydrogen bonds involving the (H_2O) groups (Fig. 5.1.), and it is these linkages on which we will focus here. For direct comparison, the atoms in each structure have been relabeled such that they are topologically equivalent (Fig. 5.2.).

The three structures seem very similar (Fig. 5.1.). The only significant difference is related to the linkage of the ($Ca\varphi_8$) polyhedra. In all three structures, the ($Ca\varphi_8$) polyhedra form edge-sharing dimers. However, the different linkages between these dimers give rise to three distinctly different sheets of polyhedra (Fig. 5.3.). In brandtite (Fig. 5.3a), dimers share edges with other dimers along the **c** direction to form zig-zag chains that link in the **b** direction by sharing polyhedron corners. The resultant sheet is parallel to (100), and each polyhedron shares two edges and two vertices with the four adjacent polyhedra. In collinsite (Fig. 5.3b), dimers share edges with other dimers along the [011] and [01-1] directions to form a sheet in which all linkages involve sharing of polyhedron edges. This sheet is parallel to (1$\underline{1}$0), and each polyhedron shares three edges with the three adjacent polyhedra. In fairfieldite
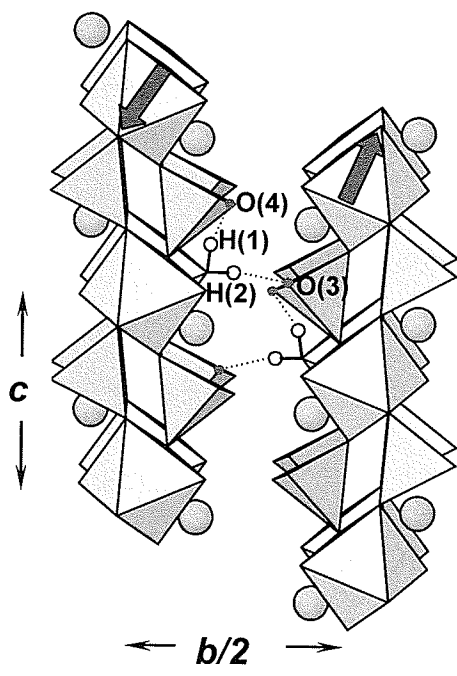
5.1(a)
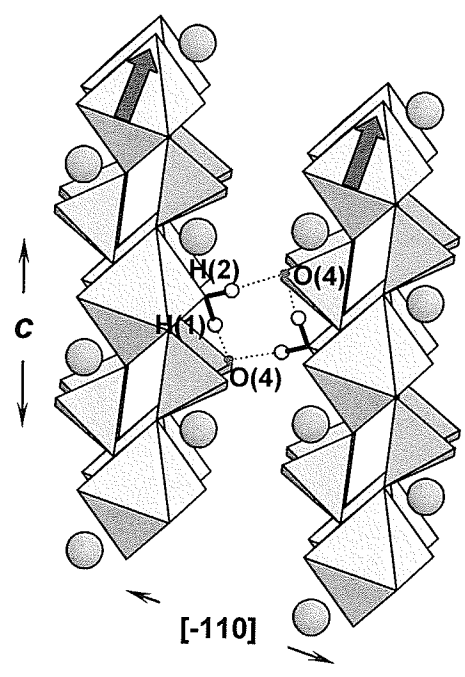
5.1(b)
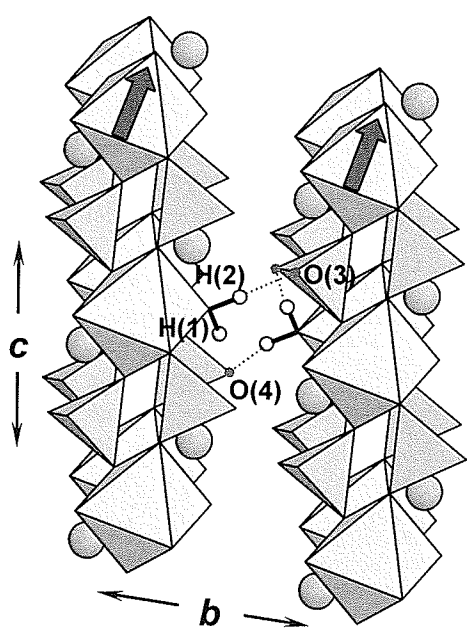
5.1(c)
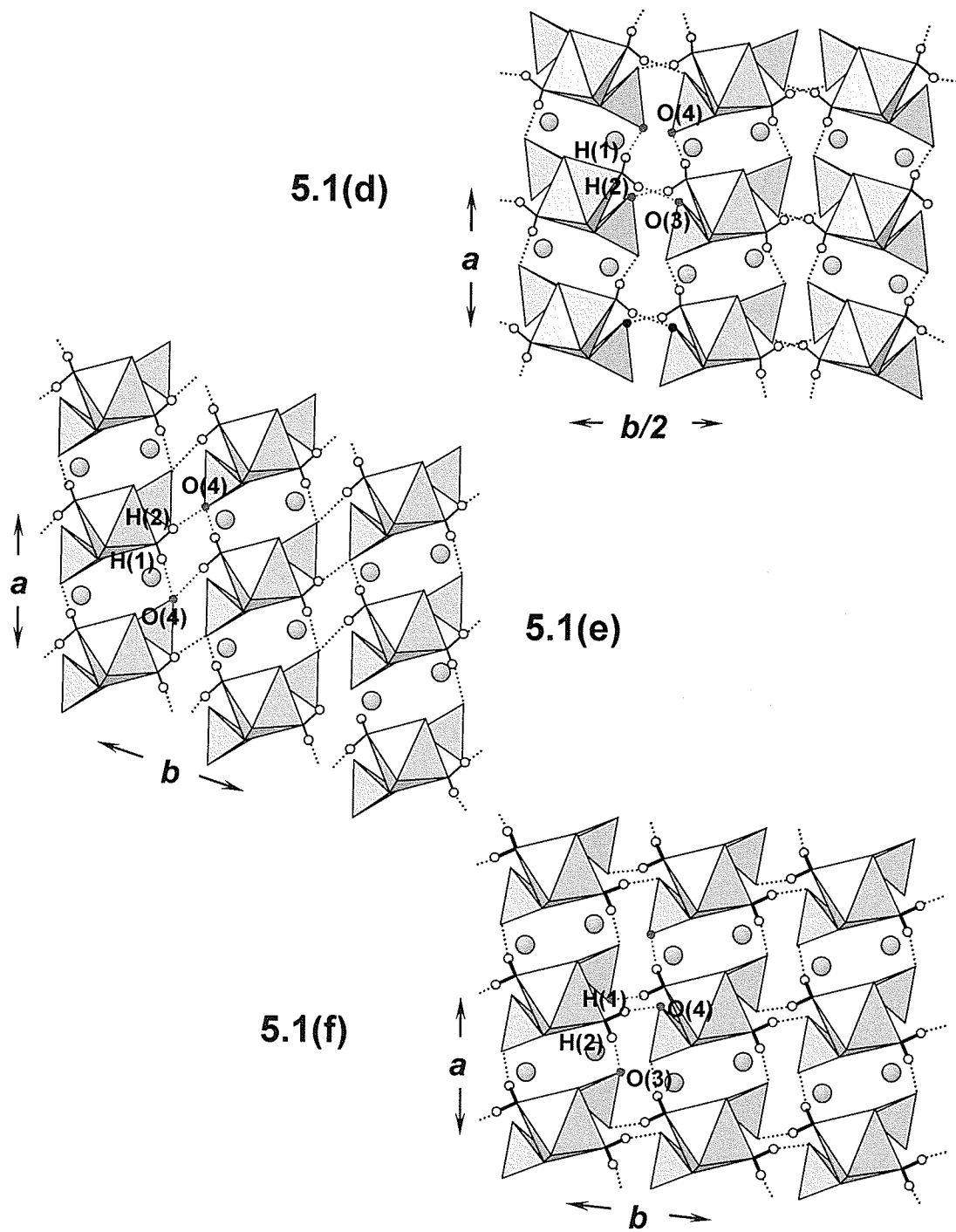
Figure 5.1. The crystal structures of (a), (d) brandtite, (b), (e) collinsite, and (c), (f) Fairfieldite projected onto (100). M octahedra are lemon yellow, T tetrahedra are pale green, Ca is tan and H are small white circles. Hydroxyl bonds as shown as solid lines, hydrogen bonds are shown as red or black dotted lines, acceptor anions for (red) hydrogen bonds are shown as red circles. The red arrows show the relative attitude or 'tilt direction' of the octahedra in adjacent chains.
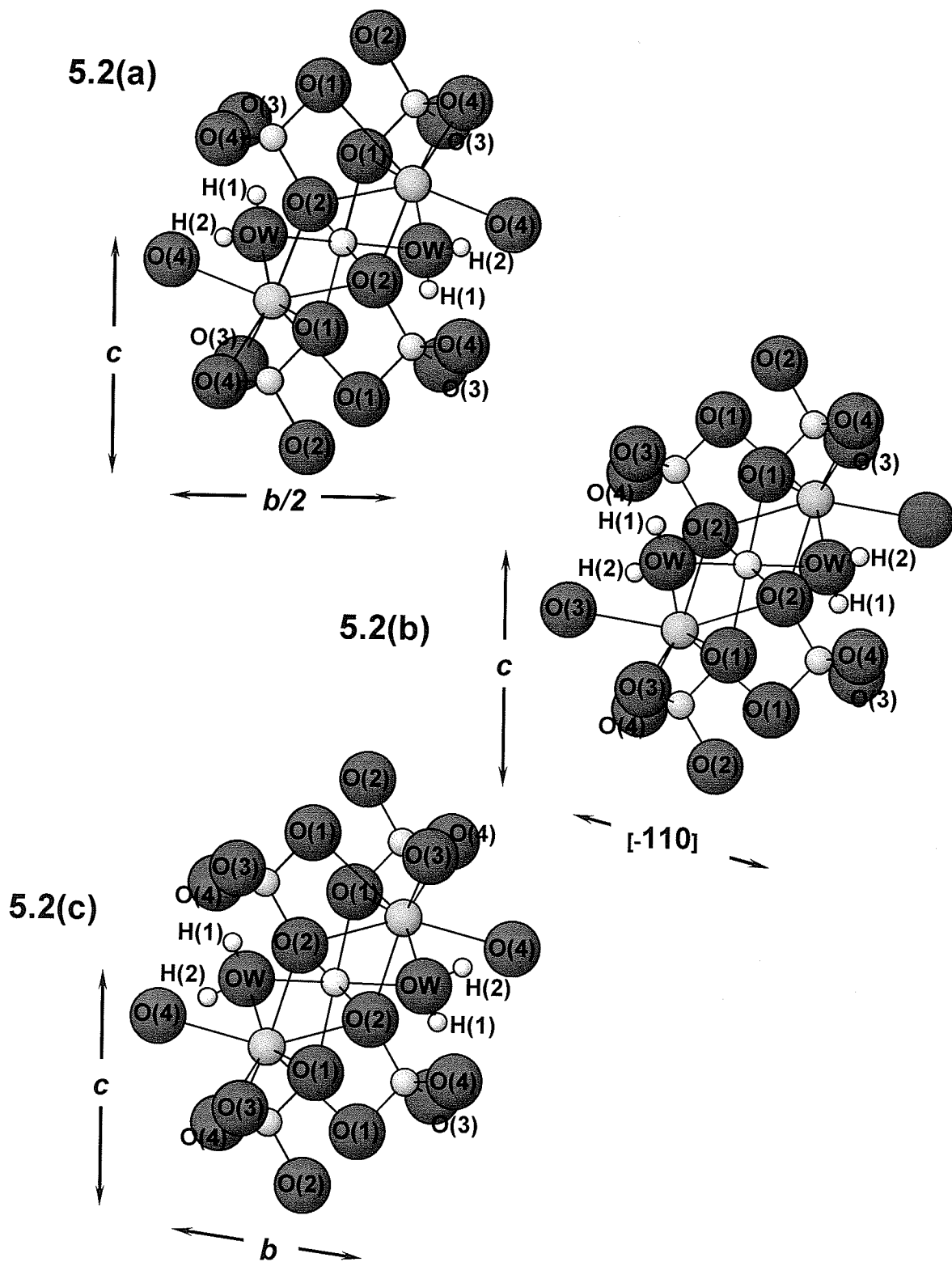
Figure 5.2. The atom-labeling schemes used in (a) brandtite, (b) collinsite, and (c) fairfieldite. Legend as in Figure 5.1, O-atoms are shown as large red circles.

5.3(a)

5.3(b)

5.3(c)
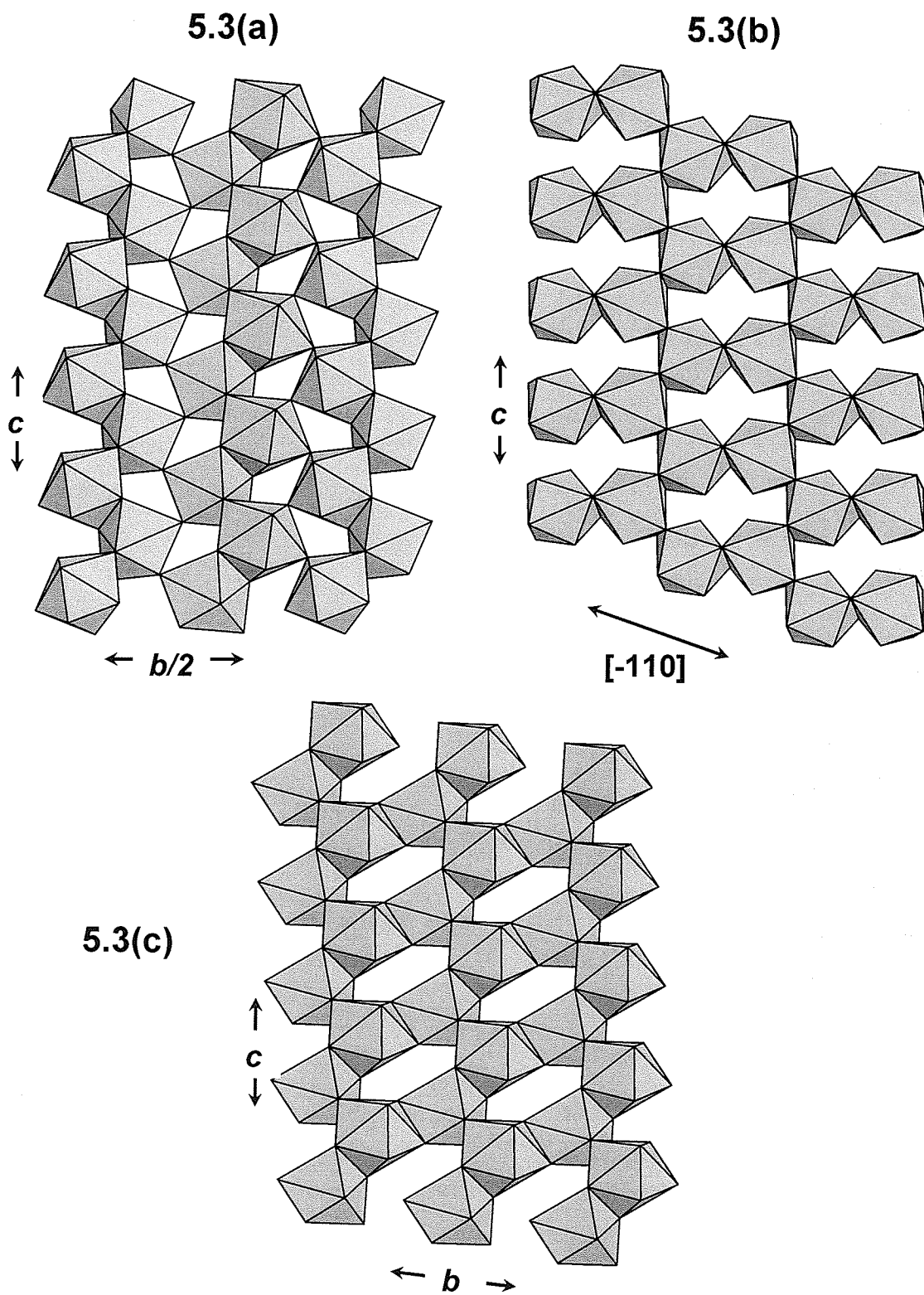
Fig. 5.3. The layers formed by Ca polyhedra in (a) brandtite, (b) collinsite, and (c) fairfieldite; the layers are parallel to (010), (-110) and (010), respectively.

(Fig.5.3c), dimers share edges with other dimers along the c direction to form zig-zag chains, and the polyhedra of these chains share edges with the polyhedra of chains adjacent in the b direction, again forming a sheet in which all linkages occur through polyhedron edges. The resultant sheet is parallel to (100), and each polyhedron shares three edges with the three adjacent polyhedra.

5.7 Interstitial linkage

The interstitial interactions are particularly interesting in these groups of minerals as the structural units are topologically identical in all three groups. There are three distinct factors involved in the interstitial linkage of the chains: (1) the attitude and offset of the adjacent chains, (2) the coordination of Ca by anions of adjacent chains, and (3) the arrangement of hydrogen bonds.

5.8 Attitude of adjacent chains

In brandtite, the upper faces of the octahedra of adjacent chains [when the structures are viewed perpendicular to (011)] point in alternate directions (see red arrows, Figure 5.1a), whereas in collinsite and fairfieldite, the corresponding faces of octahedra of adjacent chains point in the same direction (Figures 5.1b, c). In brandtite, the chains adjacent in the **b** direction are tilted in opposite directions, imparting a wave-like modulation to the sheet of $(Ca\varphi_8)$ (φ=unspecified anion) polyhedra (Figure 5.1d). In collinsite, the chains adjacent in the **b** direction are tilted in the same direction; when combined with the relative displacement of adjacent chains (Figure 5.1e), this results in the sheet of $(Ca\varphi_8)$ polyhedra being parallel to (10-1). In fairfieldite, the chains adjacent in the **b** direction are tilted in the same direction which, when combined with the

absence of a relative displacement of adjacent chains (Figure 5.1f), results in a modulated

sheet of $(Ca\varphi_8)$ polyhedra parallel to (100).

5.9 Interchain linkage by interstitial Ca

The linkage of adjacent chains in all three structure types is shown in Figure 5.4,

where adjacent chains are labeled (i) through (iv). Inspection shows that in brandtite

(Figure 5.4a), Ca (highlighted by the circle) links chains (i), (ii) and (iii), whereas in

collinsite (Figure 5.4b) and fairfieldite (Figure 5.4c), Ca links chains (ii), (iii) and (iv).

This difference in the linkage of adjacent chains is a result of the difference in attitude of

the chains in the **b** direction in these structures (Figure 5.1). In brandtite, the octahedron

faces of adjacent chains point in opposing directions (Figure 5.1a). This has the effect of

tilting the tetrahedra of adjacent chains in opposing directions relative to the octahedra to

which they are linked (Figure 5.4a), and the tetrahedra of chain (i) are within bonding

range of the Ca under consideration. In collinsite and fairfieldite, the chains point in the

same directions (Figures 5.1e,f). This has the effect of tilting the tetrahedra of adjacent

chains in the same direction relative to the octahedra to which they are linked (Figures

5.4b,c), and the tetrahedra of chain (iv) are within bonding range of the Ca under

consideration.

Close inspection of Figures 5.4b and 5.4c shows that the linkage between Ca and

chain (iii) is the same in the structures of collinsite and fairfieldite. Ca bonds to O(1)a,

O(2)a, O(3)a and OW, see extracted view of the $(Ca\varphi_8)$ polyhedra (φ = unspecified

anion) for each

5.4(a)
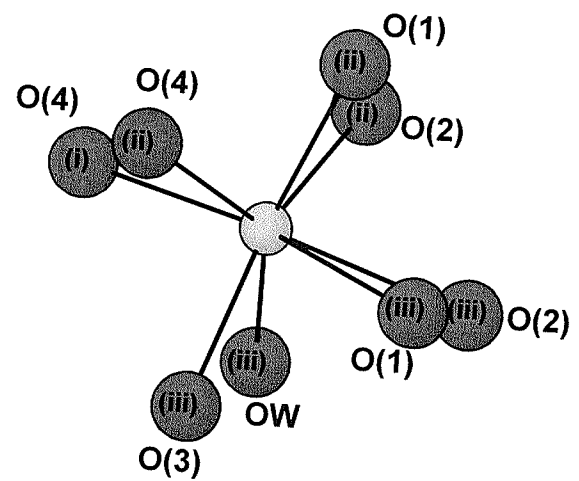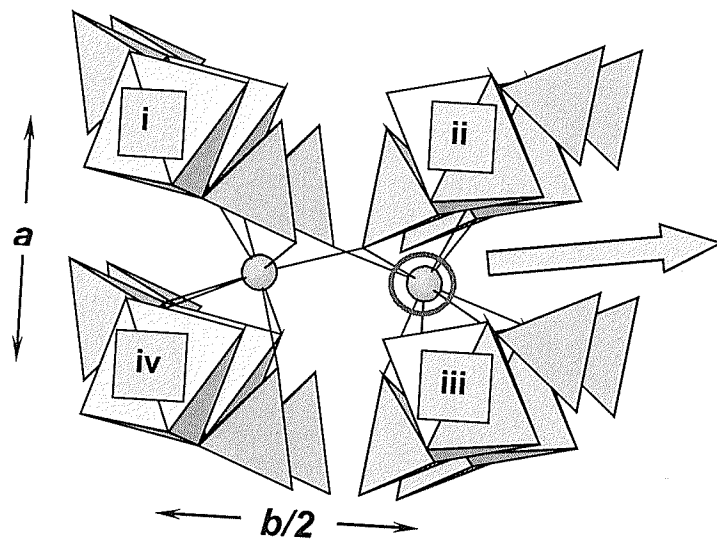
5.4(b)
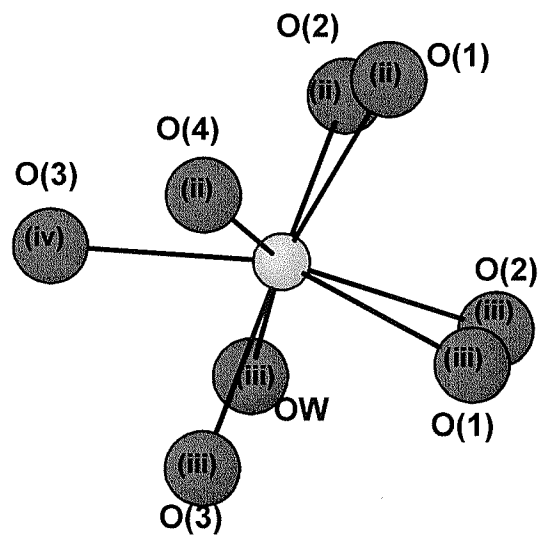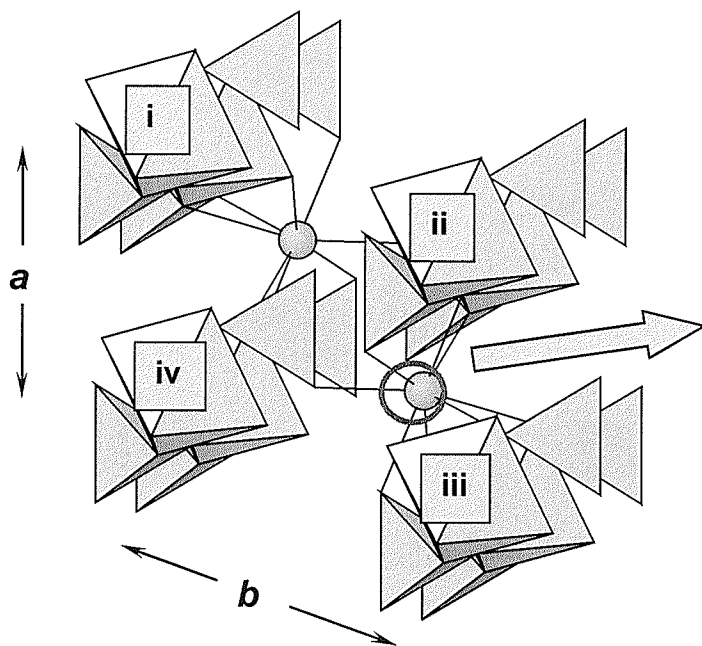
## 5.4 c)
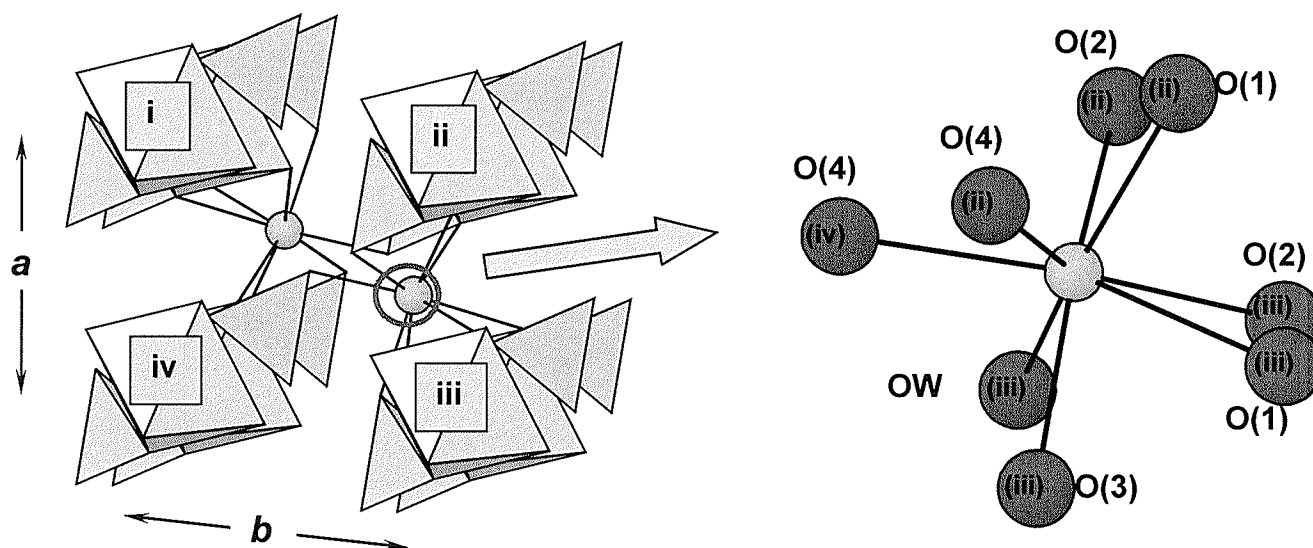
Figure 5.4. The crystal structures of (a) brandtite, (b) collinsite, and (c) fairfieldite, projected onto (001), showing the coordination of Ca by anions of different chains. Legend as in Figures 5.1 and 5.2. The chains are labeled (i) to (iv) and the anions are labeled accordingly.

Structure (Figure 5.4). Furthermore, the linkage between Ca and chain (ii) is the same in both structures: Ca bonds to O(1)b, O(2)b and O(4)b (Figs. 4b, 4c). So seven of the eight Ca-φ bonds are the same in collinsite and fairfieldite. The difference between the interchain linkage by Ca in these two structures involves their linkage to chain (iv). In collinsite, Ca links to O(3)c in chain (iv) (Figure 5.4b), whereas in fairfieldite, Ca links to O(4)c in chain (iv) (Figure 5.4c). The reason for this difference is also apparent in Figure 5.4. In both structures, the interstitial Ca links to the same tetrahedron (Figures 5.4b, c). However, in collinsite, chain (iii) is shifted further along the a direction than it is in fairfieldite; this has the effect of switching the linkage from one end of the tetrahedron in fairfieldite to the other end of the tetrahedron in collinsite.

5.10 Interstitial hydrogen-bond arrangements

The stereochemical details of the hydrogen-bonding network in each structure type is given in Table 5.7. Inspection of Figures 5.1a, b and c shows that in all three structure-types, the $[M(TO_4)_2(H_2O)_2]$ chains are repeated by the a translation to form layers of disconnected chains parallel to (100). Inspection of these layers (Figs. 5.5a, b, c) shows that the arrangement of hydrogen bonds is the same within these layers in each structure-type: the H(1) atom hydrogen-bonds to the O(4) anion, and the arrangement is the same in each case. This observation indicates that the structural differences among the minerals of these three groups must arise from differences in hydrogen-bond arrangements *between* these layers.

The hydrogen bonds involved in linkage between layers can be seen in Figures 5.1d, e, f. Inspection of Figures 5.1e, f indicate that (1) in the layers adjacent in the [010]
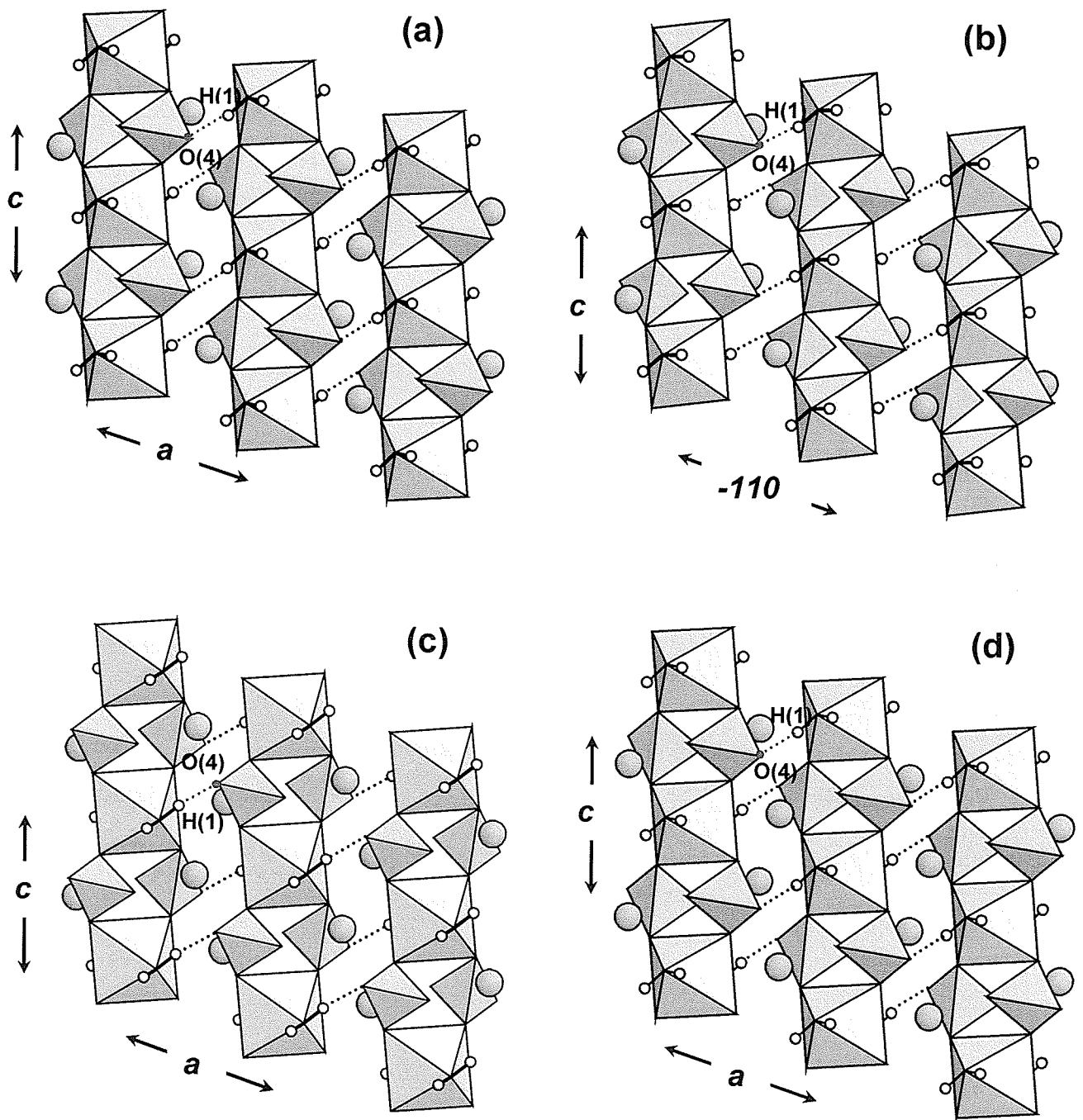
Figure 5.5. The crystal structures of (a) brandtite, (b) collinsite, (c) fairfieldite, and (d) a hypothetical $P2_1/n$ structure of the same stoichiometry, projected onto (010), showing the layers of $[M(TO_4)_2(H_2O)_2]$ chains and the intra-layer hydrogen bonds. Legend as in Figure 5.1.

interlayer direction, the constituent octahedral point in the same direction; and (2) the hydrogen bond links to different anions of the tetrahedron in the adjacent layer (Figures 5.5e, f). In the projection of Figures 5.1e, f, there are no other hydrogen-bond arrangements possible. Inspection of Figure 5.1d indicates that (1) the layers adjacent in the [010] direction *point* in opposite directions; and (2) the interlayer hydrogen bond links to the upper anion of the tetrahedron in the adjacent layer.

5.11 Other possible hydrogen-bonding arrangements

Inspection of Figure 5.1 and Table 5.7 indicates that the acceptor anions for the hydrogen-bond arrangements are always the O(3) or O(4) anions of the (TO_4) tetrahedron. In terms of the atoms that are involved in these arrangements, the following connections are topologically (but not necessarily stereochemically) possible: (1) H(1)-O(3), H(2)-O(3); (2) H(1)-O(4), H(2)-O(4); (3) H(1)-O(3), H(2)-O(4); (4) H(1)-O(4), H(2)-O(3). Arrangement (2) occurs in collinsite, and arrangement (4) occurs in brandtite and fairfieldite. In order for the other two arrangements to occur with a reasonable stereochemistry, H(1) and H(2) would have to exchange positions, and thus the arrangements would be the same as those of (2) and (4), only the atom labeling would be different.

5.12 A possible new structural arrangement with $P2_1/n$ symmetry

The description of the intersheet arrangements of hydrogen bonds given above suggests the possibility of another arrangement. In Figures 5.1e, f, we see that the intersheet hydrogen-bond links to the bottom and top, respectively, of the tetrahedron in the adjacent layer, whereas in Figure 5.1d, the interlayer hydrogen-bond links to the bottom of the tetrahedron in the adjacent layer. This suggests the possibility of interlayer

hydrogen-bonds linking to the top anion of the tetrahedron in an adjacent layer in which the octahedron points in the opposite direction. In terms of Figure 5.1d, such a linkage would require a shift of adjacent layers by ~$a/2$. This would have the result of producing a monoclinic structure with an n-glide (instead of a c-glide as in brandtite). This structure arrangement is shown in Figure 5.6, using the cell dimensions for brandtite, and the atom positions and interatomic distances are given in Tables 5.4 and 5.5. The arrangement of hydrogen bonds *within* the layers of chains is the same as in the other structure-types (Fig. 5.5d), but the hydrogen bonds *between* layers link to the top anion of the tetrahedron in the adjacent layer (*i.e.*, the O(4) anion (Figure 5.6b) rather than the O(3) anion as in brandtite (Figure 5.1d)]. Of course, the layer of X-cation polyhedra in the $P2_1/n$ structure will also be different (Figure 5.7). Although this layer superficially resembles the analogous sheet in brandtite (Figure 5.3a), careful inspection shows that the chains of edge-sharing polyhedra extending in the c direction cross-link to different vertices of chains adjacent in the [010] direction (Figure 5.7)

Inspection of the bond-valence tables for these three structure types (Table 5.8) shows that the valence-sum rule (Brown 1981, Hawthorne 1992, 1994, 1997) is obeyed reasonably well in all structures. We may evaluate the degree of agreement for each structure by calculating the RMS (Root Mean-Square) deviation for the anions of each structure. The resulting values are 0.056, 0.144 and 0.039 *vu* for brandtite, collinsite and fairfieldite, respectively. For oxysalt structures RMS deviations are usually < 0.15 *vu*, in accord with the results obtained here.

5.6(a)
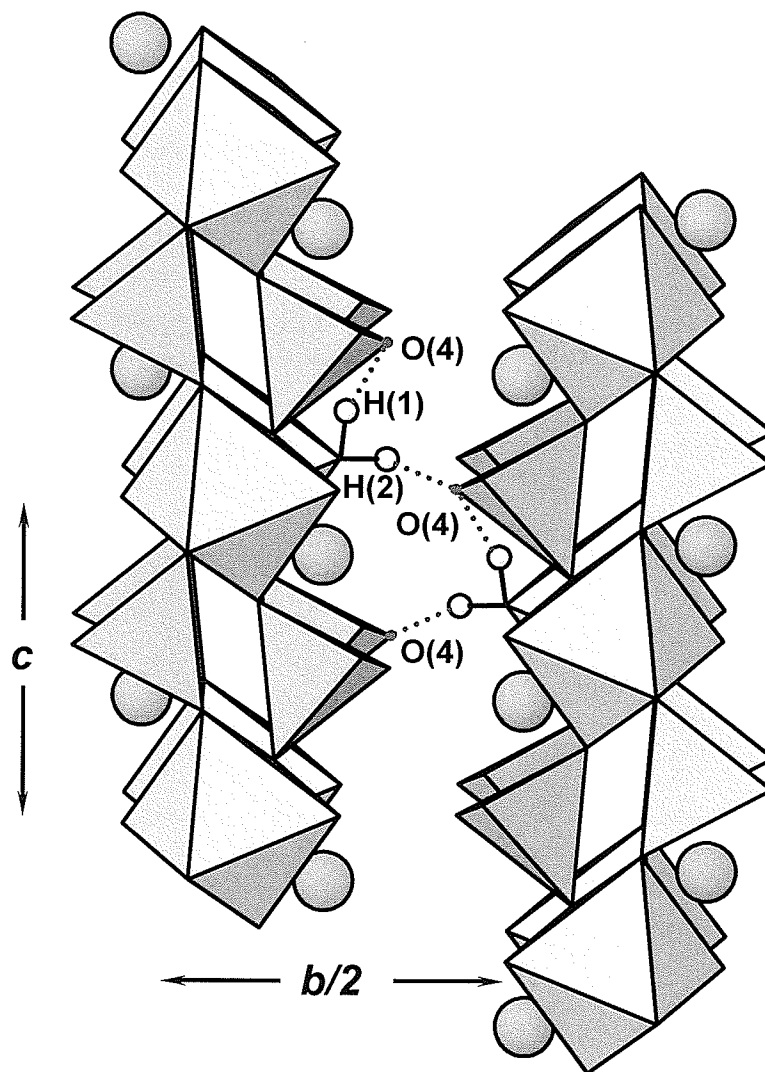
5.6(b)
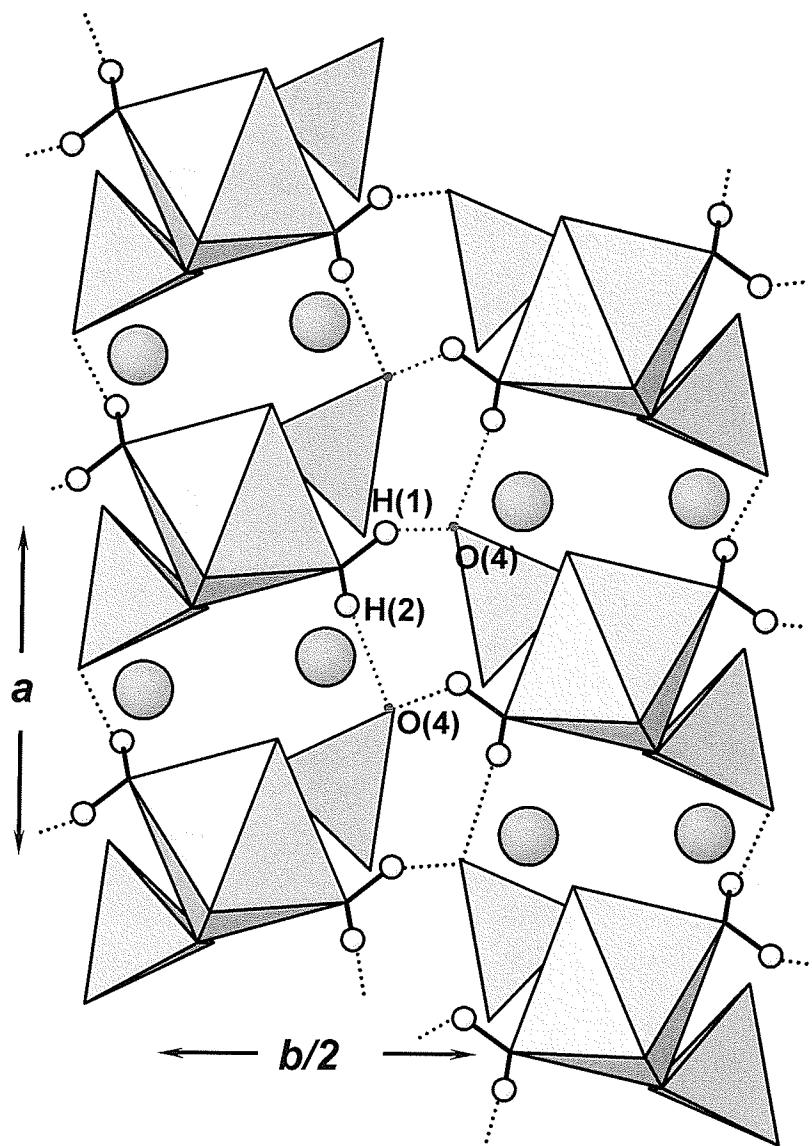
Figure 5.6. The crystal structure of a hypothetical $P2_1/n$ structure of Ca_2M $^{2+}(TO_4)_2(H_2O)_2$ stoichiometry (a) projected onto (100), and (b) projected onto (001), showing the network of inter- and intra-layer hydrogen bonds. Legend as in Figure 5.
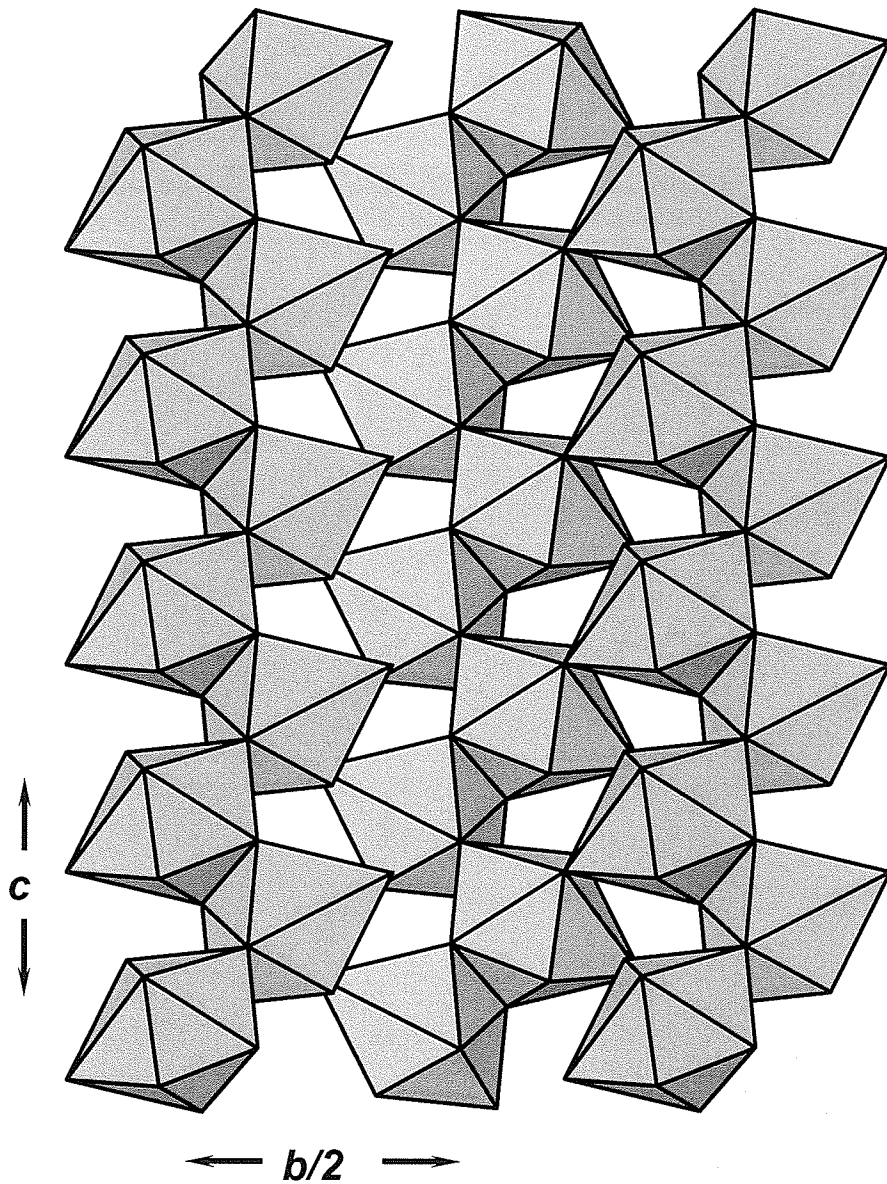
Figure 5.7. The layer of Ca polyhedra in the hypothetical $P2_1/n$ structure; legend as in Figure 5.3.

For the $P2_1/n$ arrangement derived above, the RMS deviation is ~0.23 vu, suggesting that this arrangement will not be stable owing to excessive deviation from the valence-sum rule.

The collinsite structure accommodates two hydrogen-bonds to the O(4) anion and no hydrogen bonds to the O(3) anion. The $P2_1/n$ structure does not. This issue involves the coordination of the interstitial Ca atom in each structure. In collinsite, Ca has two bonds to O(3) and one bond to O(4), resulting in O(3) and O(4) coordination numbers of [3] and [4], respectively (Table 5.8). In brandtite, Ca has one bond to O(3) and two bonds to O(4), resulting in O(3) and O(4) coordination numbers of [3] and [4], respectively (Table 5.8). In the $P2_1/n$ arrangement, Ca bonds to one O(3) and two O(4) atoms, resulting in coordination numbers of [2] and [5] for O(3) and O(4), respectively. It is this difference in bond topology that results in the major deviations from the valence-sum rule for the $P2_1/n$ arrangement, and is the reason this structure is not expected to be stable.

5.13 Other possible arrangements

Another possibility of different structural arrangements arises if we consider atoms *in different layers*. This issue is illustrated in Figure 5.8 for triclinic structures of symmetry P-1. Starting from the fairfieldite structure, the γ angle is decreased relative to that in fairfieldite, which has the effect of shifting the chains parallel to [100] relative to each other (indicated by the arrows in Figure 5.8) and allowing the H(1) atom to form a hydrogen bond to the O(4) anion *in the adjacent layer* rather than in the same layer (as it does in fairfieldite). As there are no changes in coordination number of any of the anions in Figure 5.8 (relative to Figure 5.1f), there are no obvious deviations from the valence-sum rule, and there is no convincing structural reason

5.8(a)

γ = 85°

a

b

H(1)
H(2)
O(4)
O(3)

5.8(b)

γ = 102°

a

b

O(4)
H(1)
H(2)
O(4)
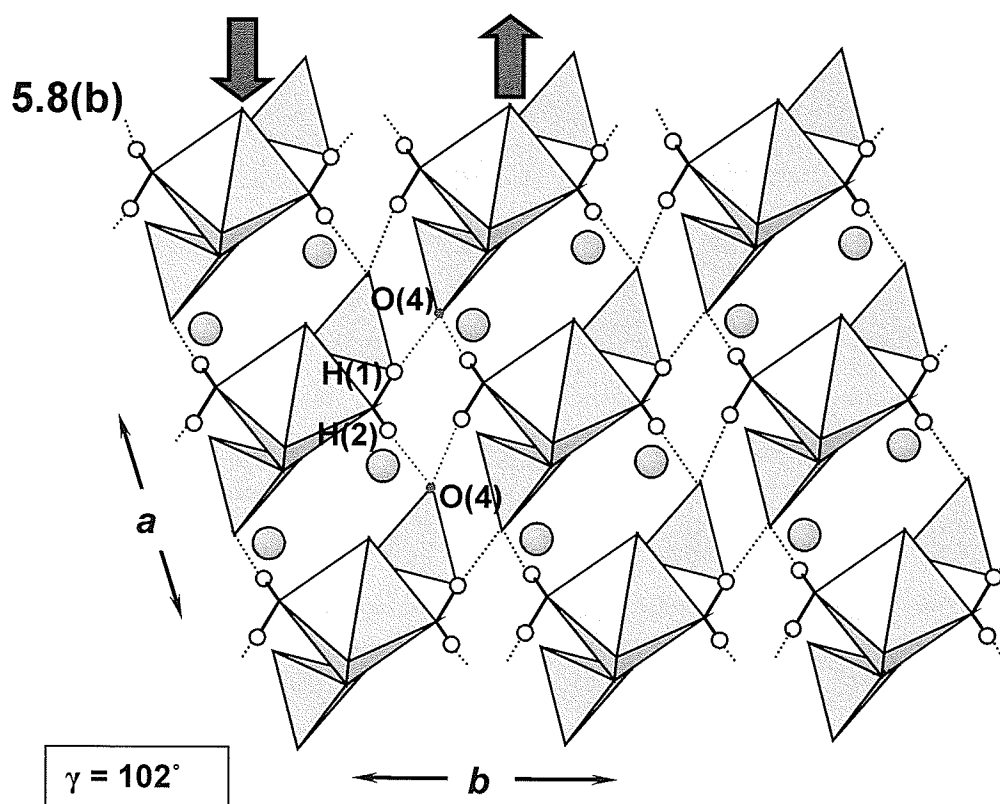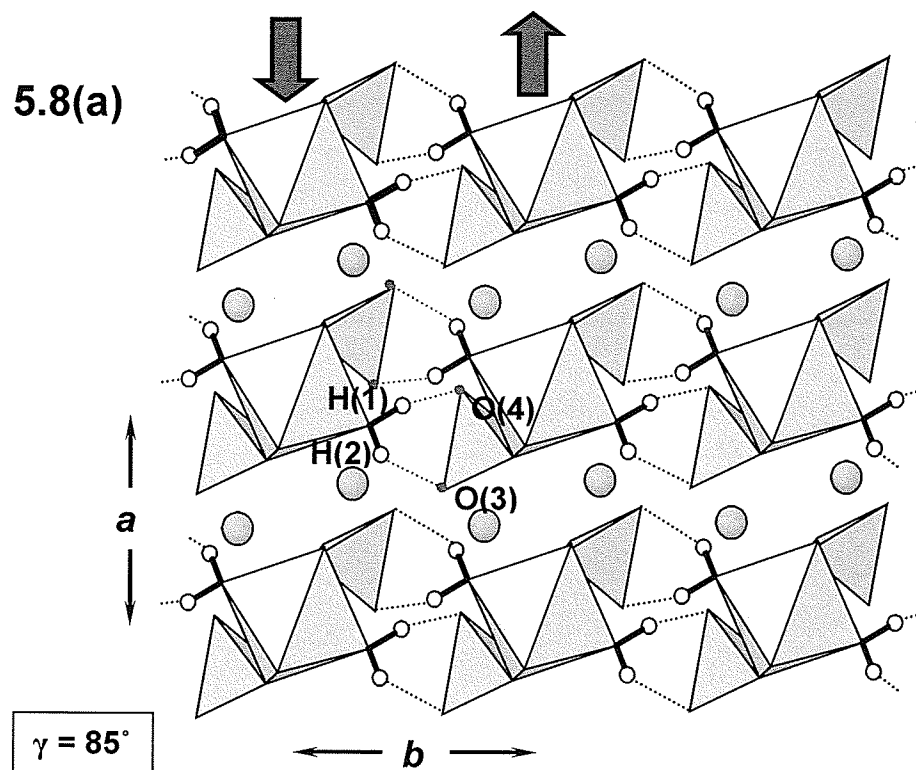
Figure 5.8. A different hydrogen-bond arrangement produced from the fairfieldite arrangement by changing the γ-angle. Legend as in Figure 5.1.

apparent as to why the arrangement of Figure 5.8 could not occur. Similar angular shear on the collinsite structure does not modify the hydrogen-bond arrangement.

5.14 Compositional aspects of the $X_2[M(TO_4)_2(H_2O)_2]$ structures

Inspection of Table 5.1 shows there are both similarities and differences with regard to the chemical compositions of the minerals in these three groups:

(1) The brandtite-group minerals are all arsenates (with the exception of kröhnkite, which is the only sulfate-mineral in any of these groups);

(2) The fairfieldite-group minerals are all phosphates;

(3) The collinsite-group minerals are both phosphates and arsenates;

(4) There are no vanadate minerals in any of these groups;

(5) There is considerable polymorphism among the arsenate minerals of these groups: the compositions $Ca_2Mg(AsO_4)_2(H_2O)_2$ (wendwilsonite and talmessite), $Ca_2Co(AsO_4)_2(H_2O)_2$ (roselite and beta-roselite) and $Ca_2Mn^{2+}(AsO_4)_2(H_2O)_2$ (brandtite and parabrandtite) occur as both structure-types.

(6) All minerals (except kröhnkite) have Ca as the dominant X-cation.

The X-cation may be monovalent (Na in kröhnkite) or divalent (Ca in all the other minerals of these three groups). Fleck & Kolitsch (2003), Kolitsch & Fleck (2005) and Fleck *et al.* (2002b) have reviewed both minerals and synthetic compounds based on the $[M(TO_4)_2(H_2O)_2]$ chains and have shown that there are a wide variety of synthetic compounds with X = Na, K, Rb, Cs, NH_4. Curiously, there are no synthetic compounds with X = Ca and no minerals (apart from kröhnkite) with monovalent X-cations. Hawthorne (1985) used the valence-matching principle (Brown 1981) to account for the

fact that no minerals of these structure types occur with other divalent cations (*e.g.*, Ba, Sr, Pb^{2+}) dominant at the X site. Liferovich *et al.* (2001) reported Sr up to 0.37 *apfu* in collinsite from the Kovdor carbonatite. One can account for the incorporation of a less than ideal cation (in terms of the valence-matching principle) into the structure by locally associating the cation with structural strain. However, where such strain fields interact, the structure may become unstable, and hence the extent of such substitutions will be limited. It would be of interest to examine this issue for (Ca,Sr) solid-solution in these structure types by synthesis, and characterize the relation between the compositions of the nascent solutions and the compositions of the crystallizing phases.

Figure 5.9 shows a type-II stability diagram (Shannon & Prewitt 1970) for these three structure types. For the phosphates, the separation into two distinct fields is quite marked: minerals of the fairfieldite group contain (relatively) large (> 0.76 Å) octahedrally coordinated cations (Fe^{2+}, Mn^{2+}), whereas phosphate minerals of the collinsite group contain (relatively) small (< 0.76 Å) octahedrally coordinated cations (Ni, Mg, Co^{2+}, Zn). For the arsenates, the situation is quite different: all compositions of arsenates (M^{2+} = Mg, Zn, Co, Mn) crystallize in both the brandtite- and collinsite-type structures. Inspection of the structures of these minerals (Figures 5.1, 5.5) show no obvious constraints on the sizes of the tetrahedra and octahedra within the structural unit itself. An explanation of the findings displayed in Figure 5.9 is not apparent. (*cf.* Keller *et al.* 2004, Kolitsch & Fleck 2005). However, it is noted that the polyhedra link *via* corners, and as there are no linkages that could be affected by articulation requirements between polyhedra, *these constraints on cation size must arise from linkage between structural units.*
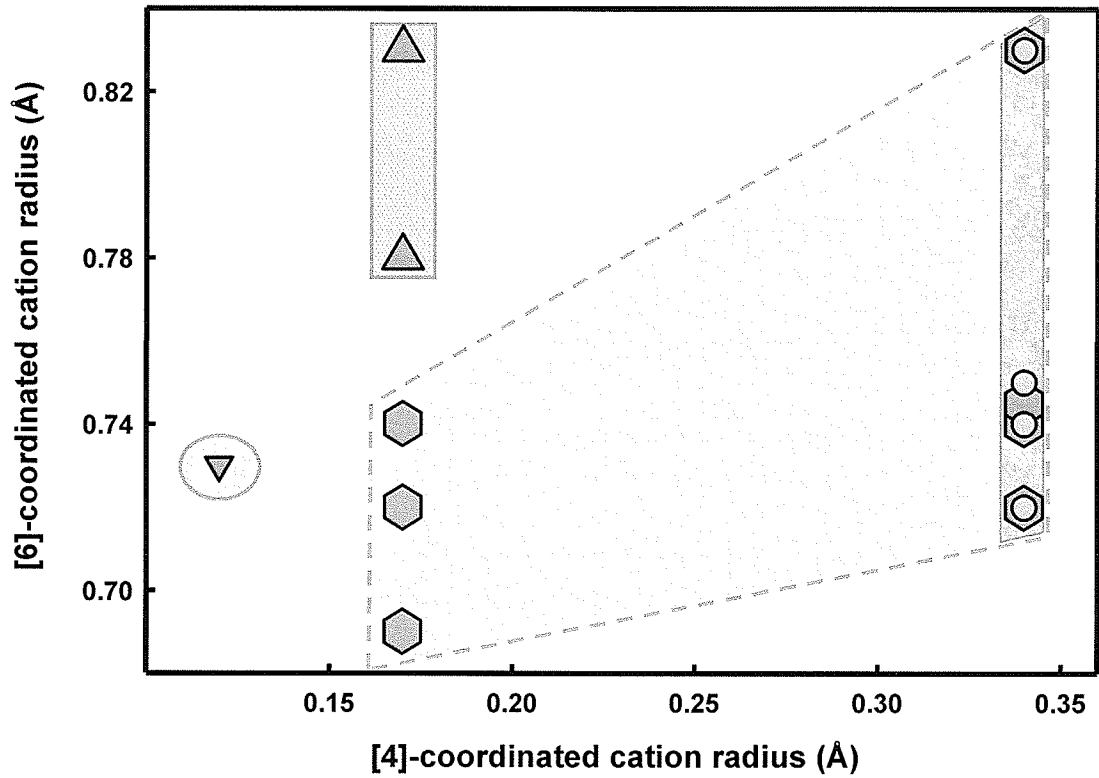
Figure 5.9. Type-II stability diagram for the $Ca_2[M(TO_4)_2(H_2O)_2]$ minerals; the fields of the brandtite-(circles), collinsite- (hexagons) and fairfieldite- (triangles) group structures are shown in blue, pink and purple, respectively.

5.15 Synthetic phases of composition X_2Y $(TO_4)_2$ $(H_2O)_2$

Recently, there has been a considerable amount of work on a wide range of synthetic phases of general composition X_2Y $(TO_4)_2$ $(H_2O)_2$ (Fleck & Kolitsch 2003, Fleck $et\ al.$ 2002a, b, Kolitsch & Fleck 2005, Wildner & Stoilova 2003). In particular, Fleck $et\ al.$ (2002b) introduced a classification of structures based on the [Y $(TO_4)_2$ $(H_2O)_2$] (kröhnkite-type) chain, dividing the over 50 compounds with this structural motif into six different types labeled A to F on the basis of differences concerning their linkage to layers as well as the stacking of the layers. The brandtite, collinsite and fairfieldite groups correspond to the type-D, -A and -B structures, respectively, in this classification.

5.16 Hydrogen bonding in the type-C structure

The type-C structure corresponds to X = K, Y = Mn^{2+}, Cd, T = S, Se (Peytavin $et\ al.$ 1974, Fleck $et\ al.$ 2002a). In this structure type, the space group is $P\underline{1}$, and the cell volume is approximately twice the cell volume of the collinsite and fairfieldite structures, and hence Z = 2. Thus there are two crystallographically distinct (H_2O) groups in the type-C structure, as distinct from one in the brandtite-, collinsite- and fairfieldite-group structures. The hydrogen-bonding arrangement is shown in Figure 5.10, where it is apparent that the two crystallographically distinct (H_2O) groups have different hydrogen-bonding schemes. The hydrogen bonds involving the H(1) and H(2) atoms have both acceptor O(4) anions in the same chain as the donor anion, a feature that does not occur in the brandtite-, collinsite- and fairfieldite structures (cf. Figures 5.1 and 5.10). The hydrogen bonds involving the H(3) and H(4) atoms are different from those in the brandtite-, collinsite- and fairfieldite-structures in that both H(3) and H(4) bond to O(3) anions of different chains (Figure 5. 10).
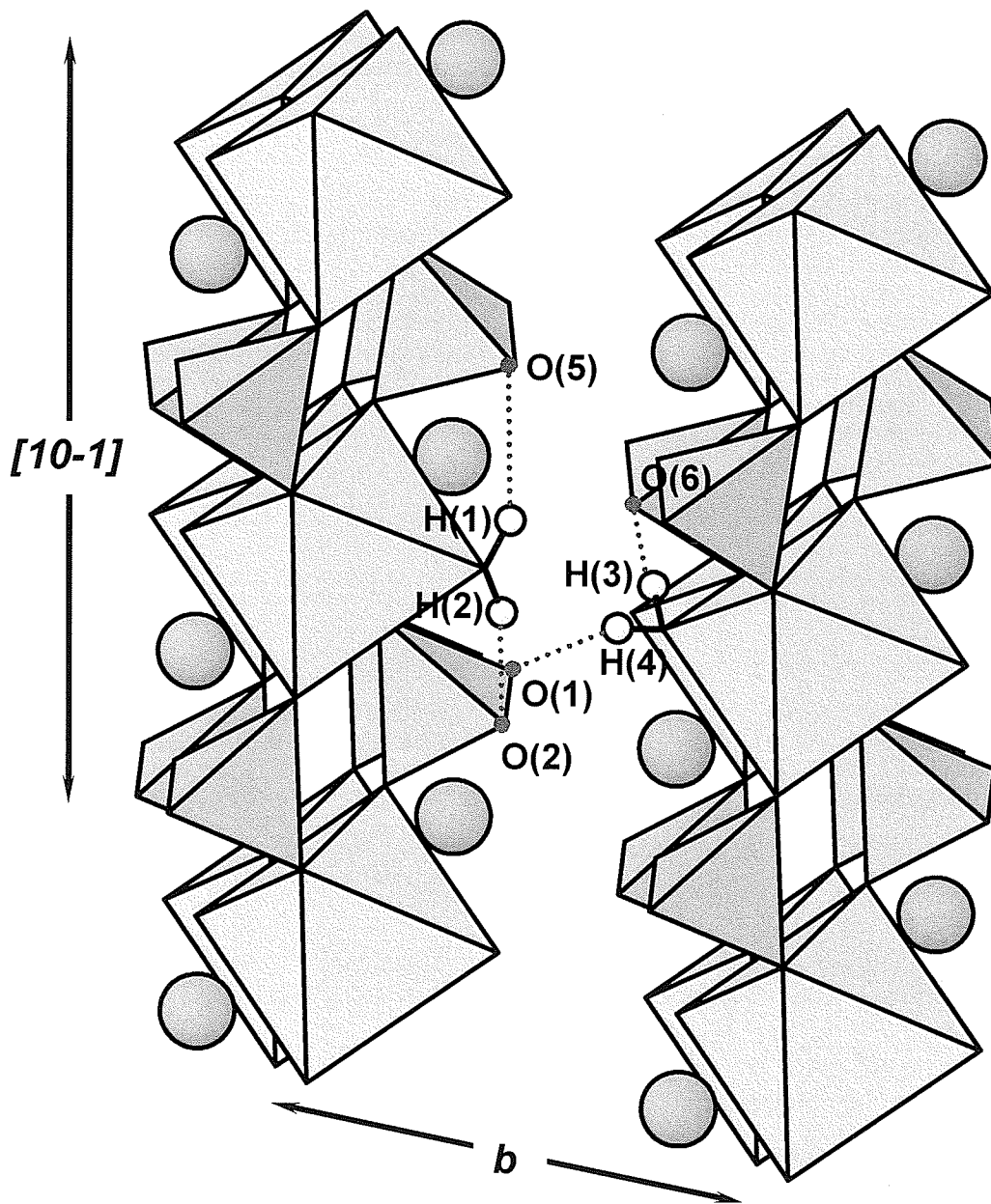
Figure 5.10. The crystal structure of $K_2Mn^{2+}(SO_4)_2(H_2O)_2$, a type-C structure showing the disposition of the hydrogen bonds; legend as in Figure 5.1.

5.17 Symmetrical hydrogen bonding in $K\ Fe^{2+}\ H\ (SO_4)_2\ (H_2O)_2$

Fleck *et al.* (2002a) showed that the H atom not associated with the (H_2O) group in this (type-E) structure forms a symmetrical hydrogen bond (see also Maciek *et al.* 1994). Symmetrical hydrogen bonds are not common. As is usually the case, the reason for the symmetrical hydrogen-bond is found in the details of the bond topology of the structure. To see this, it is instructive to compare the structures of $K\ Fe^{2+}\ H\ (SO_4)_2\ (H_2O)_2$ (a type-E structure, Figure 10.11) and $K_2\ Mn^{2+}\ (SO_4)_2\ (H_2O)_2$ (a type-C structure) in terms of their bond-valence arrangements (Table 5.9). Omitting the H(3) atom, the sum of the bond valence incident at the O(1) site in the type-E structure is 1.50 *vu*. The attitude of adjacent chains is such that O(1) atoms of adjacent chains oppose each other at a distance of 2.47 Å. Each O(1) atom requires an additional 0.50 *vu* to satisfy the valence-sum rule, and with a coordination number of [2], a central H(3) atom satisfies this requirement. However, the potential experienced by a hydrogen atom in this position is of the double-well type, and the H atom usually occupies an off-centre position in accord with this. Where in this off-centre position, the incident bond-valence sums incident at the two coordinating O atoms are ~2.3 and ~1.7 *vu*, respectively, deviating significantly from the valence-sum rule; thus there is a tendency for the H atom to move away from the former O-atom toward the latter O-atom. Where in the alternate arrangement, the bond-valence sums are reversed, ~1.7 and ~2.3 *vu*, respectively, and the H atom moves in the reverse direction. This argument suggests that the central H atom actually hops between the two asymmetric positions, and two centres of electron density are seen on the time-scale of the diffraction experiment. This mechanism is in accord with the results of Fleck *et al*

(2002a), who observed two electron-density maxima between the O(1) atoms at both

room temperature and 110 K.
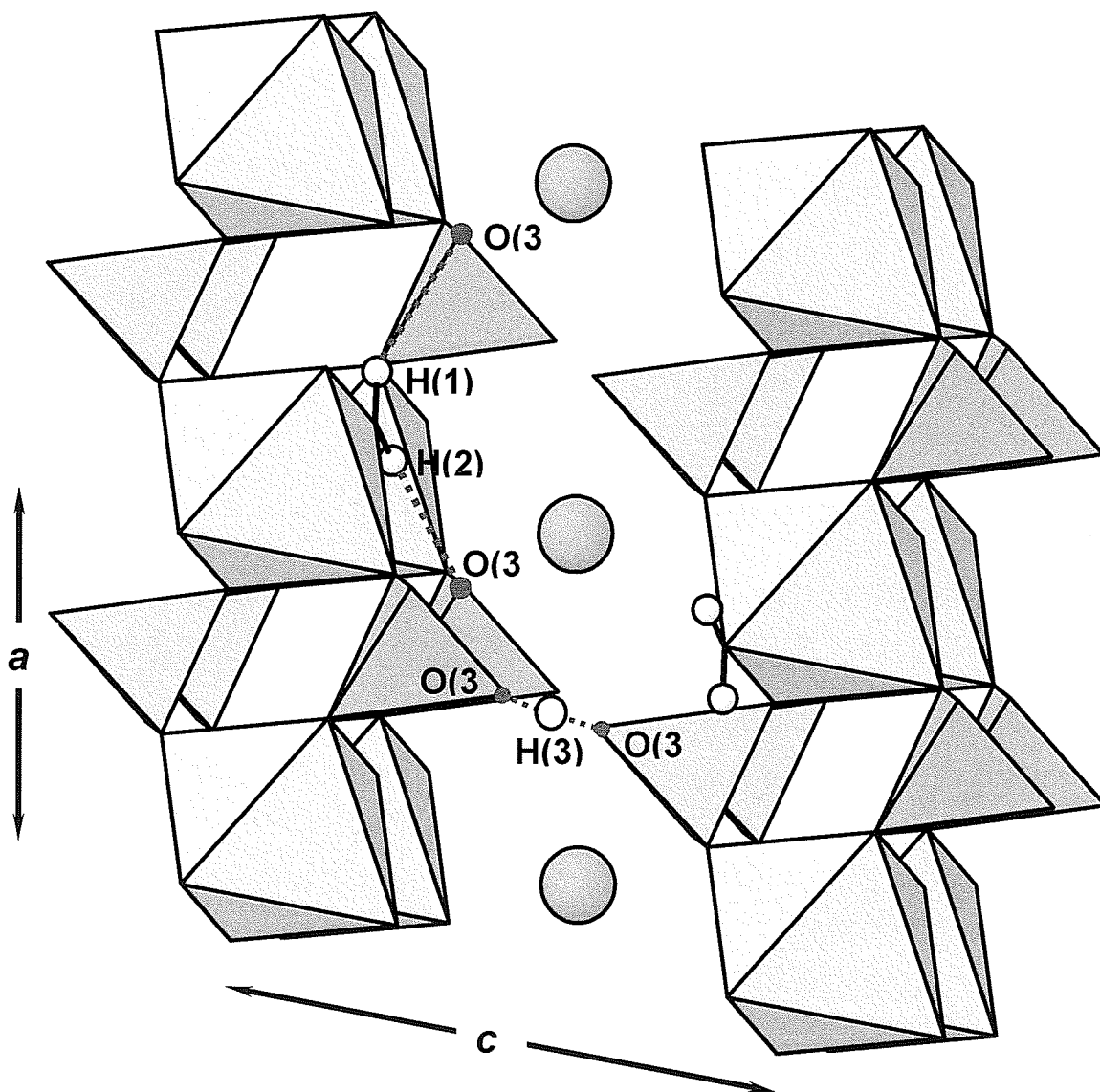
Figure 5.11. The crystal structure of $KFe^{2+}H(SO_4)_2(H_2O)_2$, a type-C structure, projected onto (010); legend as in Fig. 1. Note that the H(3) site is placed at the average of the two half-occupied (symmetry related) positions to emphasize the symmetrical nature of the hydrogen bonding.

Further inspection of the bond-valence table for K Fe^{2+} H (SO$_4$)$_2$ (H$_2$O)$_2$ (Table 5.9) shows incident bond-valence sums of 2.31 and 1.89 *vu* around the O(3) and O(4) anions. Note that according to Table 5.9, the O(3) anion receives hydrogen bonds from both H(1) and H(2), whereas the O(4) anion receives no hydrogen bonds at all. If both O(3) and O(4) each received one hydrogen-bond, the analogous bond-valence sums would be 2.11 and 2.09 *vu*, respectively. The corresponding H(1)- O(4) distance is 2.50Å, and the OW-H(1)...O(4) angle is 120°. The former distance is fairly long for a hydrogen bond, but Brown (1976) has shown that H...O interactions in the range 2.3-3.1 Å are significant (in perchloric-acid hydrates). Moreover, such long H...O distances in perchloric-acid hydrates involve O-H....O angles of 80-120°, in accord with the OW-H(1)...O(4) angle of 120° found here. Thus bond valences suggest a hydrogen-bond arrangement in KFe^{2+}H(SO$_4$)$_2$(H$_2$O)$_2$ different from that currently proposed.

Table 5.9. Bond-valence (*vu*)* tables for type-C and type-E structures.

	K(1)	K(2)	Mn²⁺	S(1)	S(2)	H(1)	H(2)	H(3)	H(4)	Σ
				Type C : K_2 Mn^{2+} $(SO_4)_2$ $(H_2O)_2$						
O(1)	0.10	0.15		1.56					0.20	2.01
O(2)		0.18 0.17		1.50			0.20			2.05
O(3)		0.18	0.36	1.45						1.99
O(4)	0.19	0.15	0.32	1.43						2.09
O(5)	0.12 0.18				1.53	0.20				2.03
O(6)	0.15				1.52			0.20		1.87
O(7)	0.10 0.11		0.32		1.44					1.97
O(8)	0.15	0.14	0.36		1.44					2.09
O(9)	0.14		0.33			0.80	0.80			2.07
O(10)		0.12	0.37					0.80	0.80	2.09
Σ	1.24	1.09	2.06	5.94	5.93	1.0	1.0	1.0	1.0	

Type E: $K2$ Fe^{2+} $H(SO_4)_2$ $(H_2O)_2$

	K	Fe²⁺	S	H(1)	H(2)	Σ	H(3)	Σ
O(1)	0.08x2↓ 0.07x2↓		1.35			1.50	0.50x2↓	2.00
O(2)	0.19x2↓	0.35x2↓	1.52			2.06		
O(3)	0.16x2↓		1.59	0.20	0.20	2.31		
O(4)		0.37x2↓	1.52			1.89		
O(5)	0.05x2↓	0.34x2↓		0.80	0.80	1.89		
Σ	1.10	2.12	5.98	1.00	1.00		1.00	

*O(1) is involved in a very short (symmetrical) hydrogen-bond.

5.2 Chapter 5 summary

Minerals of $X_2 M(TO_4)_2(H_2O)_2$ general composition show three distinct structure-types: the monoclinic kröhnkite group and the triclinic talmessite and fairfieldite groups. In all three groups, the structural units are topologically identical and the differences between the structure types involve the interstitial species, i.e. the arrangement of interstitial hydrogen bonds.

The structures and chemical compositions of three samples, brandtite (belonging to the monoclinic kröhnkite group), collinsite (belonging to the triclinic talmessite group) and fairfieldite were experimentally determined using single-crystal x-ray diffraction and electron-microprobe analysis. The hydrogen bonding arrangements in brandtite, collinsite and fairfieldite were carefully examined, described and compared. They were also compared with the hydrogen bonding arrangements of synthetic phases of the same stoichiometry. Additionally, theoretically possible alternative hydrogen bond arrangements were developed.

In the kröhnkite, talmessite and fairfieldite groups, the interstitial hydrogen bonding arrangements introduce flexibility in the way that topologically identical structural units can link together, arising in different structure types. In fact, it introduces such great flexibility that alternative hydrogen bonding arrangements are possible, whether or not they occur in nature.

THE EFFECT OF HYDROGEN ON THE STRUCTURE TOPOLOGY OF THE MAGNESIUM SULPHATES AND MINERALS WITH THE GENERAL FORMULA $M^{2+}(T^{6+}O)_4(H_2O)_n$ (n=0-7) and $M^{3+}(T^{5+}O)_4(H_2O)_n$ (n=0-3)

6.1 Introduction

The dominant members of the $MgSO_4(H_2O)_n$ series on Earth are epsomite

$MgSO_4(H_2O)_7$, hexahydrite $MgSO_4(H_2O)_6$, and kieserite $MgSO_4(H_2O)$; they occur as

important constituents of marine evaporite deposits and precipitates in saline lakes. In

addition, sanderite $MgSO_4(H_2O)_2$, starkeyite $MgSO_4(H_2O)_4$, and pentahydrite

$MgSO_4(H_2O)_5$ have been identified as efflorescent salts in a few localities in the United

States, Chile, and Germany. All of these minerals, with the exception of starkeyite have

been previously structurally and chemically characterized.

Minerals of the $MgSO_4(H_2O)_n$ series can accommodate increasing amounts of

H_2O (up to 50 wt%) by altering their crystal structures. Recently, there have been several

experimental studies aimed at the characterization of dehydration-hydration reactions

within the $MgSO_4(H_2O)_n$ series and determining stability relations between various

phases in the series. This chapter will review some of the recent research, and explore

two main themes (1) a structural / crystal-chemical explanation for observed dehydration-

hydration reactions, and (2) possible explanations for the absence of structures of

$MgSO_4(H_2O)_n$ (n=2,3) stoichiometry.

6.2 Previous work

Balarew et al., (2001) investigated experimentally and modeled

thermodynamically (according to the Pitzer method) the system $MgCl_2$-$MgSO_4$-H_2O at

50 and 75° C. At 50° C, they established the presence of four stable crystallization fields:

bischofite $MgCl_2(H_2O)_6$, hexahydrite $MgSO_4(H_2O)_6$, starkeyite $MgSO_4(H_2O)_4$, and kieserite $MgSO_4(H_2O)$, and also three metastable fields within the fields of the stable ones: starkeyite in kieserite, hexahydrite in starkeyite, and epsomite in hexahydrite (Figure 6.1). At 75° C, there is a wide field of stable kieserite and fields of metastable hexahydrite and starkeyite (Figure 6.2).

Both diagrams show that crystallization of metastable higher hydrates is possible in each crystallization field and can probably not be avoided. The authors also show that the time necessary to attain stable equilibrium increases with decreasing water content of the hydrate: in the field of crystallization of epsomite, 1–2 h; of hexahydrite, 2–5 h; of starkeyite, 2–5 days; and most slowly for kieserite, 7–20 days. The equilibration times of starkeyite and kieserite are subject to large variations depending on the absence or existence of metastable crystallization.
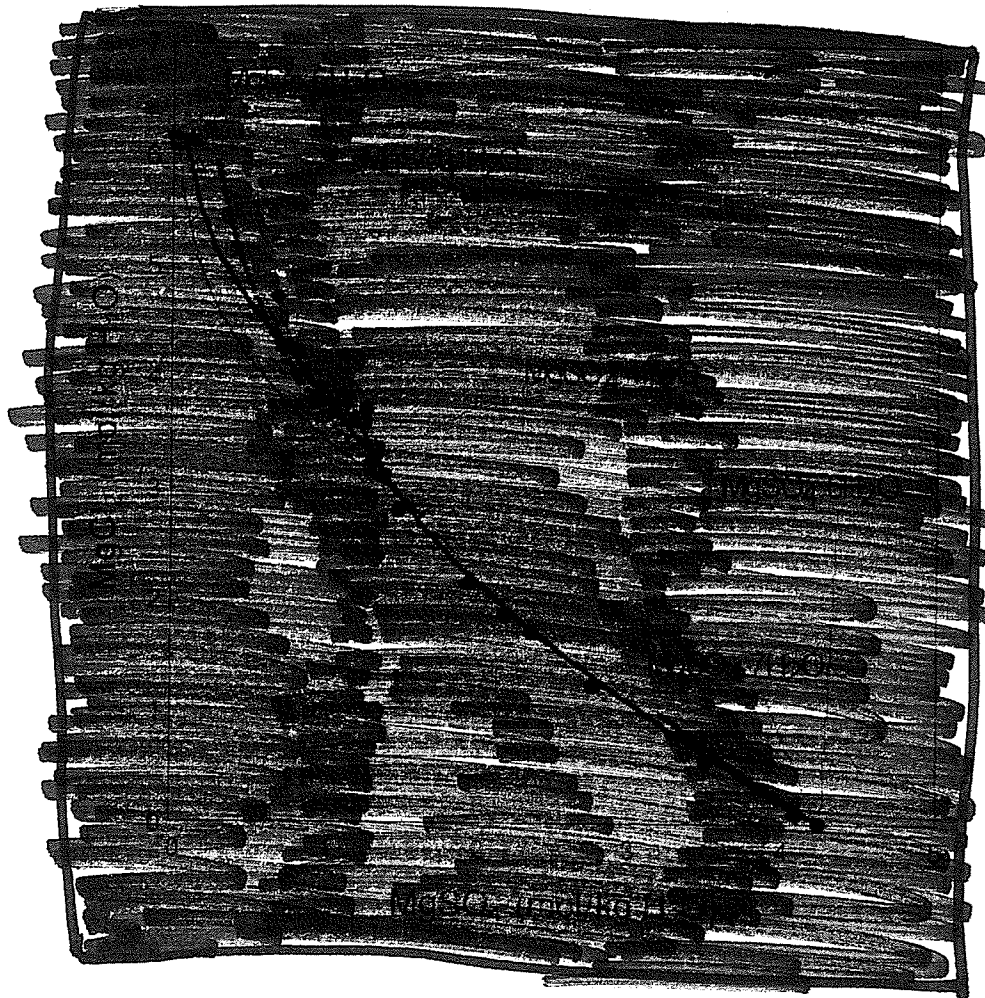
Figure 6.1. Solubilities in the system $MgCl_2$-$MgSO_4$-H_2O system at 50° C. Experimental data of the authors' work: $MgCl_2(H_2O)_6$ (★); $MgSO_4(H_2O)_7$ (□); $MgSO_4(H_2O)_6$ (●); $MgSO_4(H_2O)_4$ (♦); $MgSO_4(H_2O)$ (Δ). Calculated solubilities with parameters of this work (——). Calculated solubilities of various phases with parameters of Voigt & Voigt (1998), other lines. After Balarew et al., 2001.

Balarew, Chr., Tepavitcharova, S., Rabadjieva, D., Voigt, W. (2001) Solubility and crystallization in the system $MgCl_2$-$MgSO_4$-H_2O at 50 and 75° C. *Journal of Solution Chemistry*, **30**(9): 815-823.
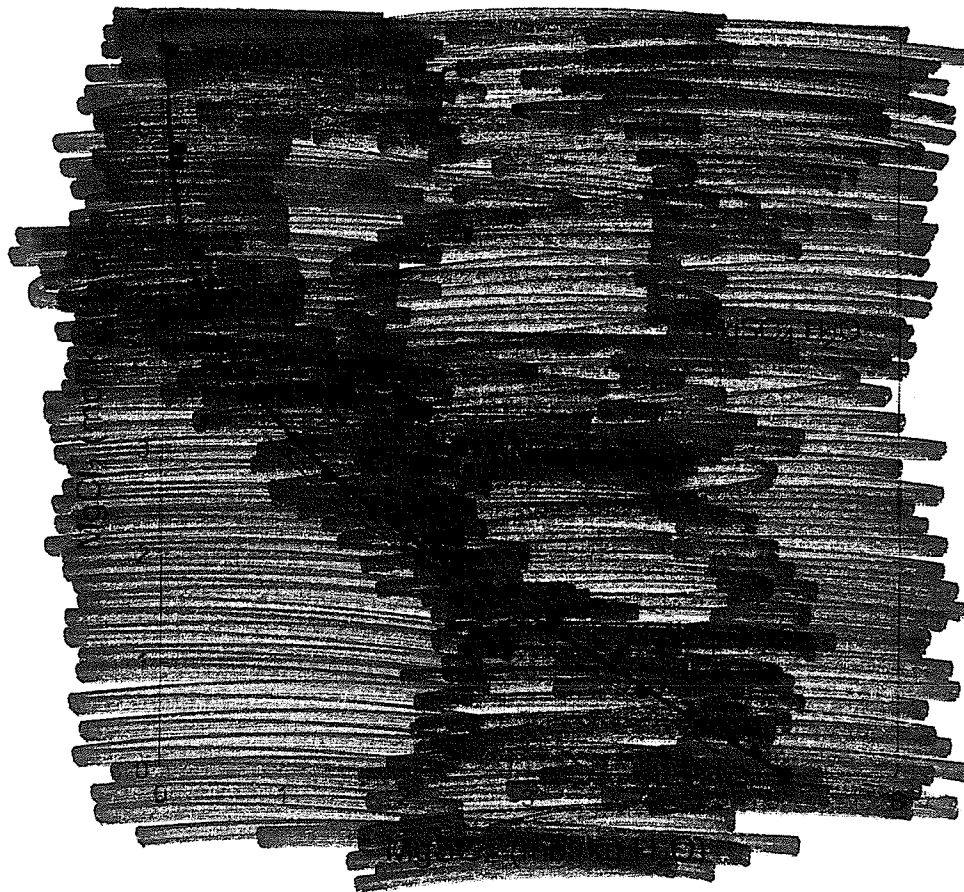
Figure 6.2. Solubilities in the system $MgCl_2$-$MgSO_4$-H_2O system at 75° C. Experimental data of the authors' work (stable phase): $MgCl_2(H_2O)_6$ (★); $MgSO_4(H_2O)$ (●). Experimental data of authors' work (metastable phase): $MgSO_4(H_2O)_6$ (▲); $MgSO_4(H_2O)_4$ (■). Calculated solubilities of various phases with parameters of this work: all lines except narrow solid line, calculated with parameters of Voigt & Voigt (1998). After Balarew et al., 2001.

Balarew, Chr., Tepavitcharova, S., Rabadjieva, D., Voigt, W. (2001) Solubility and crystallization in the system $MgCl_2$-$MgSO_4$-H_2O at 50 and 75° C. *Journal of Solution Chemistry,* **30**(9): 815-823.

60

Chou & Seal (2003) experimentally determined epsomite-hexahydrite equilibria by humidity buffer technique, and extrapolated phase equilibrium data for other relevant reactions (hexahydrite-kieserite) in the $MgSO_4$-H_2O system. The results of their work are shown in Figure 6.3. From this diagram it is apparent that phase relations between solution, epsomite, hexahydrite and kieserite are strongly influenced by temperature and relative humidity.

Chou, I.M. & Seal, R.R.II. (2003) Evaporites, water, and life, Part 1: Determination of epsomite-hexahydrite equilibria by the humidity-buffer technique at 0.1 MPa with implications for phase equilibria in the system $MgSO_4$-H_2O. *Astrobiology*, 3(3): 619-630.
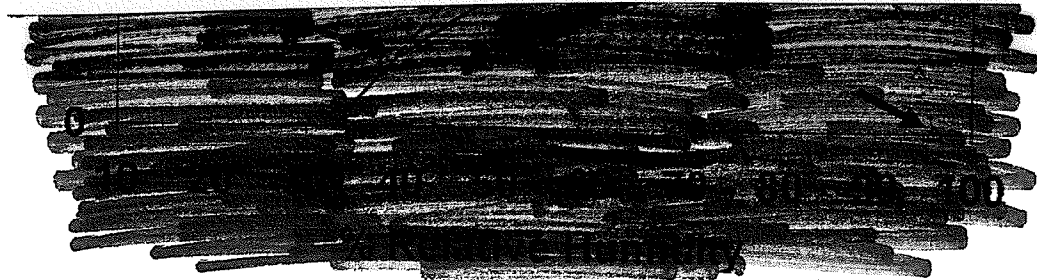
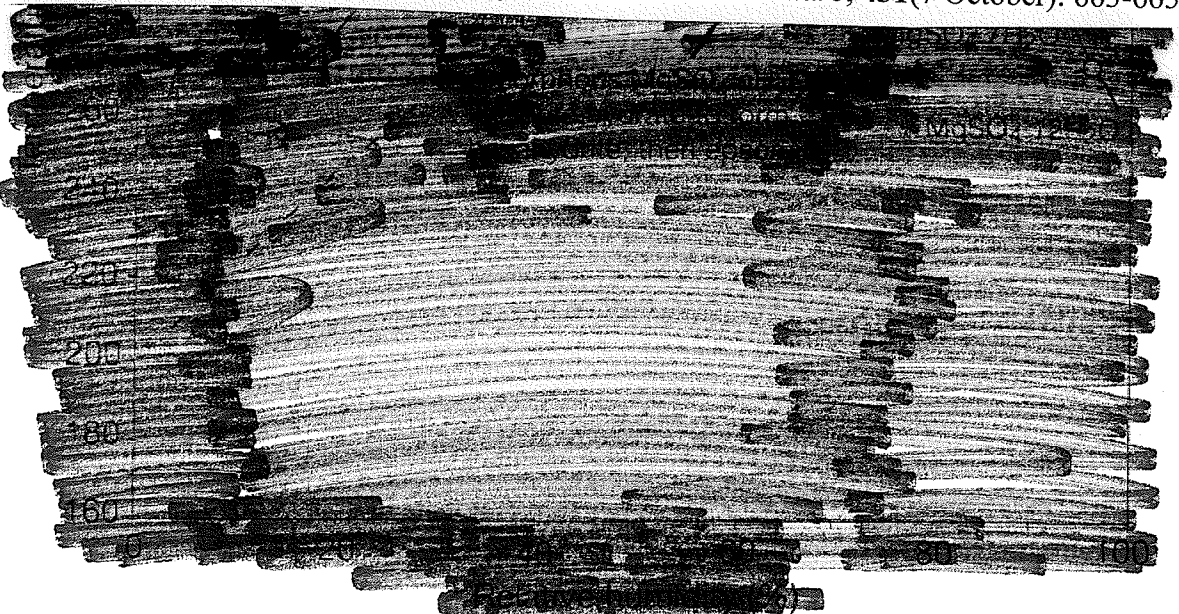**Figure 6.3.** Temperature-RH relations in the system $MgSO_4$-H_2O at 0.1 MPa. The epsomite-hexahydrite curve (solid line) and the saturated aqueous solution curve (dotted line connecting triangles) is from their study. The red arrow indicates the invariant point for the assemblage epsomite+hexahydrite+kieserite+vapour at 11° C and RH of 39% that limits the lower stability of hexahydrite. The blue arrow indicates the invariant point for the assemblage epsomite+$MgSO_4(H_2O)_{12}$ +vapour at 0.6° C and RH of 96% (from Hogenboom et al.1995 as cited in Chou &Seal 2003). Modified from Chou & Seal (2003).

Vaniman et.al. (2004) and Chipera et al. (2005) have experimentally determined the stability and transformation kinetics of various magnesium sulphate hydrates. Vaniman et al. (2004) observed that when crystals of epsomite are exposed to low humidity environments, they dehydrate and transform into hexahydrite and then into amorphous magnesium sulphate hydrate, but not kieserite. However, when the amorphous magnesium sulphate hydrate was exposed to high humidity environments, it rehydrates into hexahydrite followed by epsomite, without passing through kieserite.Kieserite crystals resisted dehydration when exposed to low humidity environments, and easily rehydrated to hexahydrite and epsomite when exposed to high humidity environments (which again, became amorphous when exposed to low humidities). Figure 6.4 shows Vaniman et al (2004) results superimposed on Chou & Seal's (2003) T-RH diagram.
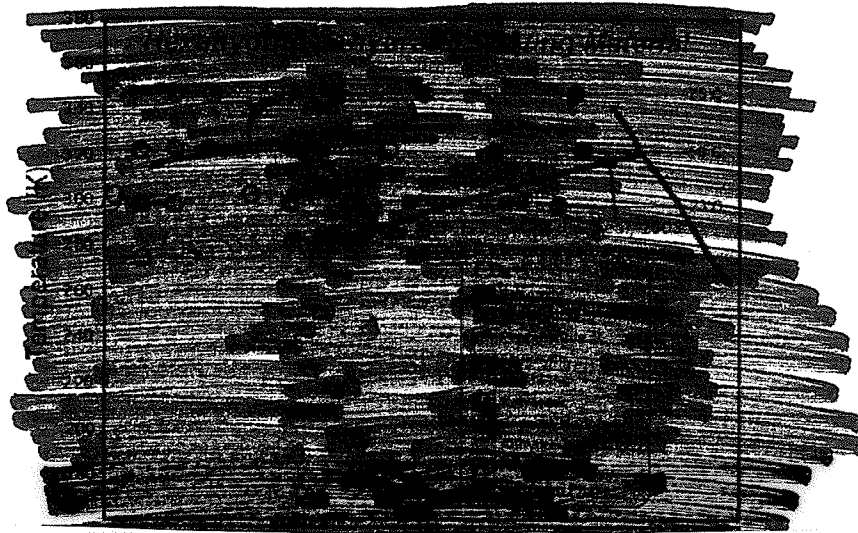
Vaniman, D.T., Bish, D.L., Chipera, S.J., Fialips, C.I., Carey, J.W., Feldman, W.C. (2004) Magnesium sulfate salts and the history of water on Mars. *Nature*, **431**(7 October): 663-665.

Figure 6.4. Results of controlled-humidity XRD experiments at 298 K plotted against stability fields for epsomite, hexahydrite and kieserite, modified from Chou & Seal (2003). Their study provides accurate constraints on the epsomite to hexahydrite transition (curve 1); their estimate of the hexahydrite to kieserite transition (curve 2) is based on thermodynamic data extrapolated from the experimentally determined solution equilibrium; an alternative estimate of this transition is based solely on thermodynamic data (curve 3). Stability of the $MgSO_4(H_2O)_{12}$ phase is poorly constrained. Their experiments show that at RH of approx. 0.5%, hexahydrite forms from solution but becomes amorphous. Hexahydrite forms and persists at RH values from approx. 55% down to at least 7%. Amorphous $MgSO_4(H_2O)_n$ formed at RH of approx. 0 5% and subsequently exposed to RH of 7-55% crystallizes to various hydrates (n = 1.25 to 6) dependent on RH; ongoing long term experiments suggest that crystalline end-products vary with RH within the upper shaded region. Above RH of approx. 55%, both amorphous $MgSO_4 (H_2O)_n$ and kieserite transform to hexahydrite and then epsomite. Modified from Vaniman et al. (2004).

63

Chipera, et al. (2005) extended the work of Vaniman et al. (2004) to include starkeyite, as it was determined to have a pronounced stability field between hexahydrite and kieserite. In the stability field of hexahydrite, starkeyite was produced by decreasing relative humidity or increasing temperature; further increases of temperature resulted in the formation of kieserite. With starkeyite as a starting product, increased temperatures caused dehydration to form kieserite. The reverse process, with kieserite as a starting material did not form starkeyite but only formed hexahydrite when the relative humidity and temperature conditions were changed to within the hexahydrite stability region. They also found that when starkeyite was exposed to low humidity environments, even for a significant length of time (<0.4% RH, 9 days), it did not transform to the amorphous magnesium sulphate hydrate phase (observed in hexahydrite dehydration by Vaniman et al., 2004). Figure 6.5 shows the controlled humidity results using reagent hexahydrite, synthetic starkeyite, and synthetic kieserite as starting materials at various RH and temperatures with the Chou & Seal (2003) experimental epsomite-hexadrite data superimposed. Sanderite formed in several experiments (Figure 6.5, yellow filled circles) and the authors state that its stability, if thermodynamically stable, appears to be rather limited. They were only able to form pentahydrite as a metastable phase during rehydration of amorphous magnesium sulphate hydrate. In no experiment have the authors ever observed the appearance of a tri-hydrate, $MgSO_4(H_2O)_3$ (Vaniman, D.T., personal communication). A graphical summary of the results of Vaniman et al., 2004 and Chipera et al., 2005 is presented in Figure 6.6.
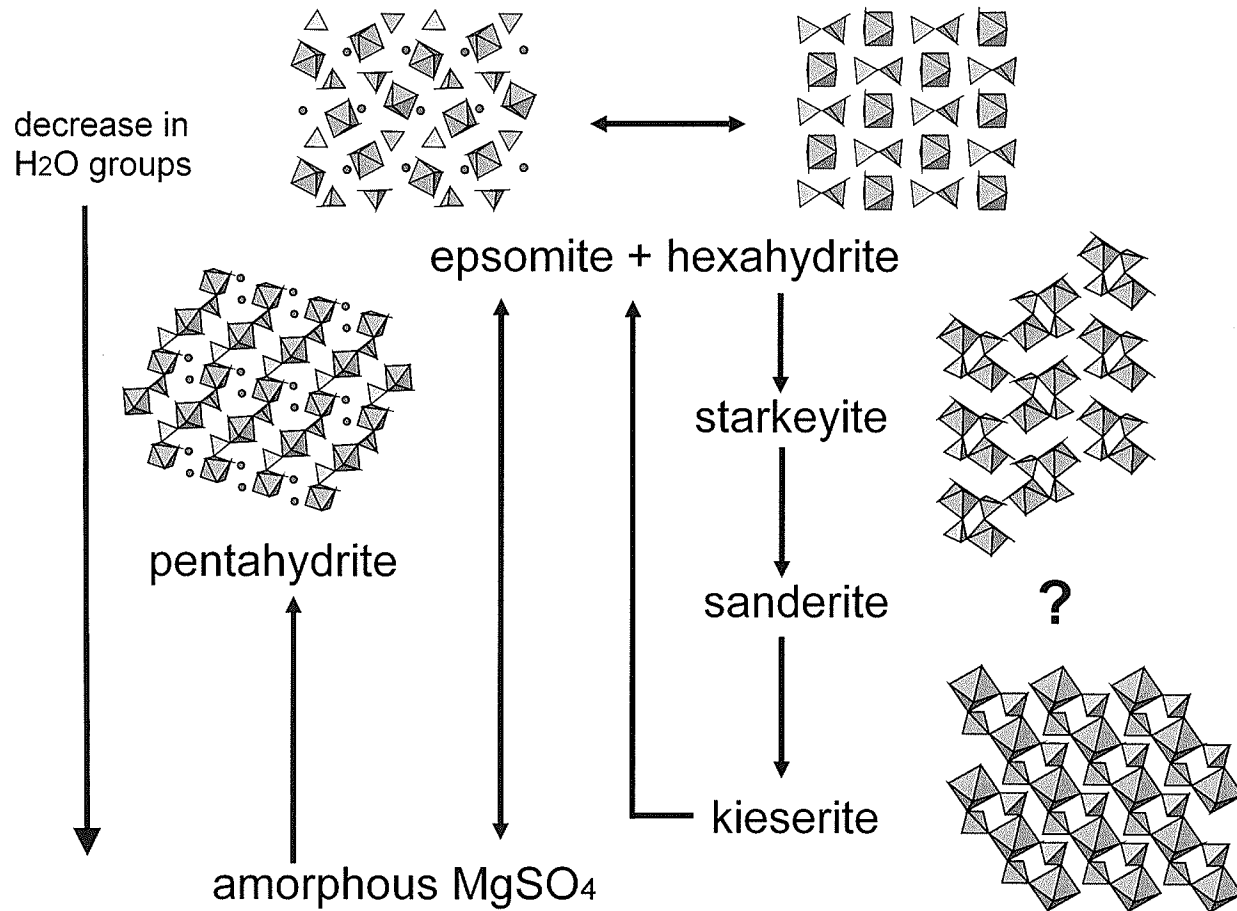
Chipera, S. J., Vaniman, D.T., Bish, D.L., Carey, J.W., Feldman, W.C. (2005) Experimental stability and transformation kinetics of magnesium sulfate hydrates that may be present on Mars. Lunar and Planetary Science Conference, **XXXVI**, March 2005, Abstract number 1497.

Figure 6.5. Experimental results at various %RH and temperatures for hexahydrite, starkeyite, and kieserite starting materials. Modified from Chipera, et al., 2005.

Graphical summary of experimental results of Vaniman et al. (2004) and Chipera et al. (2005)

decrease in H₂O groups

epsomite + hexahydrite

pentahydrite

starkeyite

sanderite

?

amorphous MgSO₄

kieserite

Figure 6.6. Graphical summary of experimental results of Vaniman et al., 2004 and Chipera et al, 2005. All clusters shown are stable; pentahydrite forms only from amorphous magnesium sulphate.

6.3 $MgSO_4(H_2O)_n$ (n=0,1, 4,5,6,7) STRUCTURES

The following discussion requires a very brief description of the crystal structures of the $MgSO_4(H_2O)_n$ (n=0,1, 4,5,6,7) minerals; the minerals and their relevant information are listed in Table 6.1.

6.3.1 *Anhydrous magnesium sulphate, MgSO₄*

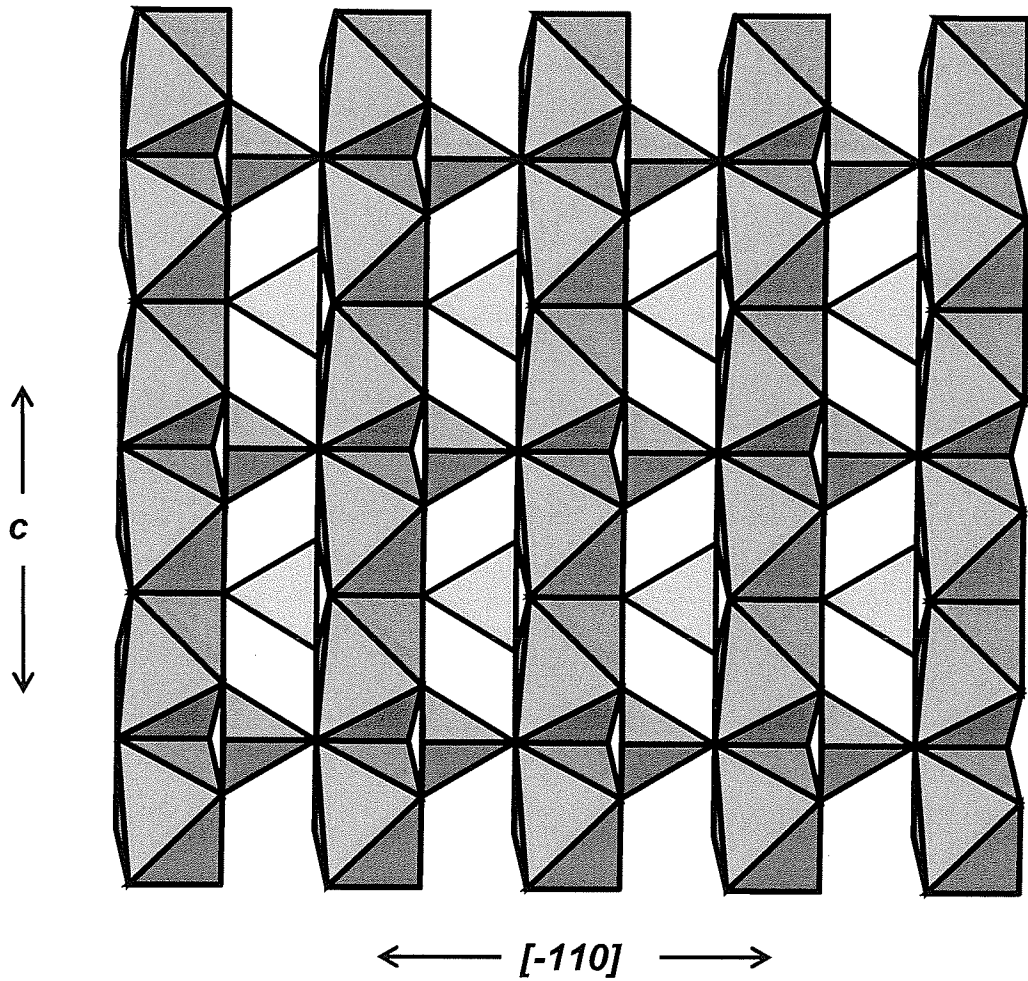The crystal structure of magnesium sulphate consists of MgO_6 octahedra that share edges to form octahedral "ribbons" parallel to c ; the octahedra are linked through their remaining two vertices by sulphate tetrahedra into a three-dimensional framework (Figures 6.7 and 6.8).

Table 6.1. Minerals of the $MgSO_4(H_2O)_n$ group.

| Mineral	Formula	Space group	Structure mode	$a(\text{Å})$	$b(\text{Å})$	$c(\text{Å})$	$\alpha(°)$	$\beta(°)$	$\gamma(°)$	Ref.
Magnesium sulfate	$MgSO_4$	Ortho. Cmcm	Frame-work	5.182(15)	7.893(2)	6.506(16)	-	-	-	1
Kieserite	$MgSO_4(H_2O)$	Mono. C2/c	Frame-work	6.891(2)	7.624(2)	7.645(2)	-	117.7(2)	-	2
Sanderite	$MgSO_4(H_2O)_2$	Mono.?	?	?	?	?	-	?	-	3
Starkeyite	$MgSO_4(H_2O)_4$	Mono. P2$_1$/n	Finite clusters	5.922(6)	13.604(4)	7.905(5)	-	90.85(17)	-	4
Pentahydrite	$MgSO_4(H_2O)_4(H_2O)$	Tric. P-1	Chains oct/tet	6.314(5)	10.565(18)	6.030(6)	81.12(20)	109.82(20)	105.108(5)	5
Hexahydrite	$MgSO_4(H_2O)_6$	Mono. C2/c	Isolated oct/tet	10.110(5)	7.212(4)	24.410(10)	-	98.30(5)	-	6
Epsomite	$MgSO_4(H_2O)_6(H_2O)$	Ortho. P2$_1$2$_1$2$_1$	Isolated oct/tet	11.887(2)	12.013(2)	6.861(1)	-	-	-	7
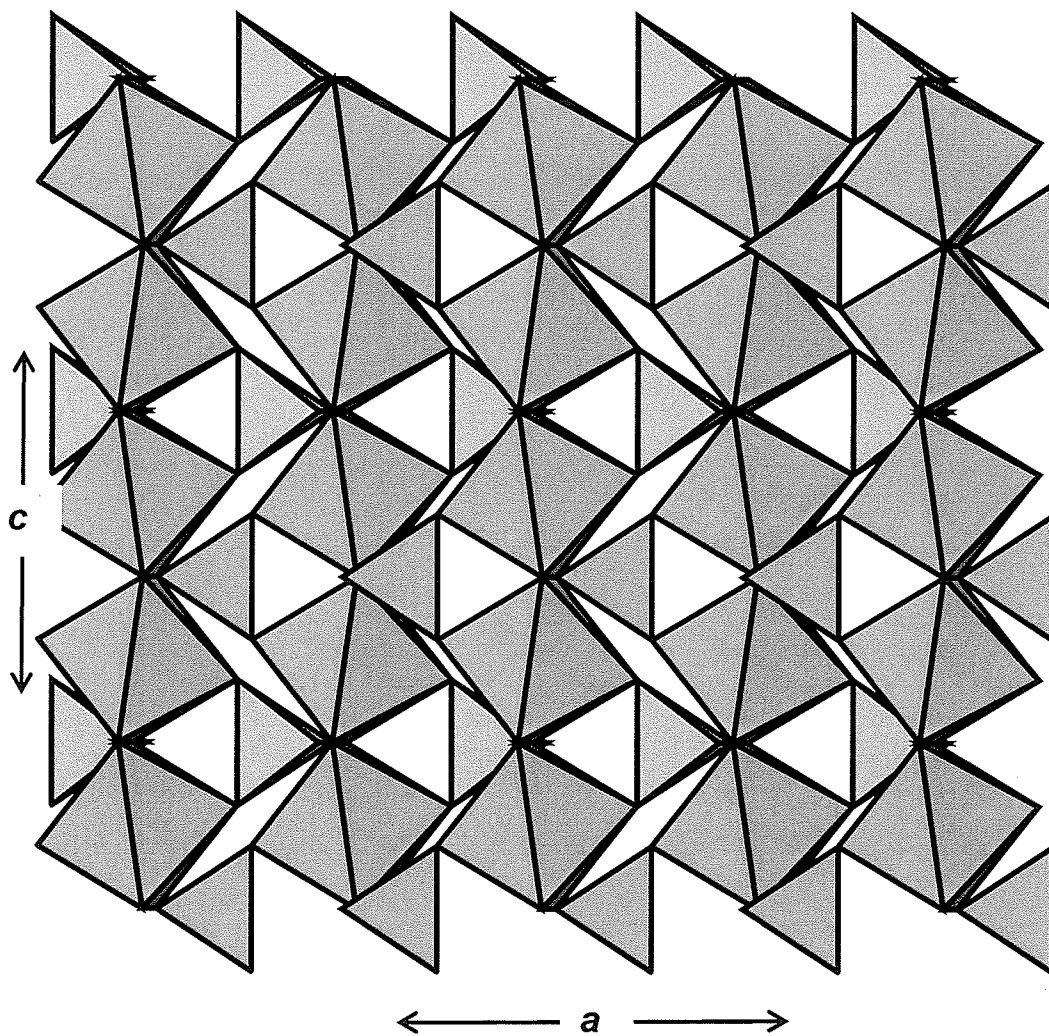
Figure 6.7. The crystal structure of magnesium sulphate, MgSO$_4$; magnesium octahedra are blue, and sulphur tetrahedra are pink.

Figure 6.8. The crystal structure of magnesium sulphate, $Mg(SO_4)$; magnesium octahedra are blue and sulphur tetrahedra are pink.

6.3.2. Kieserite, Mg(SO₄)(H₂O)

The crystal structure of kieserite consists of corner-sharing octahedral chains

parallel to c, that are linked along their length and also parallel to [110] by sulfate

tetrahedra, to form a three-dimensional framework (Figure 6.9). The oxygen "bridges"

along the length of octahedral chain are involved in (H_2O) groups.
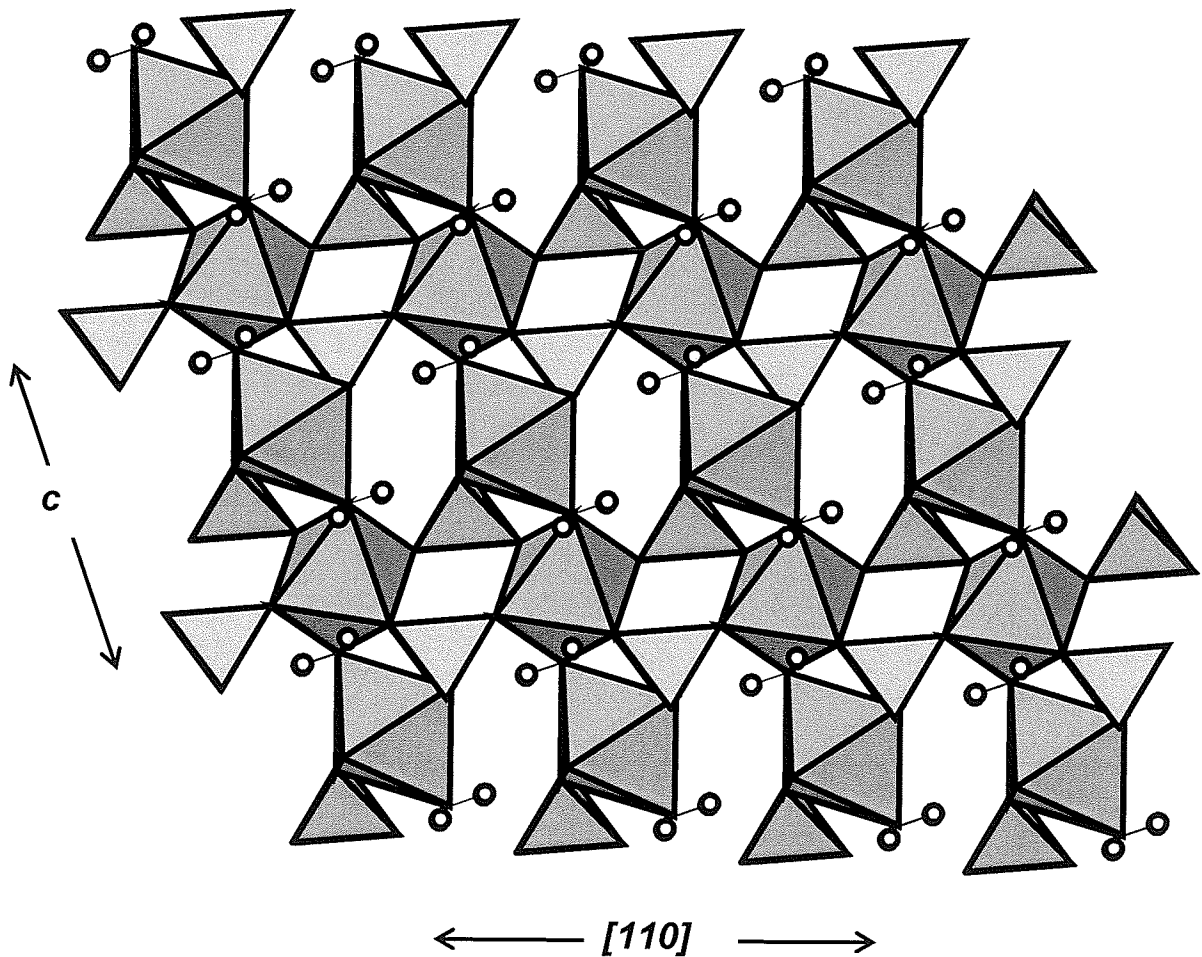
Figure 6.9. The crystal structure of kieserite, Mg(SO₄)(H₂O); magnesium octahedra are blue, sulphur tetrahedra are pink and hydrogen is white. Hydrogen bonds omitted for clarity.

71

6.3.3 Starkeyite, $Mg(SO_4)(H_2O)_4$

The crystal structure of starkeyite consists of $Mg_2(H_2O)_8(SO_4)_2$ clusters (two magnesium octahedra linked via corner-sharing with two sulphate tetrahedra) that are linked only by hydrogen bonds (Figure 6.10).
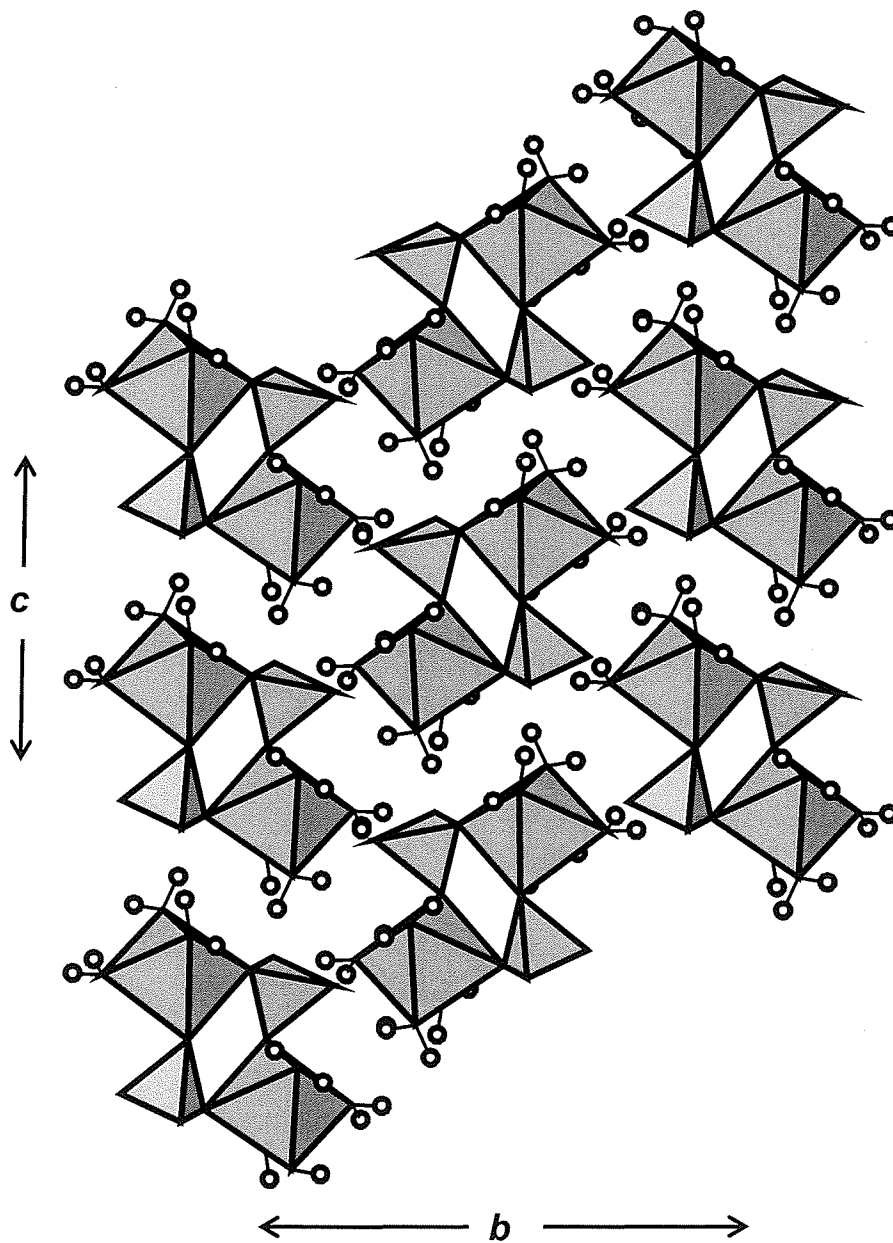
Figure 6.10. The crystal structure of starkeyite, $Mg(SO_4)(H_2O)_4$; magnesium octahedra are blue, sulphur tetrahedra are pink and hydrogen is white. Hydrogen bonds omitted for clarity.

6.3.4 Pentahydrite, Mg(SO₄)(H₂O)₅

The crystal structure of pentahydrite consists of $Mg(H_2O)_4(SO_4)$ chains composed of alternating magnesium octahedra and sulfate tetrahedra (Figure 6.11). The chains extend along [110] and are cross-linked by hydrogen bonds between the terminal octahedral H_2O groups and the sulfate tetrahedra. There is also an interstitial H_2O group that accepts and donates hydrogen bonds, further linking the structure.
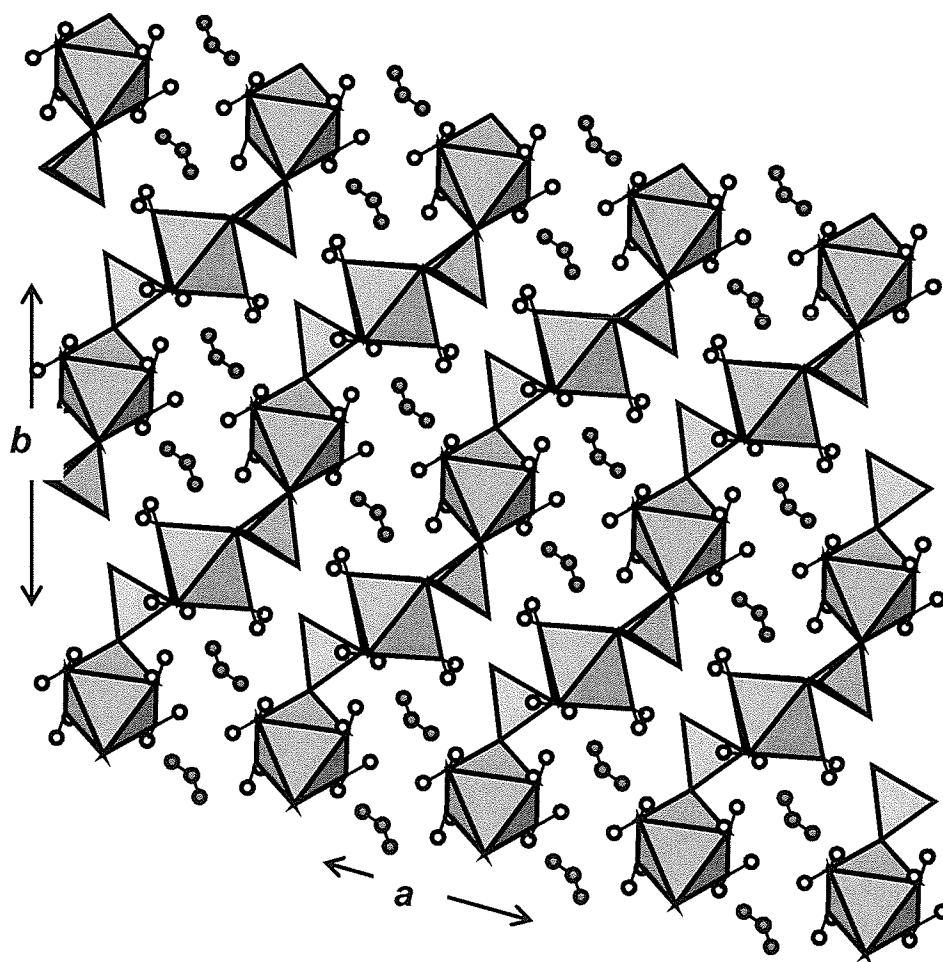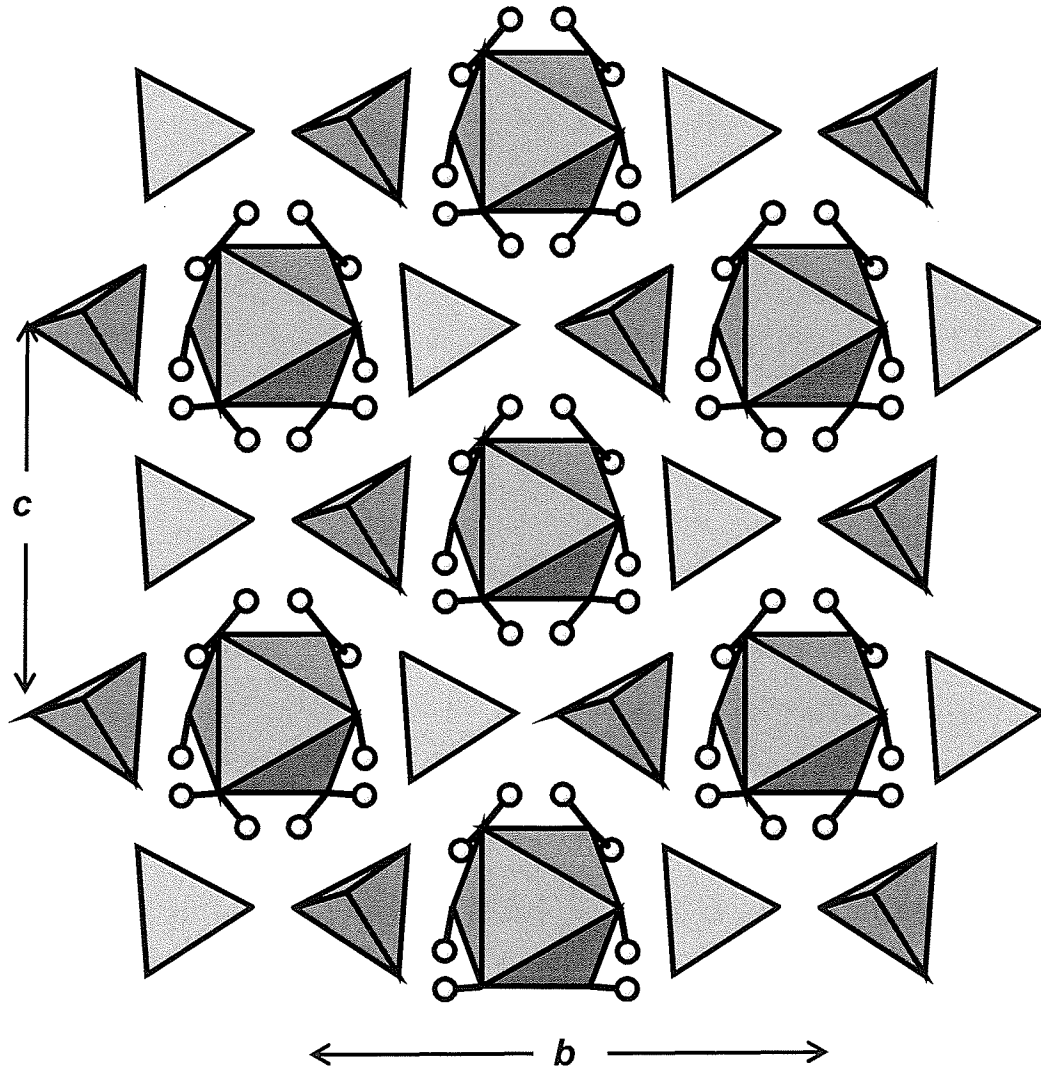

Figure 6.11. The crystal structure of pentahydrate, $Mg(SO_4)(H_2O)_5$; magnesium octahedra are blue, sulphur tetrahedra are pink, terminal H_2O groups are white and interstitial H_2O groups are dark blue. Hydrogen bonds omitted for clarity.

6.3.5 Hexahydrite, Mg(SO₄)(H₂O)₆

The crystal structure of hexahydrite consists of isolated $Mg(H_2O)_6$ octahedra

linked only by hydrogen bonds to isolated sulphate tetrahedra (Figure 6.12).

Figure 6.12. The crystal structure of hexahydrite, $Mg(SO_4)(H_2O)_6$; magnesium octahedra are blue, sulphur tetrahedra are pink and hydrogen is white. Hydrogen bonds omitted for clarity.

6.3.6 Epsomite, Mg(SO₄)(H₂O)₇

The crystal structure of epsomite consists of isolated $Mg(H_2O)_6$ octahedra, that are, like hexahydrite, linked to isolated sulphate tetrahedra by hydrogen bonds; in addition to the H_2O required to fully hydrate magnesium, there is an interstitial H_2O group that accepts and donates hydrogen bonds, further linking the structure (Figure 6.13).
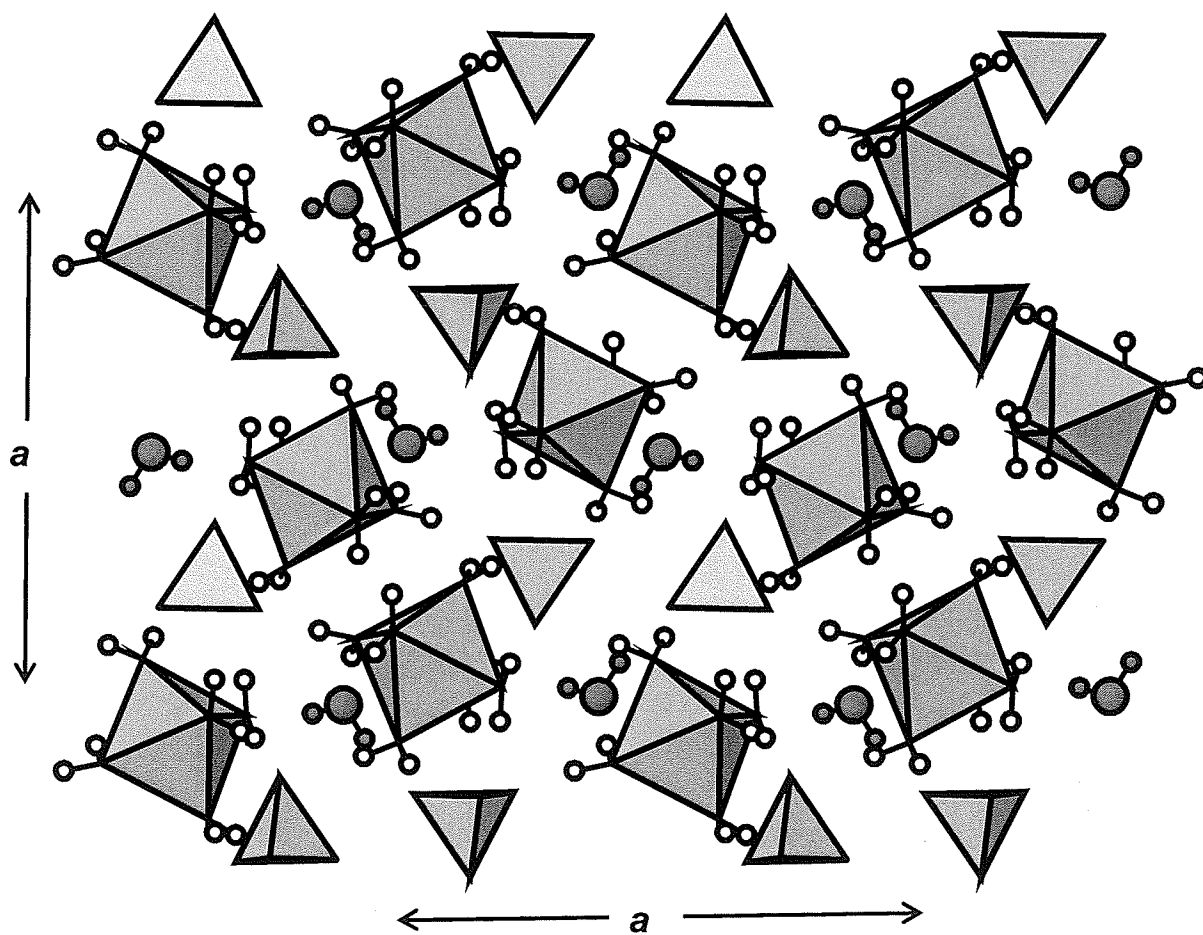
Figure 6.13. The crystal structure of epsomite, $Mg(SO_4)(H_2O)_7$; magnesium octahedra are blue, sulphur tetrahedra are pink, terminal H_2O groups are white and interstitial H_2O goups are dark blue. Hydrogen bonds omitted for clarity.

6.4 Other structures of interest

Since the structures of sanderite $MgSO_4(H_2O)_2$ and $MgSO_4(H_2O)_3$ are not known, it is instructive to examine other minerals or compounds of $M^{2+}(TO_4)(H_2O)_{2 \text{ and } 3}$ stoichiometry. Although these minerals and compounds do not form in natural evaporitic environments, their crystal structures can provide some insight into what the structures of the the di- and tri- hydrates might be, and why they do not (generally) occur. These minerals and compounds include magnesium tungstate dihydrate $Mg(WO_4)(H_2O)_2$, bonattite $Cu^{2+}(SO_4)(H_2O)_3$, chromium(II) sulphate trihydrate $Cr^{2+}(SO_4(H_2O)_3$ and bobjonesite $VO(SO_4)(H_2O)_3$; their relevant details are listed in Table 6.2.
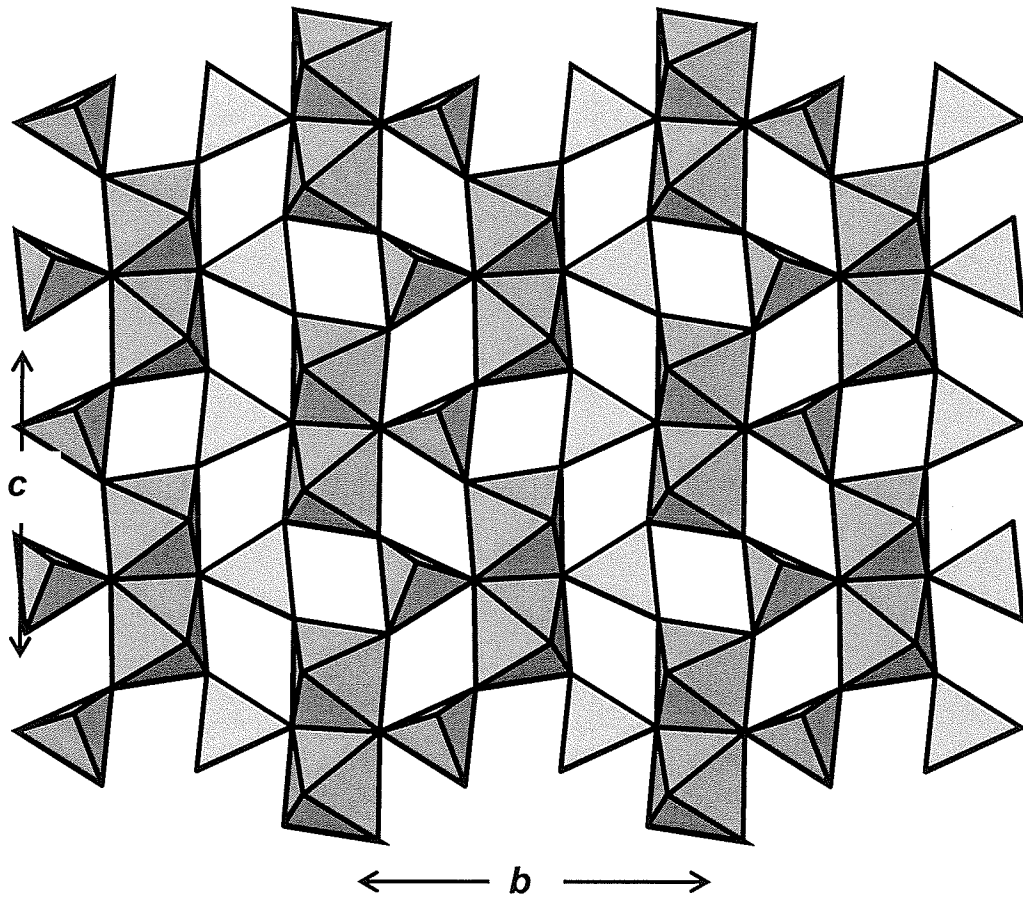
6.4.1 Magnesium tungstate dihydrate, Mg(WO₄)(H₂O)₂

The crystal structure of magnesium tungstate dihydrate consists of $Mg_2O_6(H_2O)_4$ edge-sharing dimers linked into "corrugated" sheets by WO_4 groups. The sheet is shown in Figure 6.14, and also end-on in Figure 6.15. The H_2O groups are not shown because hydrogen positions in this structure were not determined experimentally.

Bond-valences were calculated for the magnesium tungstate dihydrate structure (Table 6.11). Inspection of the table shows that the two hydrogens of each H_2O group bond to an oxygen that is itself bonded only to one magnesium, bringing the sum of incident bond-valence at the oxygen close to the ideal value of 2. Visual inspection of Figures 6.14 and 6.15 show that these oxygens are the terminal oxygens of the Mg octahedra thus the H_2O groups will project out into the interstitial space between the sheets; additional structural linkage will be provided by hydrogen bonds to the one oxygen of the WO_4 group that does not bond to anything else.

76

Table 6.2. Minerals and compounds of $M(TO_4)(H_2O)_n$ (n=2,3) stoichiometry.

| Mineral/ compound	Formula	Space group	Structure mode	a(Å)	b(Å)	c(Å)	α(°)	β(°)	γ(°)	Ref.
Magnesium tungstate dihydrate	$MgWO_4(H_2O)_2$	Mono. $P2_1/c$	Infinite sheets	5.917(1)	10.243(2)	8.566(1)	-	90.05(2)	-	8
Bonattite	$CuSO_4(H_2O)_3$	Mono. Cc	Framework	5.592(5)	13.029(10)	7.341(6)	-	97.05(12)	-	9
Chromium(II) sulphate trihydrate	$Cr^{2+}SO_4(H_2O)_3$	Mono. Cc	Framework	5.7056(8)	13.211(2)	7.485(1)	-	96.73(1)	-	10
Bobjonesite	$VOSO_4(H_2O)_3$	Mono.	Finite clusters	7.394	7.4111	12.0597	-	106.55°	-	11

Figure 6.14. The crystal structure of magnesium tungstate dihydrate, Mg(WO$_4$)(H$_2$O)$_2$; magnesium octahedra are blue and tungsten tetrahedra are pink.
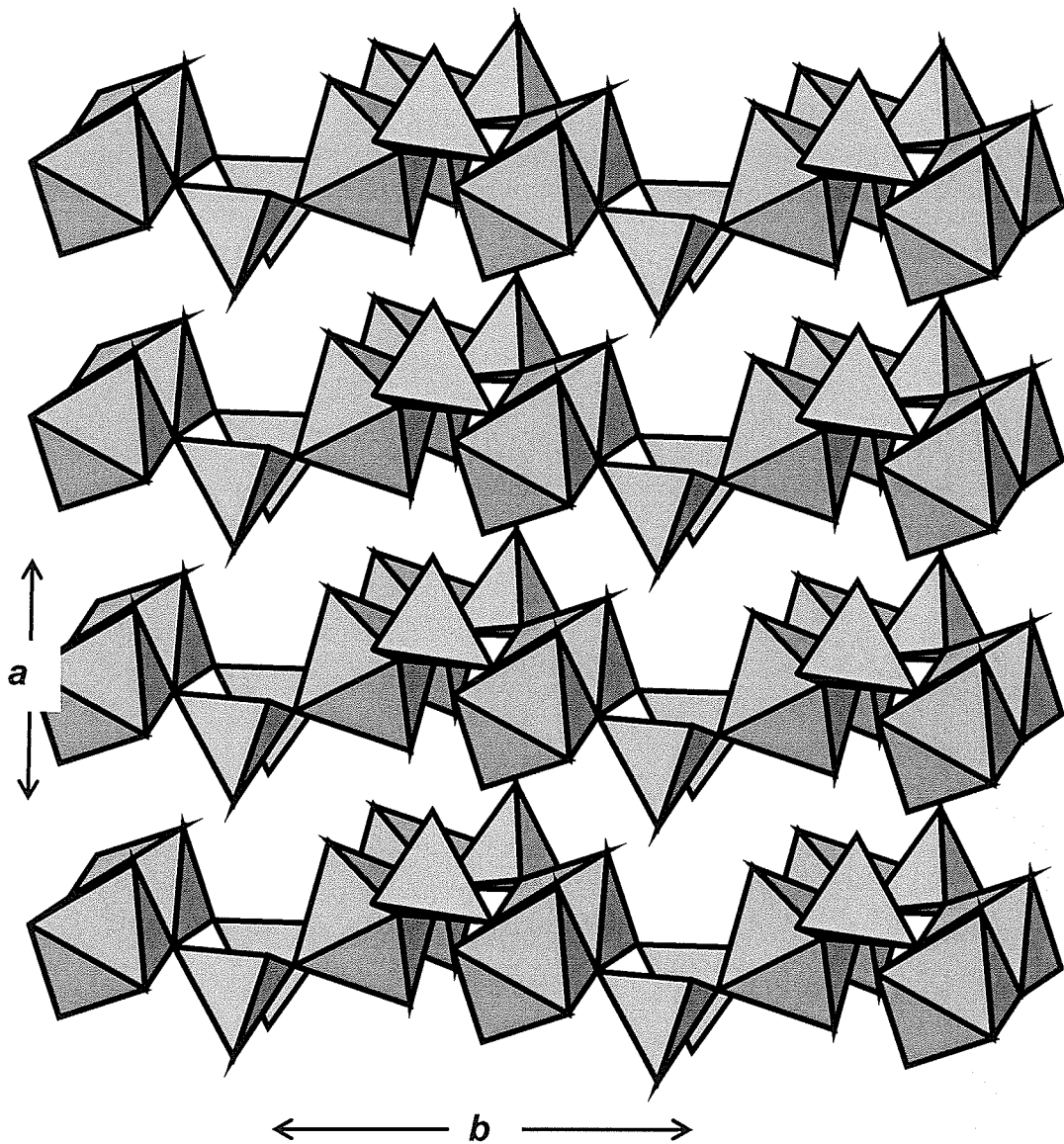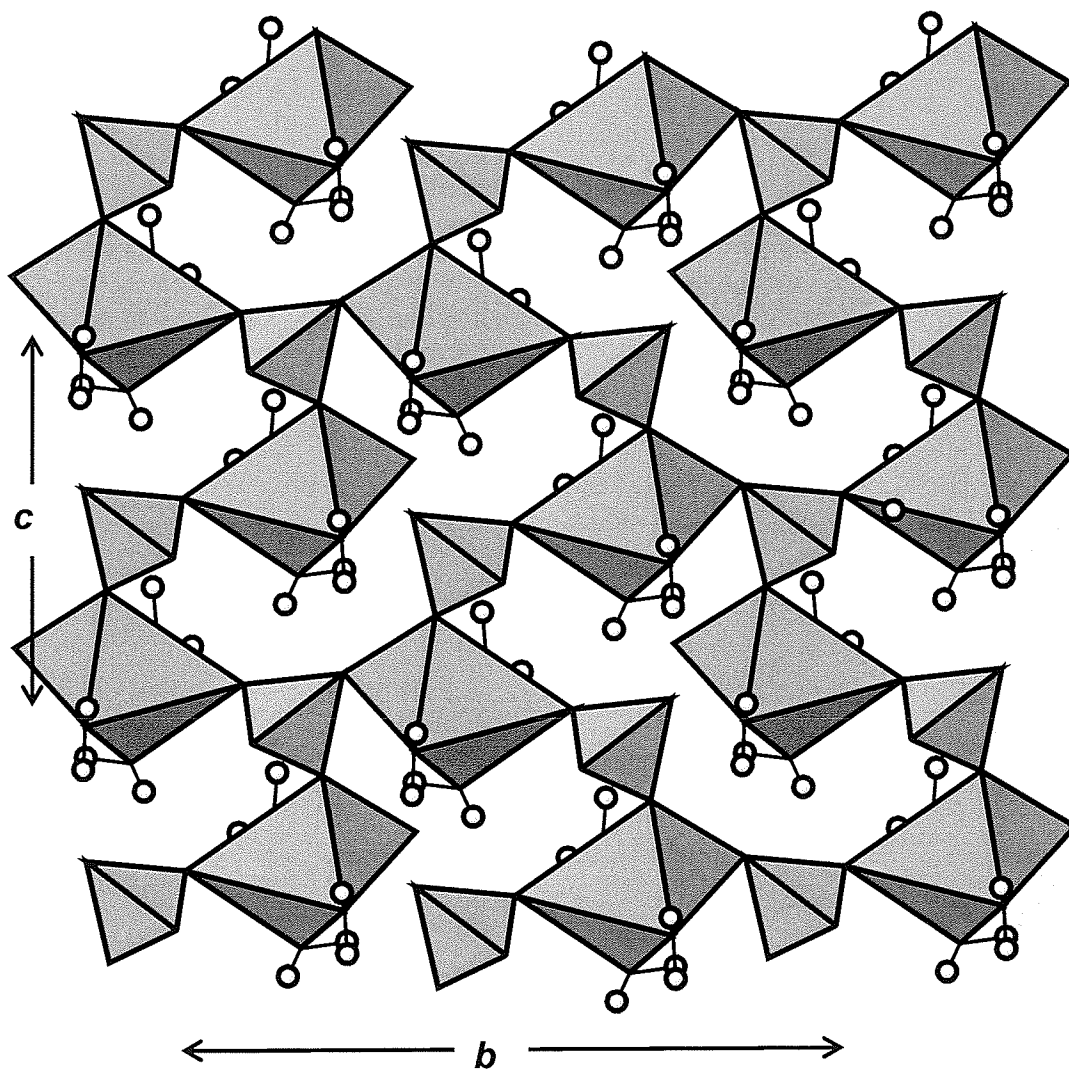
Figure 6.15. The crystal structure of magnesium tungstate dihydrate, $Mg(WO_4)(H_2O)_2$; magnesium octahedra are blue and tungsten tetrahedra are pink.

6.4.2 Bonattite, $Cu^{2+}(SO_4)(H_2O)_3$ and chromium(II) sulphate trihydrate, $Cr^{2+}(SO_4)(H_2O)_3$

The crystal structures of bonattite (Figure 6.16) and chromium (II) sulphate trihydrate (Figure 6.17) consist of distorted M^{2+} octahedra each coordinated by three H_2O groups and sharing corners with three SO_4 groups forming rather unusual frameworks further linked by hydrogen bonds to SO_4 groups.
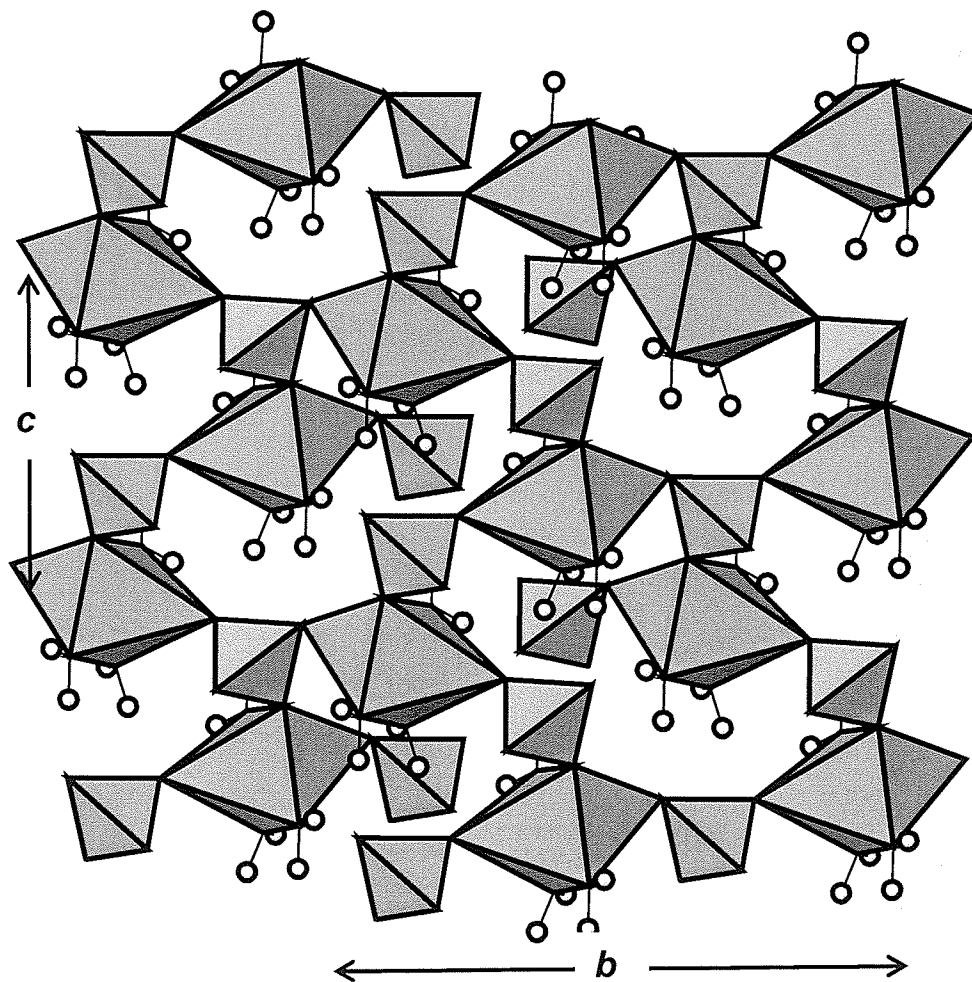
Figure 6.16. The crystal structure of bonattite, $Cu(SO_4)(H_2O)_3$; copper octahedra are blue, sulphur tetrahedra are pink and hydrogen is white. Hydrogen bonds omitted for clarity. Note the elongation of the copper octahedra.

Figure 6.17. The crystal structure of chromium (II) sulphate tri-hydrate, $Cr^{2+}(SO_4)(H_2O)_3$; chromium octahedra are blue, sulphur tetrahedra are pink and hydrogen is white. Hydrogen bonds omitted for clarity. Note the elongation of the chromium octahedra.
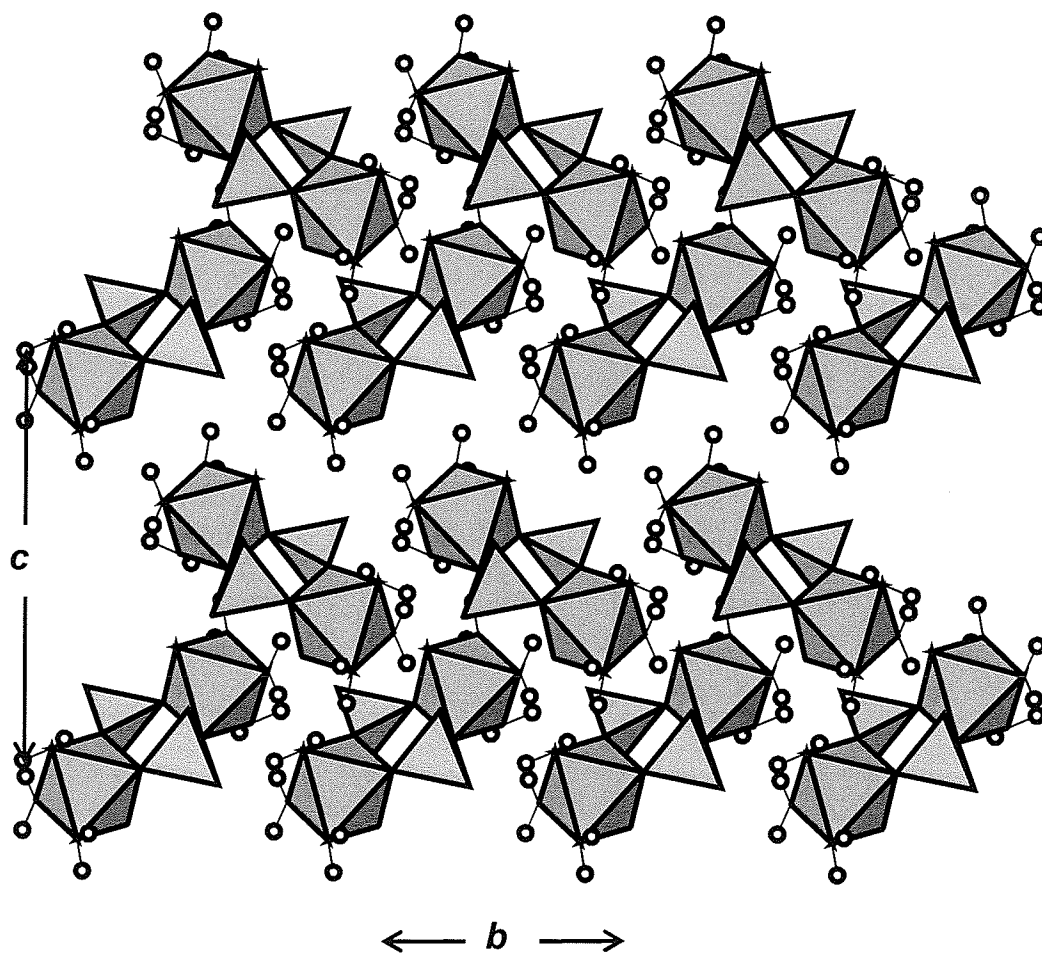
6.4.3 Bobjonesite, $VO(SO_4)(H_2O)_3$

The crystal structure of bobjonesite consists of $(VO)_2O_4(H_2O)_6(SO_4)_2$ clusters (two vanadium octahedra each coordinated by three H_2O groups and linked via corner-sharing with two sulphate tetrahedra) that are linked only by hydrogen bonds (Figure 6.18). Note that one corner of each vanadium octahedra is not linked to anything else; this is due to the very strong vanadyl bond which provides enough bond valence to the oxygen involved so that it does not require further coordination.

Figure 6.18 . The crystal structure of bobjonesite, $VO(SO_4)(H_2O)_3$; vanadium octahedra are blue, sulphur tetrahedra are pink and hydrogen is white. Hydrogen bonds omitted for clarity.

6.5 Observed dehydration –rehydration behavior of the magnesium sulphate hydrates

Bond-valences were calculated for the structures of anhydrous magnesium sulphate, kieserite, starkeyite, pentahydrite, hexahydrite, epsomite, magnesium tungstate dihydrate, bonattite, and chromium (II) sulphate trihydrate, and will (in some cases) be referred to in the following discussions (Tables 6.3-6.11).

Vaniman et al. (2004) observed that epsomite dehydrates into hexahydrite then amorphous magnesium sulphate hydrate relatively quickly in low humidity conditions; the process can be reversed in high humidity conditions (amorphous magnesium sulphate to hexahydrite to epsomite), however, it requires more time than dehydration. Kieserite is never formed during these transitions. Balarew et al. (2001) pointed out the fact that the crystallization of kieserite requires significant structural reorganization as it has the most complicated coordination pattern of the magnesium sulphate hydrates. This would require time and energy, hence the kinetics of kieserite formation are slow and high temperatures are required. Inspection of the bond valence table (Table 6.4) and Figure 6.9 shows that in kieserite the H_2O group is linked to two magnesium; incident bond valence on the oxygen involved (O(3)) is quite high (being ~0.2 valence units (vu) greater that the ideal value of 2.0 for oxygen) hence the H_2O group must form two relatively strong hydrogen bonds. As such, this type of configuration is not ideal.

*hydrogen bond valences not included in all tables

Table 6.3 Bond valence table for magnesium sulphate:

	Mg	S	Σ
O(1)	0.42 x 2 ↓	1.34 x 2↓	1.76
O(2)	0.32 x 2→, x 4↓	1.20 x 2↓	1.88
Σ	2.20	5.08	

Table 6.4 Bond valence table for kieserite:

	Mg	S	H	Σ
O(1)	0.39x 2 ↓	1.54 x 2↓	0.2→	2.13
O(2)	0.37 x 2↓	1.49 x 2↓	0.2	2.06
O(3)	0.29 x 2→↓		0.8 x 2→	2.17
Σ	2.10	6.07	1.0	

Table 6.5 Bond valence table for starkeyite:

	Mg	S	H(1)	H(2)	H(3)	H(4)	H(5)	H(6)	H(7)	H(8)	Σ
O(1)	0.35	1.48									1.83
O(2)	0.35	1.52									1.87
O(3)		1.48									1.48
O(4)		1.53									1.53
O(5)	0.38		0.8	0.8							1.98
O(6)	0.34				0.8	0.8					1.94
O(7)	0.38						0.8	0.8			1.98
O(8)	0.36								0.8	0.8	1.96
Σ	2.16	6.01									

Table 6.6 Bond valence table for pentahydrite:

	Mg(1)	Mg(2)	S	H(1)	H(2)	H(3)	H(4)	H(5)	H(6)	H(7)	H(8)	H(9)*	H(10)*	Σ
O(1)	0.34x2↓		1.48											1.82
O(2)		0.33x2↓	1.49											1.82
O(3)			1.54											1.54
O(4)			1.27											1.27
O(5)	0.37x2↓			0.8	0.8									1.97
O(6)	0.38x2↓					0.8	0.8							1.98
O(7)		0.38x2↓						0.8	0.8					1.98
O(8)		0.4x2↓								0.8	0.8			2.0
O(9)*												0.8	0.8	1.6
Σ	2.18	2.22	5.78											

* interstitial H_2O group

Table 6.7 Bond valence table for hexahydrite:

	Mg(1)	Mg(2)	S	H(1)	H(2)	H(3)	H(4)	H(5)	H(6)	H(7)	H(8)	H(9)	H(10)	H(11)	H(12)	Σ
O(1)			1.49													1.49
O(2)			1.56													1.56
O(3)			1.42													1.42
O(4)			1.49													1.49
O(5)	0.39x2↓			0.8	0.8											1.99
O(6)	0.39x2↓					0.8	0.8									1.99
O(7)	0.35x2↓							0.8	0.8							1.95
O(8)		0.35x2↓								0.8	0.8					1.95
O(9)		0.38x2↓										0.8	0.8			1.98
O(10)		0.37x2↓												0.8	0.8	1.97
Σ	2.26	2.20	5.96													

Table 6.8 Bond valence table for epsomite:

	Mg	S	H(1)	H(2)	H(3)	H(4)	H(5)	H(6)	H(7)	H(8)	H(9)	H(10)	H(11)	H(12)	H(13)*	H(14)*	Σ
O(1)		1.55															1.49
O(2)		1.50															1.56
O(3)		1.51															1.42
O(4)		1.46															1.49
O(5)	0.37		0.8	0.8													1.99
O(6)	0.33				0.8	0.8											1.99
O(7)	0.38						0.8	0.8									1.95
O(8)	0.38								0.8	0.8							1.95
O(9)	0.33										0.8	0.8					1.98
O(10)	0.37												0.8	0.8			1.97
O(11)*															0.8	0.8	1.6
Σ	2.16	6.02															

* interstitial H_2O group

Table 6.9 Bond valence table for bonattite:

	Cu	S	H(1)	H(2)	H(3)	H(4)	H(5)	H(6)	$\sum$
O(1)	0.49	1.44							1.93
O(2)	0.12	1.49							1.61
O(3)		1.52							1.52
O(4)	0.14	1.58							1.72
O(5)	0.45		0.8	0.8					2.05
O(6)	0.46				0.8	0.8			2.06
O(7)	0.47						0.8	0.8	2.07
$\sum$	2.13	6.03							

Table 6.10 Bond valence table for chromium (II) sulphate trihydrate:

	Cr	S	H(1)	H(2)	H(3)	H(4)	H(5)	H(6)	$\sum$
O(1)		1.53							1.53
O(2)	0.48	1.48							1.96
O(3)	0.15	1.53							1.68
O(4)	0.15	1.49							1.64
O(5)	0.45		0.8	0.8					2.05
O(6)	0.47				0.8	0.8			2.07
O(7)	0.46						0.8	0.8	2.06
$\sum$	2.16	6.03							

Table 6.11 Bond valence table for magnesium tungstate dihydrate:

	Mg	W	H(1)	H(2)	H(3)	H(4)	$\sum$
O(1)	0.39	1.53					1.92
O(2)	0.41	1.58					1.99
O(3)		1.52					1.52
O(4)	0.32 0.36	1.28					1.96
O(5)	0.32		0.8	0.8			1.92
O(6)	0.35				0.8	0.8	1.95
$\sum$	2.16	5.91					

Kieserite resists further dehydration (Vaniman, et al. 2004). Dehydration to anhydrous magnesium sulphate would require loss of one water molecule per formula unit followed by a change in the way magnesium octahedra are linked i.e. from corner-sharing in kieserite to edge-sharing in anhydrous magnesium sulphate (refer to Figures 6.8 and 6.9). The stability of structures increases when the number of shared edges (and faces) is minimized. Increased sharing of edges also increases the incident bond valence on magnesium to greater than the ideal value of 2.0 vu (see bond valence table, appendix). Kieserite easily rehydrates, first to hexahydrate and then to epsomite. Ab initio calculations (Richens, 1999 and references therein) point to a favourable six-coordinate hydration for Mg^{2+} (as in hexahydrite), and the stable seven-coordinate structure for Mg^{2+} consists of six primary shell H_2O groups with the seventh in the secondary shell, hydrogen bonded to two of the primary shell H_2O groups (as in epsomite, except the hydrogen bonds are to the SO_4 groups). Similarly, Balarew et al, (2001) state that the highest crystallization rate, and the lowest supersaturation required for nucleation, is to be expected for salts with crystal structures containing Mg^{2+} as the hexa-aqua complex, $[Mg(H_2O)_6]$ (epsomite and hexahydrite).

6.6 The missing structures: sanderite and $MgSO_4(H_2O)_3$

6.6.1 Sanderite $MgSO_4(H_2O)_2$

Sanderite is a poorly characterized mineral, however it is has been considered a valid mineral species since 1952. The type localities are the Hansa I shaft, Empelde, and the Niedersachsen shaft, near Wathlingen, Austria, where it is said to occur as efflorescences on kieserite (Berdesinski, 1952). Hodenberg & Kuhn (1967) synthesized $MgSO_4(H_2O)_2$, verifying the stoichiometry with thermogravimetric techniques and

powder x-ray diffraction. Chipera et al. (2005) have successfully synthesized $MgSO_4(H_2O)_2$ by dehydration of hexahydrite at 75° C and 1-5% RH (in a gas-mixing apparatus) for a few weeks (Vaniman, D.T., pers. comm.). The authors state that its stability field, if thermodynamically stable, seems limited. Vaniman (pers. comm) cautions that all synthesis attempts result in mixed phases (also stated by Balarew, et al. 2001), and that a categorization based on the amount of water can be misleading (e.g. a 50:50 mix of sanderite and starkeyite might be interpreted as $MgSO_4(H_2O)_3$). At any rate, the crystal structure of sanderite has not been solved, due in part to the fact that its stability field is limited, making it both a difficult material to synthesize and analyze, or remove from its natural environment without further hydration.

There is one inorganic compound of sanderite stoichiometry, $M^{2+}(T^{6+}O_4)(H_2O)_2$: magnesium tungstate dihydrate, $MgWO_4(H_2O)_2$. One could speculate that sanderite might adopt the same structure. The structure of magnesium tungstate dihydrate is shown in Figures 6.14 and 6.15. First inspection shows that the structure seems similar to that of gypsum $CaSO_4(H_2O)_2$ (Figure 6.19); however, calcium is [8]-coordinated whereas magnesium is [6]-coordinated, and the Ca polyhedra share edges forming continuous polyhedral strips whereas the Mg octahedra share edges to form dimers.

Is it possible to substitute sulphur for tungsten in the magnesium sulphate dihydrate structure? W-O bond lengths in magnesium tungstate dihydrate range from 1.74-1.83 Å , S-O bond lengths are shorter, ranging from 1.44-1.48 Å. Replacing W with S would bring the octahedral dimers and their terminal H_2O groups much closer together,

possibly too close for structural stability. This could potentially be a reason for the

limited stability field observed for sanderite.
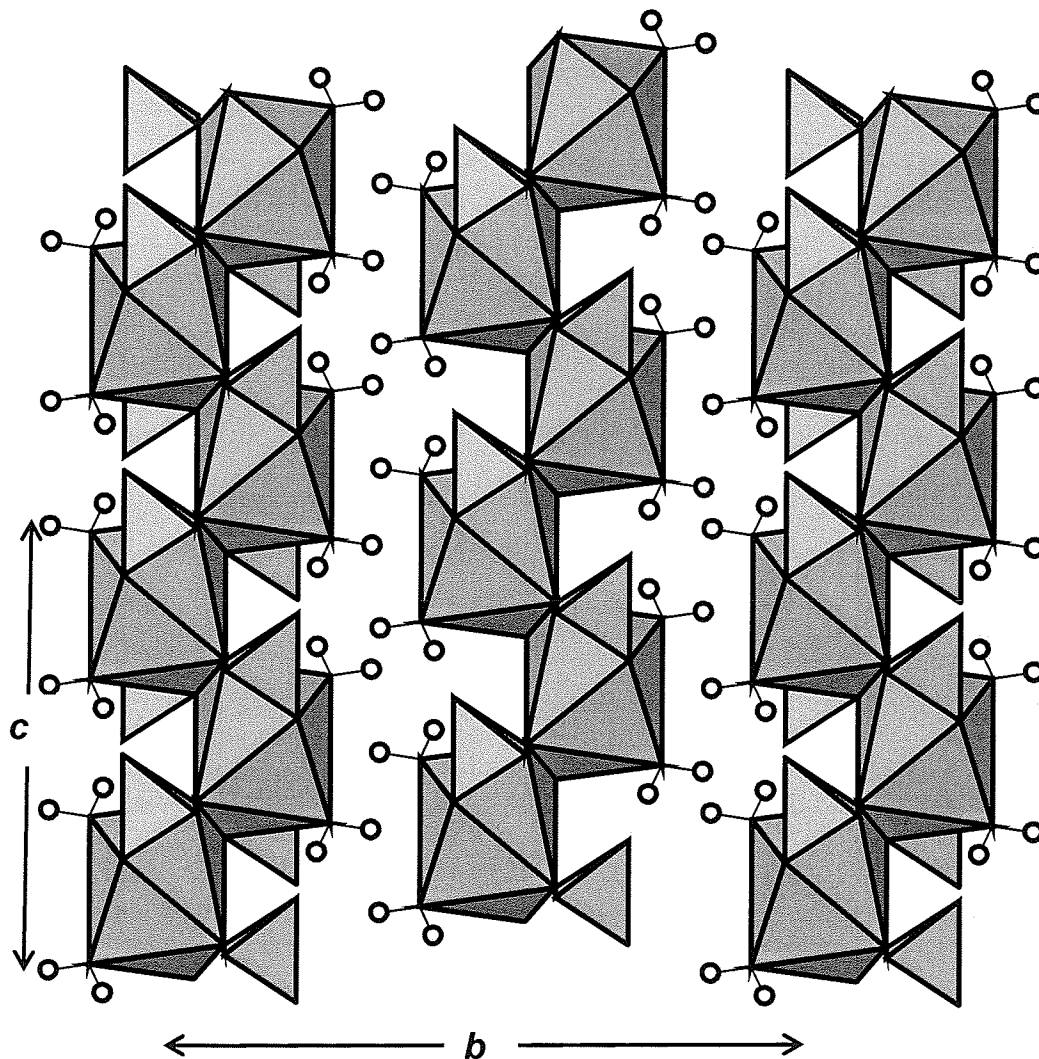
Figure 6.19 The crystal structure of gypsum, $Ca(SO_4)(H_2O)_2$; calcium polyhedra are blue, sulphur tetrahedra are pink, and terminal H_2O groups are white. Hydrogen bonds omitted for clarity.

6.6.2 MgSO$_4$(H$_2$O)$_3$

MgSO$_4$(H$_2$O)$_3$ does not occur in nature (at Earth surface temperatures, pressure, and RH). Hodenberg & Kuhn (1967) crystallized MgSO$_4$(H$_2$O)$_3$ from MgCl$_2$-MgSO$_4$-H$_2$O solutions. In the dehydration-hydration experiments of Vaniman et al. (2004) and Chipera et al. (2005), MgSO$_4$(H$_2$O)$_3$ was never observed . There are three simple salts with M^{x+}(T^{6+}O4)(H$_2$O)$_3$ stoichiometry: the rare minerals bonattite Cu^{2+}(SO$_4$)(H$_2$O)$_3$ and bobjonesite VO(SO$_4$)(H$_2$O)$_3$, and the compound chromium (II) sulphate trihydrate Cr^{2+}(SO$_4$)(H$_2$O)$_3$.

The structures of bonattite and chromium (II) sulphate trihydrate (Figures 6.16 and 6.17, respectively) consist of M^{2+} octahedra each coordinated by three H$_2$O groups and sharing corners with three SO$_4$ groups, forming rather unusual frameworks further linked by hydrogen bonds to SO$_4$ groups. Inspection of the figures shows that both of these structures contain M^{2+} cations in very distorted octahedral coordination, with four short bonds (approx. 1.96 Å in bonattite and 2.05 Å in chromium (II) sulphate trihydrate)and two long bonds (approx. 2.4 Å in bonattite and 2.46 Å in chromium (II) sulphate trihydrate) to oxygen. This is a characteristic Jahn-Teller distortion that can occur for d-block elements, such as Cu^{2+} and Cr^{2+}).

The crystal structure of bobjonesite is based on finite clusters composed of two vanadium octahedra each coordinated by three H$_2$O groups and linked via corner-sharing with two sulphate tetrahedra, that are linked only by hydrogen bonds (Figure 6.18). Note that one corner of each vanadium octahedra is not linked to anything else; this is due to the very short, strong vanadyl bond which provides enough bond valence to the oxygen

involved so that it does not require further coordination. It is interesting to note that this is the same type of cluster seen in starkeyite with the exception of one less H_2O group.

Magnesium has a propensity to be in regular octahedral coordination; other ions (such as Cu^{2+} and Cr^{2+}) can have more flexible coordination geometry (Richens, 1999). It seems that the only $M^{x+}(T^{6+}O_4)$ minerals / compounds that can incorporate three water molecules per formula unit are those which contain M cations capable of adopting distorted coordination geometry. Figure 6.20 is a graphical representation of the condensation of starkeyite.

6.7 Polymerization sequence

The expected polymerization sequence for crystal structures is:

isolated polyhedra → finite clusters → infinite chains → sheets → framework

In the $MgSO_4(H_2O)_n$ (n=0-7) structures, the following polymerization sequence is observed (Figure 6.): *isolated polyhedra(n=6,7) → infinite chains(n=5) → finite clusters(n=4) → ??(n-2,3) → framework(n=0,1)*
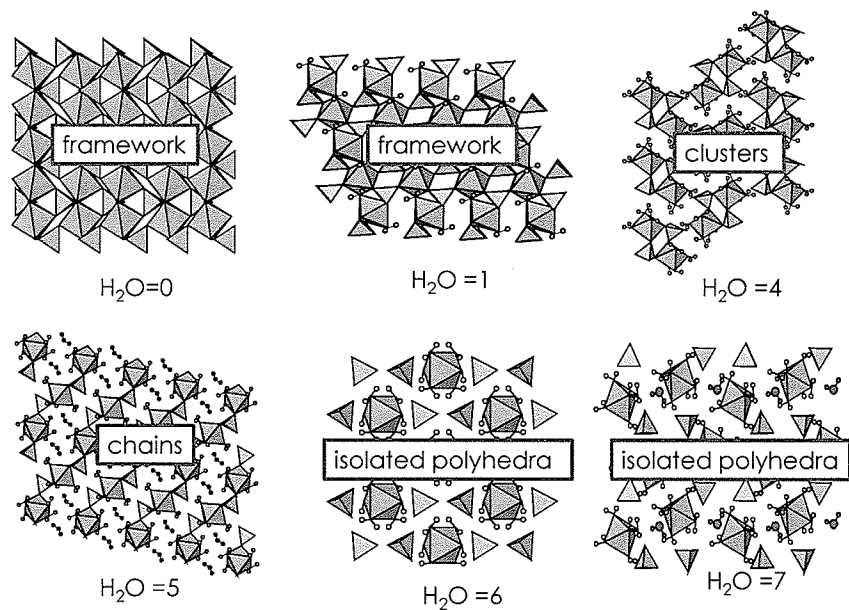
Figure 6.20. Polymerization sequence observed in the magnesium sulphates.

Two issues are evident: (1) we don't know the polymerization modes of sanderite, $Mg(SO_4)(H_2O)_2$ or $Mg(SO_4)(H_2O)_3$ because we don't know the structures (2) the polymerization modes of starkeyite, $Mg(SO_4)(H_2O)_4$ and pentahydrite, $Mg(SO_4)(H_2O)_5$ are reversed according to a typical sequence.

Magnesium tungstate dihydrate $Mg(WO_4)(H_2O)_2$, a possible structural analogue for sanderite $Mg(SO_4)(H_2O)_2$, has a sheet structure. This fits in with the expected sequence. Bonattite, $Cu^{2+}(SO_4)(H_2O)_3$, bobjonesite $VO(SO_4)(H_2O)_3$ and chromium sulphate trihydrate, $Cr^{2+}(SO_4)(H_2O)_3$ are the only known minerals and compound of this stoichiometry. Bonattite and chromium sulphate dihydrate crystal structures are frameworks, and don not fit in with the expected polymerization sequence. The

bobjonesite structure is based on finite clusters, which does not fit in with the expected sequence.

Polymerization can be described quantitatively in terms 'polymerization degree' which is the number of shared oxygen atoms / the total number of oxygen atoms, for a given unit (Table 6.12). It can also be described in terms of the changing linkage types within an entire sequence.

in the $M^{2+}T^{6+}O_4(H_2O)_n$ series (Table 6.13). As H_2O increases in the series, we observe (a) a decrease in O- M^{2+}+ T^{6+} due to hydrogen breaking linkages between octahedron and tetrahedra, (b) an increase in O- M^{2+}+ H + H as octahedra replace that linkage with H_2O, and (c) an increase in O- T^{6+}, due to the isolation of tetrahedral which become H-bond acceptors. Exceptions to these generalizations are in the trihydrate structures, and when the increase in H_2O is due to interstitial H_2O, which does not affect bonding within the structural unit.

The polymerization modes of starkeyite, $Mg(SO_4)(H_2O)_4$ and pentahydrite, $Mg(SO_4)(H_2O)_5$ are reversed according to a typical sequence. Inspection of tables 6.12 and 6.13 shows that the starkeyite and pentahydrite structures have the same type and number of linkages, however, their arrangements are different. It appears possible to have a chain with $Mg(SO_4)(H_2O)_4$ stoichiometry and a cluster with $Mg(SO_4)(H_2O)_5$ stoichiometry, which would follow the typical polymerization sequence, however they are not known to occur. At this time there is no apparent reason as to the reverse polymerization sequence of starkeyite and pentahydrite.

Table 6.12 Polymerization degree in selected $M^{2+}T^{6+}O_4(H_2O)_n$ minerals.

Mineral / Compound	Polymerization Mode	Polymerization Degree
MgSO$_4$	framework	1.0
Mg(SO$_4$)(H$_2$O)	framework	1.0
Mg(WO$_4$)(H$_2$O)$_2$	sheet	0.67
M^{2+}(SO$_4$)(H$_2$O)$_3$	framework	0.78
Mg(SO$_4$)(H$_2$O)$_4$	cluster	0.33
Mg(SO$_4$)(H$_2$O)$_5$	chain	0.33
Mg(SO$_4$)(H$_2$O)$_6$	isolated	0
Mg(SO$_4$)(H$_2$O)$_7$	isolated	0

Table 6.13 Linkages in the $M^{2+}T^{6+}O_4(H_2O)_n$ series

$M^{2+}T^{6+}O_4(H_2O)_n$ linkage	n=0	n=1	n=2	n=3	n=4	n=5	n=6	n=7
O- M^{2+} + M^{2+} + T^{6+}	1	2	1					
O- M^{2+} + T^{6+}	1		2	3	2	2		
O- M^{2+} + M^{2+}								
O- M^{2+} + M^{2+} + H + H		2						
O- M^{2+} + H + H			2	3	4	4	6	6
O- T^{6+}			1	1	2	2	4	4
O- H + H						1		1

6.8 Chapter 6 summary

Minerals of the $MgSO_4(H_2O)_n$ series (n= 0-1, 4-7) can accommodate increasing amounts of H_2O (up to 50 wt%) by altering their crystal structures. The crystal structures of those minerals were examined to (a) investigate and describe the structural modifications resulting from the addition of H_2O, (b) propose what the sanderite $Mg(SO_4)(H_2O)_2$ and $Mg(SO_4)(H_2O)_3$ crystal structures might be, and (c) provide reasons for the non-typical observed polymerization sequence in this group.

With addition of H_2O, structural modifications involve depolymerization, which can be quantitatively described by adecrease in O-M^{2+}+T^{6+} linkages as they are replaced by O-M^{2+}+H+H and O-T^{6+} linkages.

M^{2+} $(TO_4)(H_2O)_2$ structures are sheet structures, and M^{2+} $(TO_4)(H_2O)_3$ are framework structures. It is not entirely apparent at this time why these structures are not stable when M^{2+}= Mg.

A typical depolymerization sequence is not observed in the case of pentahydrite and starkeyite.It appears theoretically possible for pentahydrite and starkeyite to adopt structures that would conform to the typical sequence, e.g. $MgSO_4(H_2O)_4$ chain$\rightarrow$ $MgSO_4(H_2O)_5$ cluster (dimer). At this time it is not apparent as to why these structures do not occur.

CHAPTER 7

LOW-TEMPERATURE HYDRATED BORATES: A LINK BETWEEN SOLID AND SOLUTION

7.1 Introduction

Borates are a structurally diverse group of minerals because boron can occur in both tetrahedral and triangular coordination to oxygen, and can polymerize to form clusters, chains, sheets and framework structures. There are approximately 100 known borate minerals. Of the borates, thirty-one minerals, with nineteen distinct structure-types, contain isolated borate polyhedra; twenty-seven minerals, with twenty-five distinct structure-types, contain finite clusters of borate polyhedra; ten minerals, with ten distinct structure-types, contain chains of borate polyhedra; fifteen minerals, with thirteen distinct structure-types, contain sheets of borate polyhedra; fifteen minerals, with thirteen distinct structure-types, contain frameworks of borate polyhedra (Hawthorne et.al ,1996).

The occurrence of [4]-coordinated and [3]-coordinated boron, OH⁻ and H_2O in both minerals (low temperature) and solutions is strongly dependent on pH. In concentrated borate solutions, $B(OH)_3$ is dominant at low pH, $B(OH)_4$ at high pH and in the near neutral pH range there exist various more complicated borate complexes (Figure 7.2). It has been suggested that borate minerals crystallizing out of such solutions utilize those aqueous complexes to build their structural units, and that mineral structures may then be an indicator of the pH of the environment in which they formed.

The structures of 49 low temperature borates are examined to determine the occurrence of borate aqueous complexes as structural units; some structural units are composed of discrete borate complexes found in solution, while some are formed by a

combination of different aqueous complexes, or by multiples of the same aqueous complex.

7.2 Crystal chemistry of boron

The boron cation is small; [3] radius = 0.01Å, [4] radius = 0.11Å (Shannon, 1976) and it can occur in both triangular and tetrahedral coordination to oxygen or $(OH)^-$. Bond-valence is a measure of the strength of a chemical bond, and, in a coordination polyhedron, can be approximated by the Pauling bond-strength (cation valence divided by the cation coordination number). For example, in a BO_3 group, the bond-valence is 3/3 = 1.00 vu (valence units), and in a BO_4 group, the bond-valence is 3/4= 0.75 vu. Oxygen requires 2.0 vu to be electrically satisfied. When two BO_3 groups link together, the bond-valence requirements of the linking oxygen are satisfied (Figure 7.1a). When two BO_4 groups link together, the linking oxygen receives 1.50 vu from both boron atoms (Figure 7.1b). The linking oxygen needs another 0.50 vu to have its valence requirements satisfied; this can be accomplished by receiving bond(s) from interstitial large low-valence cations or hydrogen bonds. When a BO_3 and a BO_4 group link together, the linking oxygen receives 1.75 vu from both boron atoms (Figure 7.1c). The oxygen needs another 0.25 vu to have its valence requirements satisfied which can be accomplished by receiving a hydrogen-bond or a bond from an interstitial cation.
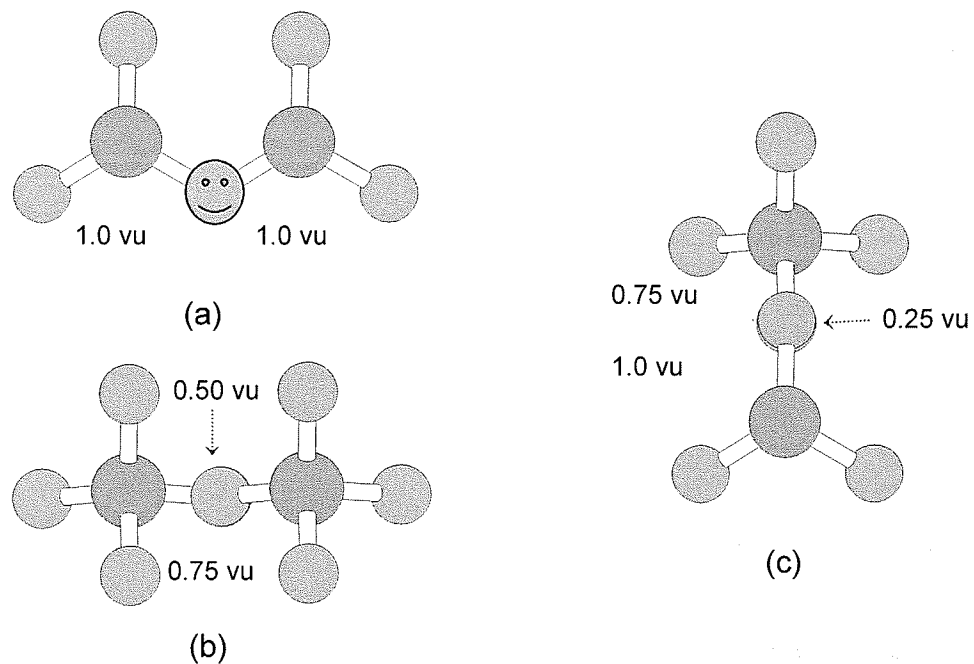
Figure 7.1. Bond valence characteristics of three configurations of borate polyhedra showing additional bond-valence requirements (red arrows) for the shared oxygen atoms. Boron atoms are green and oxygen atoms are blue.

7.3 Borate structural classification and polymerization

Hawthorne (1983) proposed that crystal structures can be classified according to polymerization of cation polyhedra with higher bond-valences. The higher bond-valence polyhedra polymerize to form homo- or heteropolyhedral clusters that are the fundamental building block (FBB) of the structure. The FBB is repeated, or polymerized to form the structural unit (SU), a complex usually anionic polyhedral array whose charge is balanced by the interstitial species, usually large low-valence cations and / or hydrogen bonds (IC) (Hawthorne, 1985). Further polymerization of these units can occur ; the

possible modes of polymerization are (a) unconnected polyhedra; (b) finite clusters; (c) infinite chains; (d) infinite sheets; and (e) infinite frameworks. In the structure of most borate minerals, the boron-oxygen bonds are of much higher bond-valence than the other cation-oxygen bonds; therefore the structures of borate minerals can be hierarchically classified based on the linkage of (BO_3) triangles and (BO_4) tetrahedra.

The crystal structure of borate have been studied, resulting in some general rules regarding their structure and classification (Christ, 1960)(Christ & Clark, 1977). More recently, Hawthorne et al. (1996) and Grice et al. (1999) have developed a hierarchical structural classification for borate minerals based on the polymerization of the fundamental building blocks of the structures of borate minerals.

Burns et al. (1995) derived all topologically and geometrically possible finite borate clusters and identified those clusters which occur as fundamental building blocks (FBB) of the structures of borate minerals. Many clusters were not observed, while some clusters were very common and it was shown that 3-membered rings are important as FBBs.

7.4 Paragenesis of borates

Low- temperature hydrated borate minerals form primarily by evaporation of saline lakes or during diagenesis of the resulting lacustrine sediments. Hanshaw (1963) and Christ et al. (1967) used paragenetic relations and thermodynamic data for several Na, Na-Ca and Ca-Mg borate minerals to construct their phase relations on a log [Na]6[H]2 / [Ca]4 – log H_2O – 1/T diagram. Christ et al. (1967) calculated the topology of the activity-activity diagrams for log [Na^+] / [H^+] and log [Ca^{2+}] / [H^+], respectively, vs. log (H_2O). Smith and Medrano (1996) reviewed these phase relations and indicated

that the chemical composition and occurrence of saline borate minerals depend on the

composition, temperature and pH of the primary parent solutions from which they

crystallize and the secondary solutions with which they interact during weathering and

diagenesis.

Schindler and Hawthorne (2001 a,b,c) interpreted the crystal structures and

chemical compositions of oxy-hydrated borate oxysalt minerals in terms of bond-valence

and they established a connection between the crystal structures of borate minerals and

the conditions (pH, $\log[H_2O]$) at which they are stable. They showed that average

basicity of borate clusters in solution is a linear function of the pH of that solution at

maximum concentrations of the cluster and it is also a linear function of the proportion of

[4]-coordinated boron. They developed pH-$\log[H_2O]$ activity-activity diagrams for the

borates. Some of their general observations were that structural units of borates with

similar paragenesis occurred in contiguous fields of the diagrams, and that

polymerization trends changed systematically across the diagram from isolated polyhedra

at high activity of [H_2O] to frameworks at low activity of [H_2O].

7.5 Aqueous borate complexes

Ingri (1963) summarized previous work which showed that the aqueous

complexes [$B(OH)_3$], [$B_5O_6(OH)_4$]$^-$, [$B_3O_3(OH)_4$]$^-$, [$B_3O_3(OH)_5$]$^{2-}$, [$B_4O_5(OH)_4$]$^{2-}$ and

[$B(OH)_4$]$^-$ occur in highly concentrated aqueous borate solutions (Figure 7.2).In

concentrated borate solutions at low pH, $B(OH)_3$ is the dominant complex and at high pH

$B(OH)_4^-$ is the dominant complex. In the intermediate pH range of ~7-10, there exist

various other complexes.

Raman spectroscopy (Maya 1976, Janda & Heller 1979a) and 11B-NMR

spectroscopy (Janda & Heller 1979b, Salentine 1983) have confirmed the presence and

pH ranges for all these aqueous complexes except $[B_3O_3(OH)_5]^{2-}$. Raman and 11B-NMR

spectroscopy (Heller et al. 2001) and FTIR spectroscopy (Zhihong et al. 2003) confirmed

the existence of the aqueous complex $[B_3O_3(OH)_5]^{2-}$.

7.6 Linking aqueous borate complexes with borate mineral structures

It has been suggested that borate minerals crystallizing from concentrated borate

solutions might use the aqueous borate complexes to build their structures (Christ, 1960).

If this is the case, the structures of borate minerals may indicate the pH of the

environment in which they formed. Figure 7.3 shows the structures of the borate

complexes known to occur in solution. The important question is: *can we relate aqueous*

borate complexes to the structural units of borate minerals? To do this, the structures of

49 borate minerals are examined to determine if is is possible to construct the structures

using aqueous borate "building blocks". The borate minerals examined are known to

have evaporatic or diagenetic occurrences, where pH plays a significant role in

determining chemical composition (Table 7.1). The structures of these 49 minerals are

built with 28 different structural units. Of these 28 structural units, 5 exist as discrete

aqueous borate complexes in solution; the other 23 structural units are formed by some

combination of different aqueous complexes, or by multiples of the same aqueous

complex.
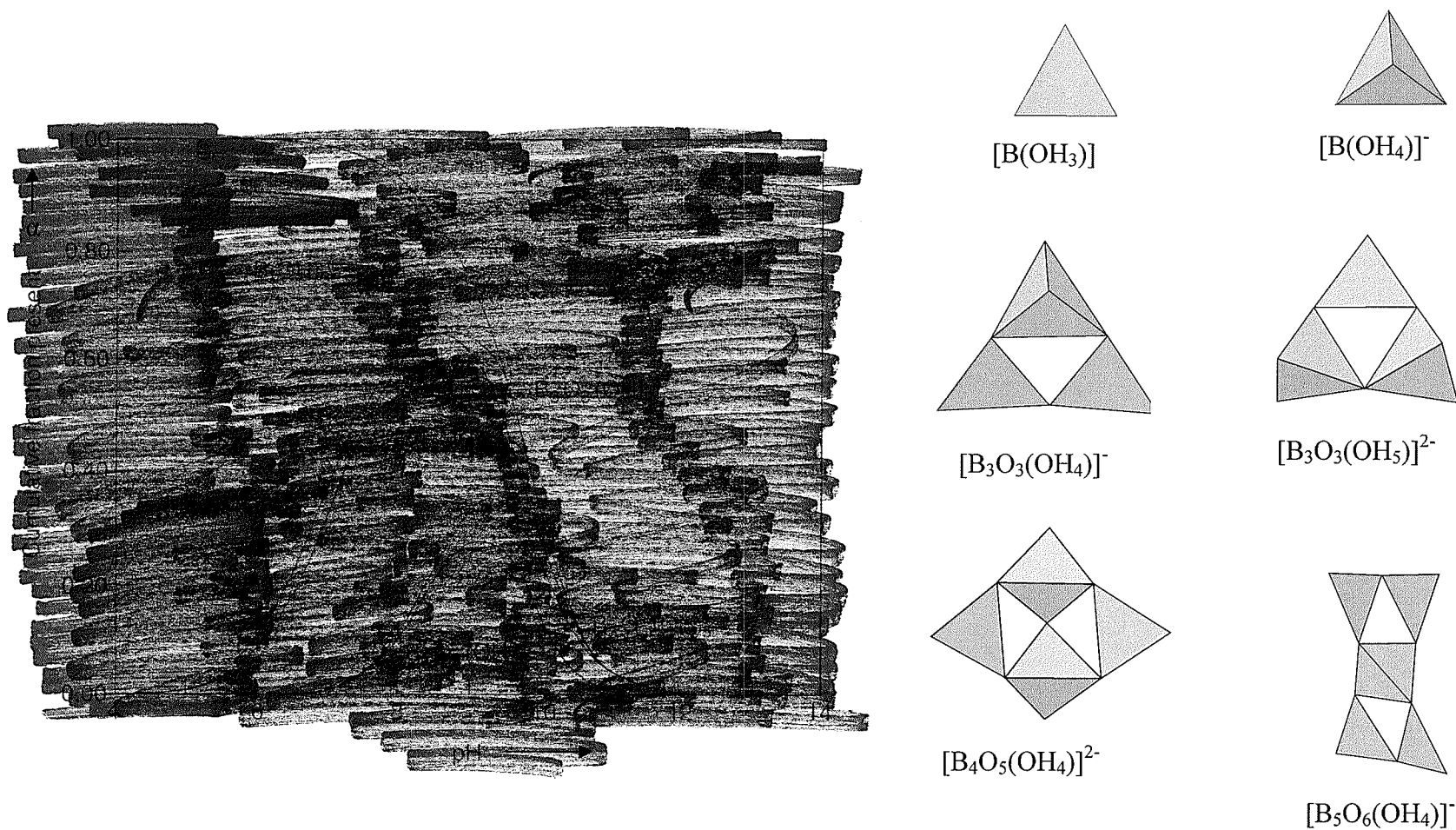
Figure 7.2 Speciation of borate clusters in 0.4M B(OH)₃ solution (after Ingri, 1963) and the structures of the borate clusters.

Ingri, N. (1963): Equilibrium studies of polyanions containing B(III), Si(IV), Ge(IV) and V(V). *Svensk Kemisk Tidskrift*. **74**(4). 199-230.

Table 7.1 Low-temperature hydrated borates.

Structural unit	Mineral	Formula	B polym.	AB[vu]	AAV[vu]	[4]B%	Occurrence*
$[B(OH)_3]^{3-}$	sassolite	$[B(OH)_3]$	iso. poly.	0.14	0	0	EP (FA)
$[B_2O_4(OH)]^{3-}$	szaibelyite	$Mg_2(OH)[B_2O_4(OH)]$	dimer	0.64	0.33	0	EP (HY, CM)
"	sussexite	$Mn_2(OH)[B_2O_4(OH)]$	"	"	"	"	"
$[B(OH)_4]^-$	bandylite	$Cu[B(OH)_4]Cl$	iso.poly	0.45	0.25	100	EP (CM)
"	teepleite	$Na_2[B(OH)_4]Cl$	"	"	"	"	"
"	frolovite	$Ca[B(OH)_4]2$	"	"	"	"	"
"	hexahydroborite	$Ca[B(OH)_4]_2(H2O)_2$	"	"	"	"	EP (MT, PG)
$[B_2O(OH)_6]^{2-}$	pentahydroborite	$Ca[B_2O(OH)_6](H_2O)_2$	dimer	0.46	0.25	100	EP
	pinnoite	$Mg[B_2O(OH)_6]$	"	"	"	"	"
$[B_3O_3(OH)_5]^{2-}$	inderite	$Mg[B_3O_3(OH)_5](H_2O)_5$	trimer	0.38	0.18	66	EP, DG
"	kurnakovite	$Mg[B_3O_3(OH)_5](H_2O)_5$	"				
"	inyoite	$Ca[B_3O_3(OH)_5](H_2O)_4$	"				
"	meyerhofferite	$Ca[B_3O_3(OH)_5](H_2O)$	"				
"	inderborite	$CaMg[B_3O_3(OH)_5]_2(H_2O)_6$	"				
$[B_3O_4(OH)_3]^{2-}$	colemanite	$Ca[B_3O_4(OH)_3](H_2O)$	chain	0.37	0.18	66	EP, DG
"	hydroboracite	$CaMg[B_3O_4(OH)_3]_2(H_2O)_3$	"	"	"	"	"
$[B_6O_{10}(OH)_2]^{4-}$	fabianite	$Ca_2[B_6O_{10}(OH)_2]$	sheet	0.37	0.18	66	EP, DG
$[B_3O_3(OH)_4]^-$	ameghinite	$Na[B_3O_3(OH)_4]$	cluster	0.26	0.1	33	EP
$[B_4O_5(OH)_4]^-$	borax	$Na_2[B_4O_5(OH)_4](H_2O)_8$	cluster	0.31	0.14	50	EP, DG
"	tinconalite	$Na_2[B_4O_5(OH)_4](H_2O)_3$	"	"	"	"	"
"	hungchaoite	$Mg[B_4O_5(OH)_4](H_2O)_7$	"	"	"	"	"
$[B_4O_6(OH)_2]^{2-}$	kernite	$Na_2[B_4O_5(OH)_2](H_2O)_3$	chain	0.3	0.14	50	EP, DG
$[B_4O_7]^{2-}$	diomignite	$Li_2[B_4O_7]$	framework	0.28	0.14	50	PG

107

Structural unit	Mineral	Formula	B polym.	AB[vu]	AAV[vu]	[4]B%	Occurrence*
$[B_5O_6(OH)_6]^{3-}$	ulexite	$NaCa[B_5O_5(OH)_6](H_2O)_5$	cluster	0.35	0.17	60	EP
$[B_5O_7(OH)_4]^{3-}$	probertite	$NaCa[B_5O_7(OH)_4](H_2O)_3$	chain	0.35	0.17	60	DG
$[B_5O_8(OH)_2]^{3-}$	tuzlaite	$NaCa[B_5O_8(OH)_2](H_2O)_3$	sheet	0.34	0.17	60	EP, DG
$[B_5O_9]^{3-}$	hilgardite-group	$Ca[B_5O_9]Cl(H_2O)$	framework	0.33	0.17	60	EP, DG
$[B_5O_7(OH)_3]^{2-}$	ezcurrite	$Na_2[B_5O_7(OH)_3](H_2O)_2$	chain	0.26	0.12	40	EP, DG
$[B_5O_8(OH)]^{2-}$	biringuccite	$Na_2[B_5O_8(OH)](H_2O)$	sheet	0.24	0.12	40	EP (FA)
"	nasinite	$Na_2[B_5O_8(OH)](H_2O)_2$	"	"	"	"	"
$[B_5O_8(OH)^{2-}$ x $[B(OH)_3]$	gowerite	$Ca[B_5O_8(OH)][B(OH)_3](H_2O)_3$	sheet&	0.25	0.12	50	EP
"	veatchite group	$Sr[B_5O_8(OH)][B(OH)_3](H_2O)_3$	iso.poly.	0.14	0	"	"
$[B_6O_7(OH)_6]^{2-}$	mcallisterite	$Mg_2[B_6O_7(OH)_6]_2(H_2O)_9$	cluster	0.25	0.1	50	EP
"	admontite	$Mg_2[B_6O_7(OH)_6]_2(H_2O)_7$	"	"	"	"	"
"	aksaite	$Mg[B_6O_7(OH)_6](H_2O)_2$	"	"	"	"	"
"	rivadavite	$Na_6Mg[B_6O_7(OH)_6]_4(H_2O)_{10}$	"	"	"	"	"
$[B_6O_8(OH)_4]^{2-}$	aristarainite	$NaMg[B_5O_8(OH)_4]_2(H_2O)_4$	chain	0.23	0.1	50	EP
$[B_6O_8(OH)_5]^{3-}$	kaliborite	$KMg_2H[B_7O_8(OH)_5](H_2O)_4$	chain	0.31	0.14	50	EP, DG
$[B_6O_9(OH)_2]^{2-}$	nobleite	$Ca[B_6O_9(OH)_2](H_2O)_3$	sheet	0.22	0.1	50	DG
"	tunellite	$Sr[B_6O_9(OH)_2](H_2O)_3$	"	"	"	"	"
$[B_4O_4(OH)_7]^{3-}$	hydrochlorborite	$Ca_2[B_3O_3(OH)_4][BO(OH)_3]Cl(H_2O)_7$	cluster	0.4	0.2	75	EP
$[B_5O_7(OH)_5]^{4-}$	priceite	$Ca_4[B_5O_7]_2(H_2O)_7$	chain	0.42	0.21	80	EP (MT,PG)

Structural unit	Mineral	Formula	B polym.	AB[vu]	AAV[vu]	[4]B%	Occurrence*
$[B_7O_{13}]^{5-}$	boracite group	$M_3[B_7O_{13}]Cl$, M=Mg, Fe^{2+}, Mn^{2+}	framework	0.38	0.19	85-100	EP, DG
$[B_5O_6(OH)_6]^{3-}$	brianroulstonite	$Ca_3[B_5O_6(OH)_6](OH)Cl_2(H_2O)_8$	sheet	"	"	"	"
$[B_8O_{11}(OH)_4]^{2-}$	strontioborite	$Sr[B_8O_{11}(OH)_4]$	sheet	0.19	0.08	37.5	EP
$[B_9O_{13}(OH)_6]^{5-}$	penobsquisite	$Ca_2Fe2+[B_9O_{13}(OH)_6]Cl(H_2O)_4$	framework	0.33	?	50	EP
$[B_{11}O_{15}(OH)_9]^{6-}$	preobrazhenskite	$Mg_3[B_{11}O_{15}(OH)_9]$	sheet	0.33	0.15	63	EP
$[B_{14}O_{20}(OH)_6]^{4-}$ "	ginorite strontioginorite	$Ca_2[B_{14}O_{20}(OH)_5](H_2O)_5$ $Sr_2[B_{14}O_{20}(OH)_5](H_2O)_5$	sheet "	0.2 "	0.09 "	42 "	EP "
$[B_{26}O_{34}(OH)_{24}]^{14-}$ "	pringleite ruitenbergite	$Ca_9[B_{26}O_{34}(OH)_{24}]Cl_4(H_2O)_{13}$ "	framework "	0.32 "	0.15 "	54 "	EP "

*EP= evaporitic; DG=diagenetic; FA=fumarolic; HY=hydrothermal; CM= contact metamorphic ;
MT= metamorphic; PG= pegmatite

7.6 Monoborates and diborates (pyroborates)

7.6.1 Triangular mono- and diborate crystal structures with $[B(OH)_3]^0$ and $[B_2O_4(OH)]^{3-}$ structural units

$[B(OH)_3]^0$ is the dominant aqueous complex in concentrated borate solutions at pH < 6. Sassolite, $[B(OH)_3]$, is the only mineral with this structural unit. The structure is made up of layers of $B(OH)_3$ triangles that are hydrogen-bonded together to form sheets; intersheet attraction is through Van der Waals interactions (Figure 7.3).
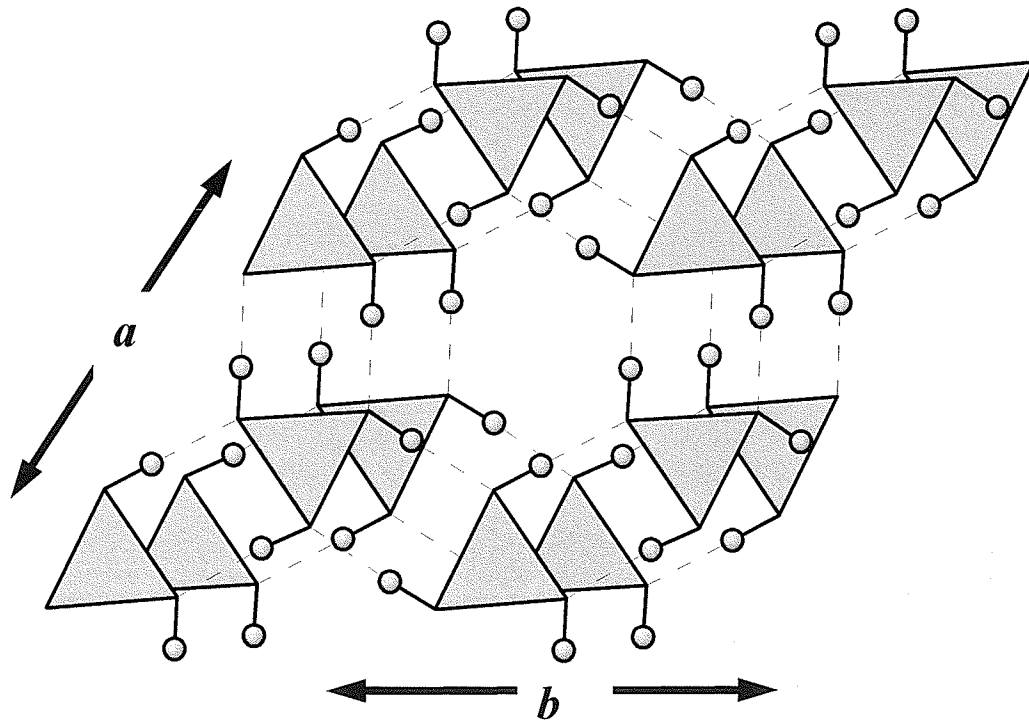
Figure 7.3 The crystal stucture of sassolite $[B(OH)_3]$. The isolated $[B(OH)_3]$ groups are pink and hydrogen is blue.

$[B(OH)_3]^0$ can polymerize to form dimers according to the following scheme:

$$2 \ [B(OH)_3]^0 \rightarrow [B_2O(OH)_4]^0 + H_2O$$
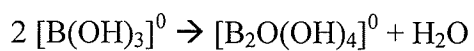
These dimers are not known to exist as aqueous complex in solution, but a deprotonated version of the dimer is found as the structural unit in the minerals szaibelyite $Mg_2(OH)[B_2O_4(OH)]$ and sussexite $Mn_2(OH)[B_2O_4(OH)]$ (Figure 7.4); hydrogen is "split out" so that those oxygens may bond to the octahedrally coordinated Mn and Mg cations to form the respective crystal structures.
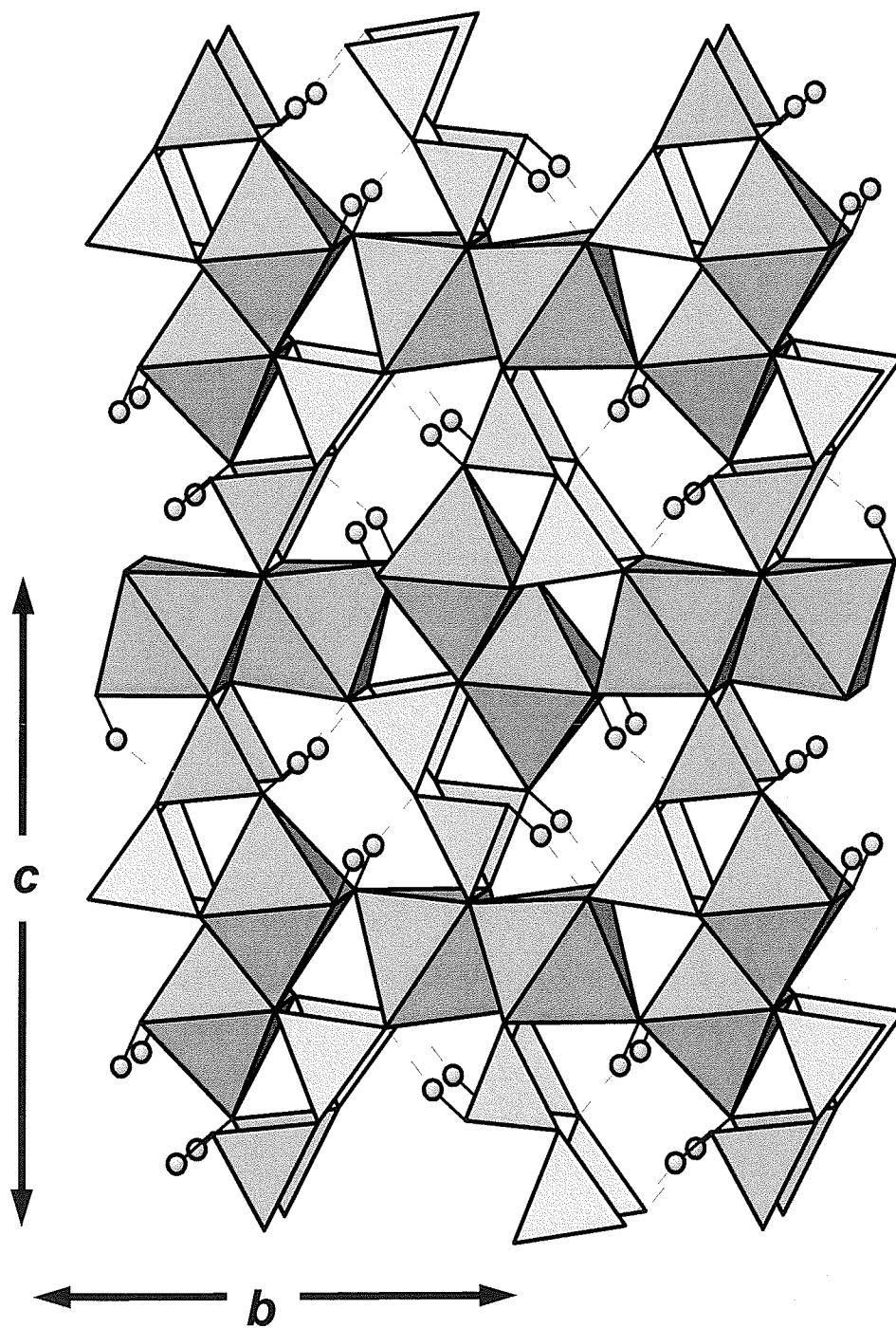
Figure 7.4. The crystal structure of sussexite $Mn_2(OH)[B_2O(OH)]$. The $[B_2O(OH)]$ dimers are light pink, Mn octahedral are dark pink and hydrogen is blue.

7.6.2 Tetrahedral mono- and diborate crystal structures with $[B(OH)_4]^-$ and $[B_2O(OH)_6]^{2-}$ structural units

$[B(OH)_4]^-$ is the dominant aqueous complex in concentrated borate solutions at pH >6. There are four minerals with $[B(OH)_4]^-$ as the structural unit: bandylite, $Cu[B(OH)_4]Cl$, teepleite, $Na_2[B(OH)_4]Cl$, frolovite, $Ca[B(OH)_4]_2$ and hexahydroborite, $Ca[B(OH)_4]_2(H_2O)_2$. $[B(OH)_4]^-$ can be polymerized to form dimers according to the following scheme:

$$2\ [B(OH)_4]^- \rightarrow [B_2O\ (OH)_6]^{2-} + H_2O$$
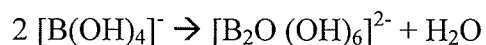
These dimers are not known to exist as aqueous complexes in solution, but are found as the structural unit in the minerals pinnoite $Mg[B_2O(OH)_6]$ and pentahydroborite $Ca[B_2O(OH)_6](H_2O)_2$. (Figure 7.5)

113
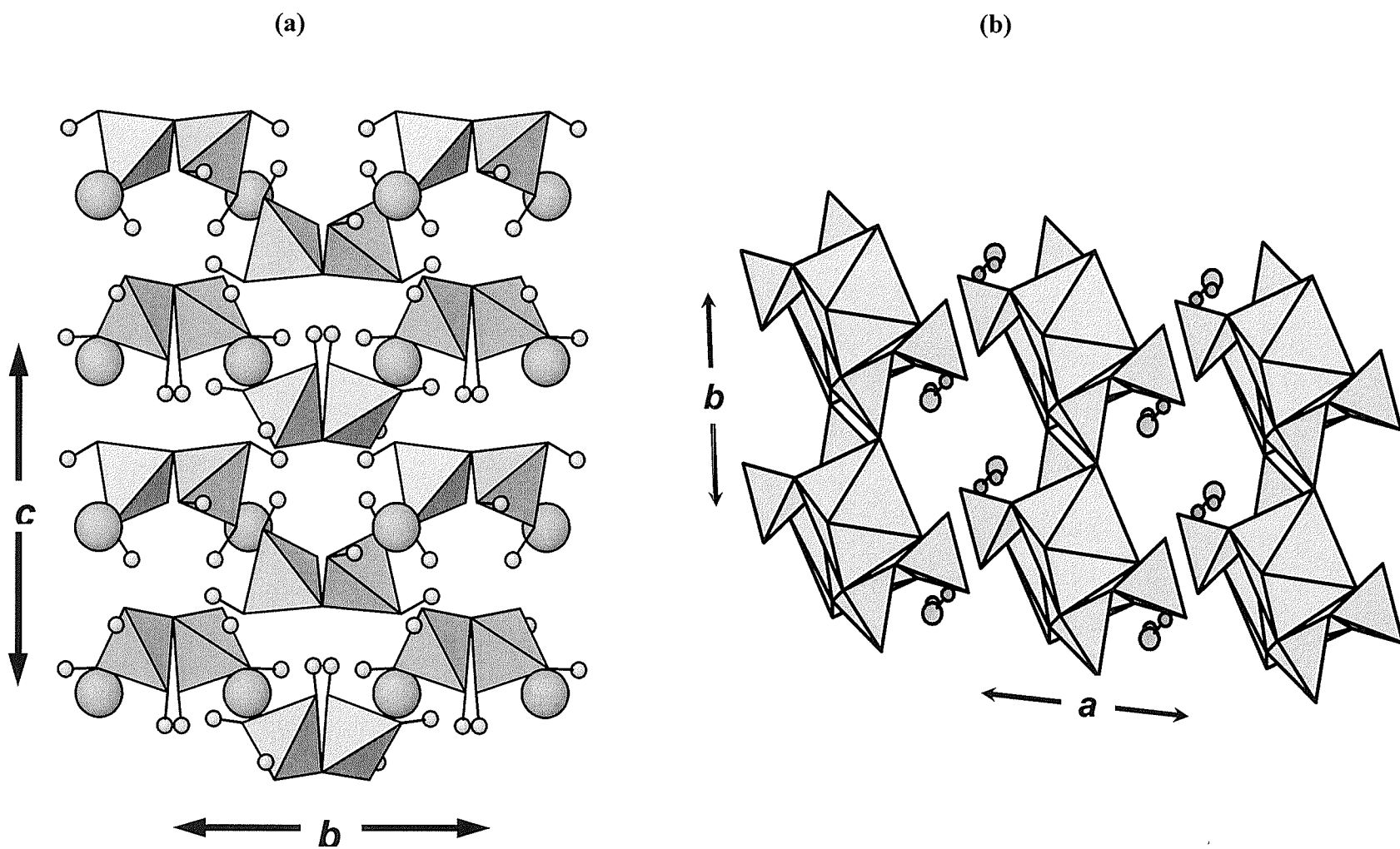
Figure 7.5. The crystal structures of (a) pinnoite $Mg[B_2O(OH)_6]$ and (b) pentahydroborite $Ca[B_2O(OH)_6](H_2O)_2$.

114

Further polymerization of the diborate structural units (dimers) to form strictly four-membered tretrahedral or four-membered triangular structural units does not occur (there are no known minerals with these as structural units), however, it is possible for them to polymerize with each other to form a combined tetrahedral and triangular tetraborate structural unit (see tetraborate section).

7.7 Triborates

7.7.1 Triborate crystal structures with [B₃O₃(OH)₄]⁻ structural units

$[B_3O_3(OH)_4]^-$ is found as an aqueous complex in concentrated borate solutions in the pH range of 6-10. It is a three-membered ring consisting of two B triangles and one B tetrahedron (Figure 7.6)
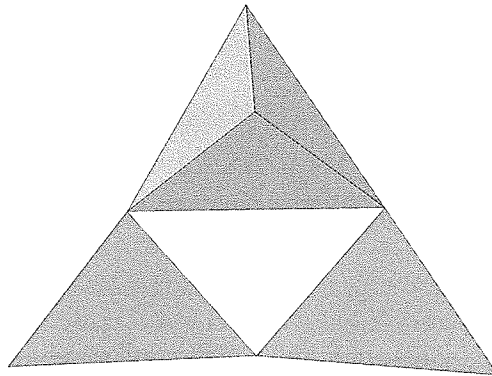
Figure 7.6. The structure of $[B_3O_3(OH)_4]^-$; terminal hydrogen atoms omitted.

It can be formed from the polymerization of the triangular pyroborate group with an isolated tetrahedral group, or by the polymerization of two B triangles and one B tetrahedron, according to the following schemes:

$$[B_2O(OH)_4] + [B(OH)_4]^- \rightarrow [B_3O_3(OH)_4]^- + 2 \; H_2O$$

$$2[B(OH)_3] + [B(OH)_4]^- \rightarrow [B_3O_3(OH)_4]^- + 3 \; H_2O$$
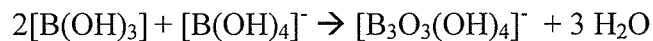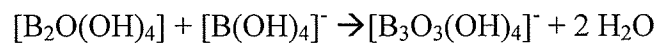
Ameghinite $Na[B_3O_3(OH)_4]$ is the only mineral with this structural unit which occurs in the structure as finite clusters (Figure 7.7). It is surprising to note that although this polyborate anion has been shown to be the most dominant aqueous complex in the pH range of 6-10, it occurs as a structural unit in only one mineral.
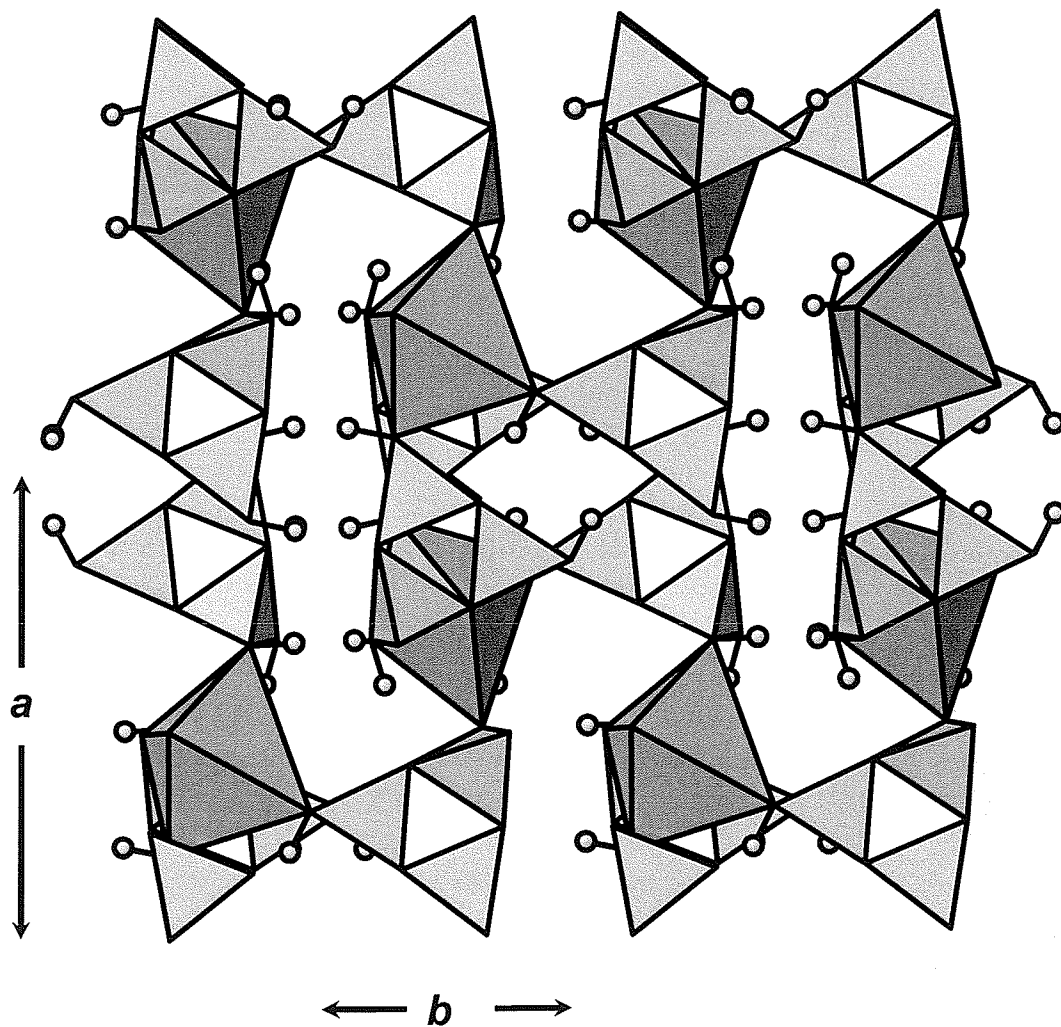
Figure 7.7. The crystal structure of ameghinite Na[B₃O₃(OH)₄]; B triangles are light pink. B tetrahedra are purple, Na polyhedra are dark pink and hydrogen is blue.

7.7.2 Triborate crystal structures with $[B_3O_3(OH)_5]^{2-}$ structural units

$[B_3O_3(OH)_5]^{2-}$ is found as an aqueous complex in concentrated borate solutions in the pH range of 6-12. It is a three-membered ring consisting of one B triangle and two B tetrahedrons (Figure 7.8).
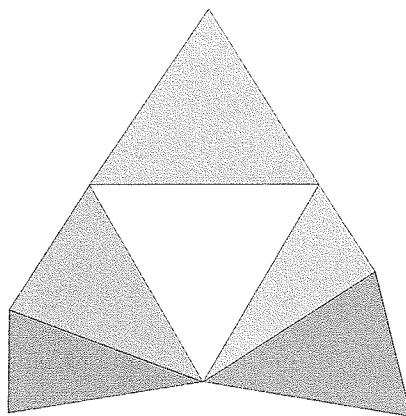
Figure 7.8. The structure of $[B_3O_3(OH)_5]^{2-}$; terminal hydrogen atoms omitted.

It can be formed from the polymerization of the tetrahedral diborate group with an isolated triangular group, or by the polymerization or by polymerization of two B tetrahedra and one B triangle according to the following schemes:

$$[B_2O(OH)_6]^{2-} + [B(OH)_3]^0 \rightarrow [B_3O_3(OH)_5]^{2-} + 2H_2O$$

$$2[B(OH)_4]^- + [B(OH)_3]^0 \rightarrow [B_3O_3(OH)_5]^{2-} + 3H_2O$$
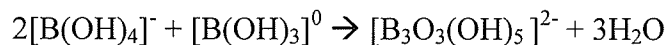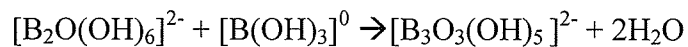
Polymerization of this structural unit produces excess H_2O which is incorporated into the crystal structures of the minerals in which it occurs; all minerals with the $[B_3O_3(OH)_5]^{2-}$ structural unit contain significant amounts of H_2O.

Inderite $Mg[B_3O_3(OH)_5](H_2O)_5$, kurnakovite $Mg[B_3O_3(OH)_5](H_2O)_5$, inyoite $Ca[B_3O_3(OH)_5](H_2O)_4$, meyerhofferite $Ca[B_3O_3(OH)_5](H_2O)$ and inderborite $CaMg[B_3O_3(OH)_5](H_2O)_6$ have this borate polyanion as their structural unit in which it occurs as a finite cluster (Figure 7.9)

7.9(a)

c

b

7.9(b)

b

a
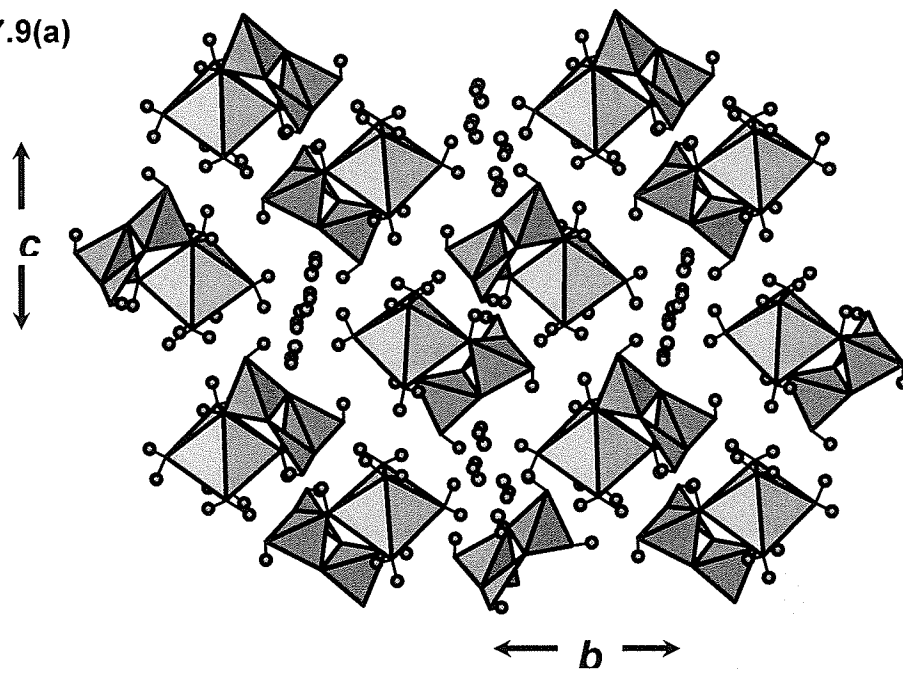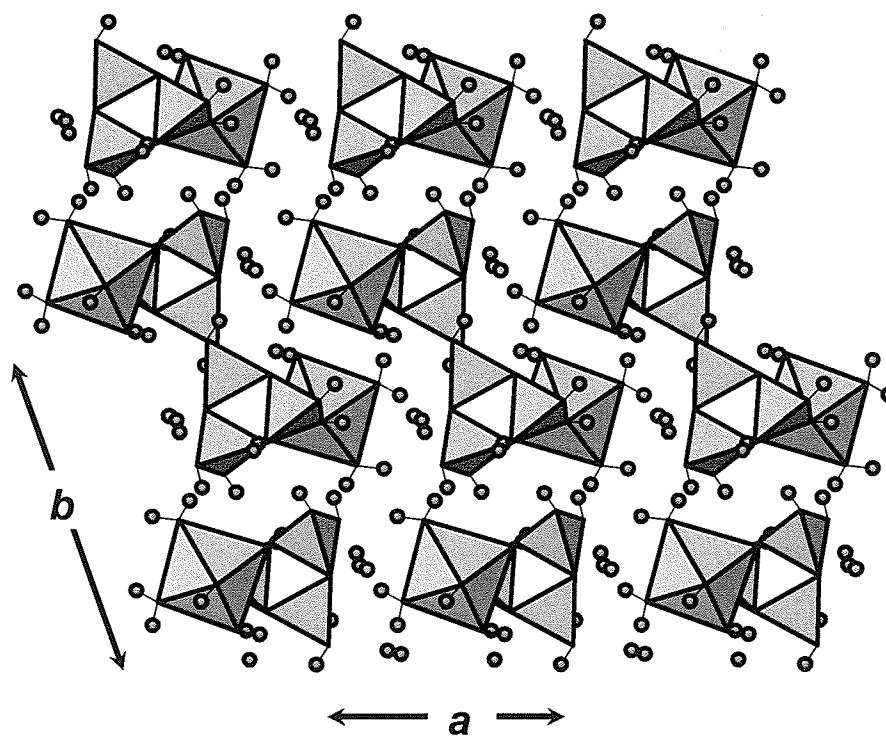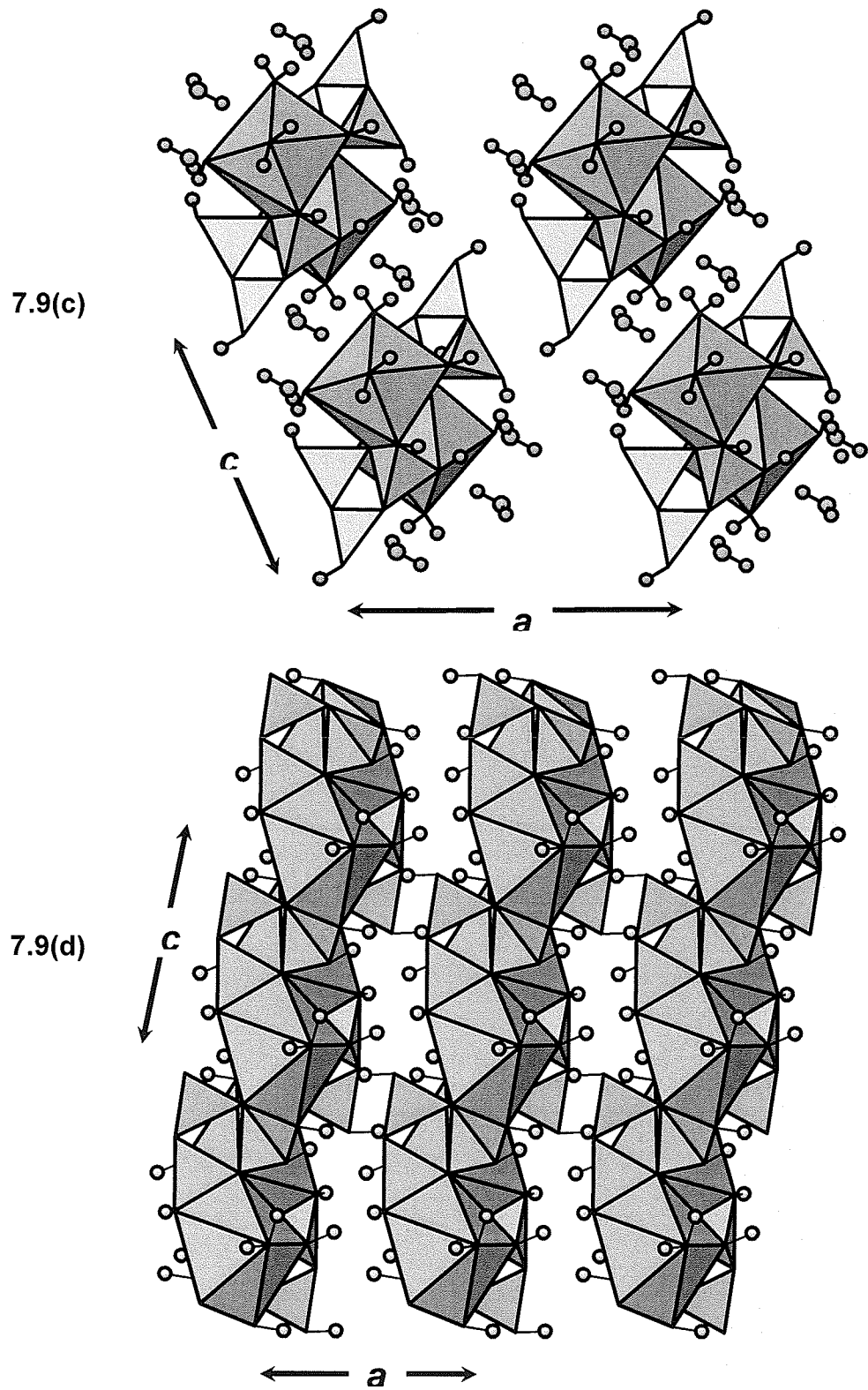
Figure 7.9. The crystal structures of (a) inderite (b) kurnakovite (c) inyoite, and (d) meyerhofferite.

This finite cluster can be further polymerized into the chains found in colemanite $Ca[B_3O_4(OH)_3](H_2O)$ and into the sheets found in fabianite $Ca[B_3O_5(OH)]$ by progressive condensation and the "splitting off" of water (Figure 7.10):

$$[B_3O_3(OH)_5]^{2-} \text{ (cluster)} \rightarrow [B_3O_4(OH)_3]^{2-} \text{ (chain)} + H_2O$$

$$[B_3O_4(OH)_3]^{2-} \text{ (chain)} \rightarrow [B_3O_5(OH)]^{4-} \text{ (sheet)} + H_2O$$
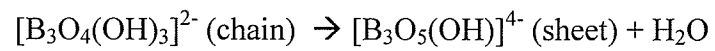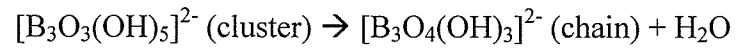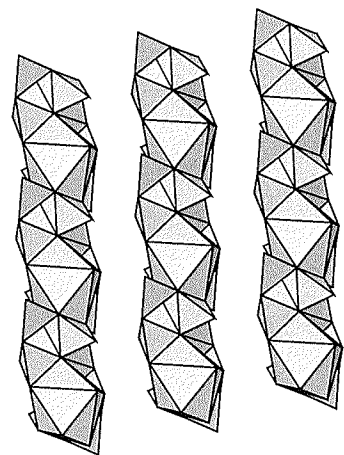
meyerhofferite
Ca[B$_3$O$_3$(OH)$_5$](H$_2$O)
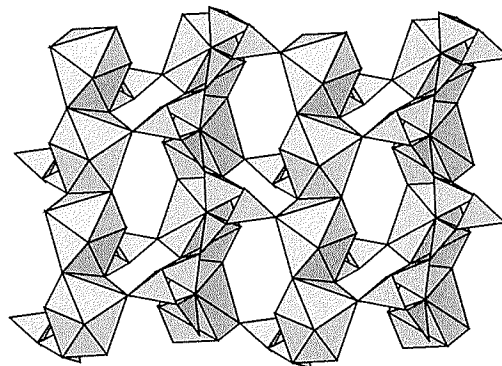
colemanite
Ca[B$_3$O$_4$(OH)$_3$](H$_2$O)

fabianite
Ca[B$_3$O$_5$(OH)]

$$[B_3O_3(OH)_5]^{2-} \text{ (}cluster\text{)} \rightarrow [B_3O_4(OH)_3]^{2-} \text{ (}chain\text{)} \rightarrow [B_3O_5(OH)]^{4-} \text{ (}sheet\text{)}$$
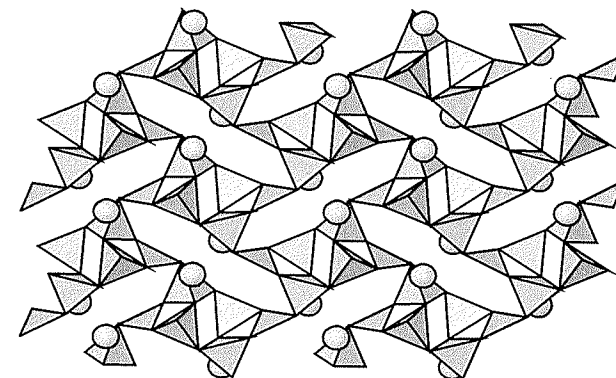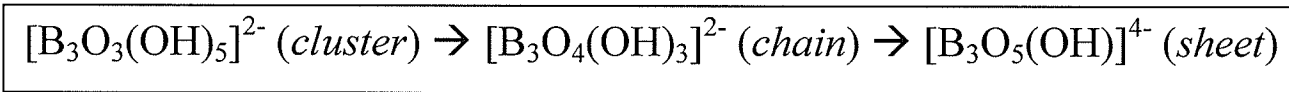
Figure 7.10 Polymerization of the [B$_3$O$_3$(OH)$_5$]$^{2-}$ structural unit from finite clusters to chains to sheets.

123

7.8 Tetraborates: structural unit $[B_4O_5(OH)_4]^{2-}$

$[B_4O_5(OH)_4]^{2-}$ is found as an aqueous complex in concentrated borate solutions in the pH range of 5-11. It is a cluster of four B polyhedra; two three-membered rings consisting of one B triangle and two B tetrahedrons sharing the two B tetrahedra (Figure 7.11).
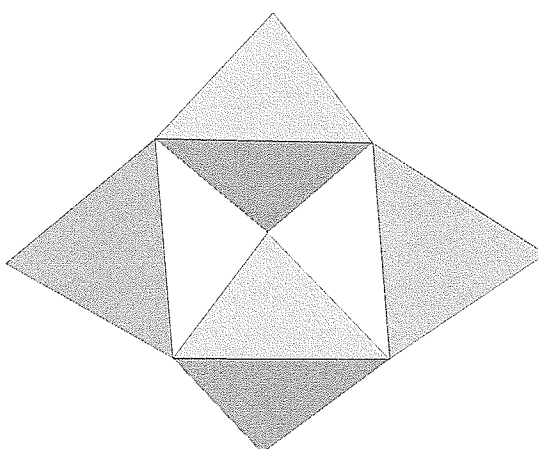
Figure 7.11. The structure of $[B_4O_5(OH)_4]^{2-}$; terminal hydrogen atoms omitted.

It can be formed from the polymerization of the three-membered $[B_3O_3(OH)_5]^{2-}$ group with an isolated $[B(OH)_3]^0$ group according to the following scheme:

$$[B_3O_3(OH)_5]^{2-} + [B(OH)_3]^0 \rightarrow [B_4O_5(OH)_4]^{2-} + 2H_2O$$
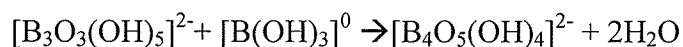
It could also be formed by the polymerization of the three-membered $[B_3O_3(OH)_4]^-$ group with an isolated $[B(OH)_4]^-$ tetrahedron, but this seems less likely; we have the correct number of [3] and [4] B polyhedra, but it would require more "reorganization" of polyhedra ie. complete disconnection of all components of the $[B_3O_3(OH)_4]^-$ group so

124

that the [4] B became the shared part of the two rings. All else being equal the favoured reaction is the likely the one where the least number of stronger B – O bonds are broken.

Borax $Na_2[B_4O_5(OH)_4](H_2O)_8$, tinconalite $Na_2[B_4O_5(OH)_4](H_2O)_3$ and hungchaoite $Mg[B_4O_5(OH)_4](H_2O)_7$ have this borate polyanion as their structural unit in which it occurs as a finite cluster (Figure 7.12).

$$[B_4O_5(OH)_4]^{2-} \text{ (cluster)} \rightarrow [B_4O_6(OH)_2]^{2-} \text{ (chain)} + (H_2O)$$

$$[B_4O_6(OH)_2]^{2-} \text{ (chain)} \rightarrow [B_4O_7]^{2-} \text{ (framework)} + 2\ (H_2O)$$
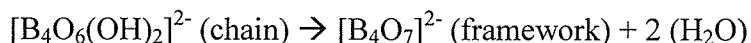
There do not appear to be any chain, sheet or framework structures composed of $[B_4O_5(OH)_4]^{2-}$ clusters in any configuration.

There are two tetraborates with different structural units: hydrochlorborite and kernite. Hydrochlorborite $Ca_2[B_3O_3(OH)_4[BO(OH)_3]Cl(H_2O)_7$ has a structural unit which is a three-membered $[B_3O_8]$ ring singly decorated by $[BO_3]$ (Figure 7.14) It might better fit with the triborates. The kernite $Na_2[B_4O_5(OH)_2](H_2O)_3$ structure is based on chains with a basic unit formula of $B_4O_6(OH)_2$; a three-membered $[B_3O_8]$ ring singly decorated by $[BO_3]$ (Figure 7.13).

7.12 (a)

a

← *c/2* →

7.12 (b)

c/2

← *a* →

126
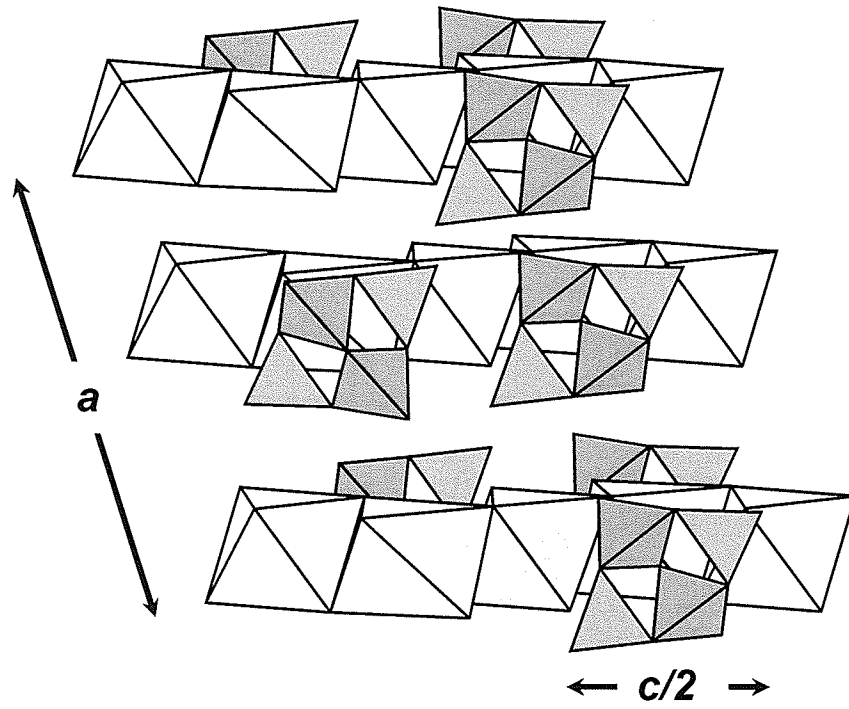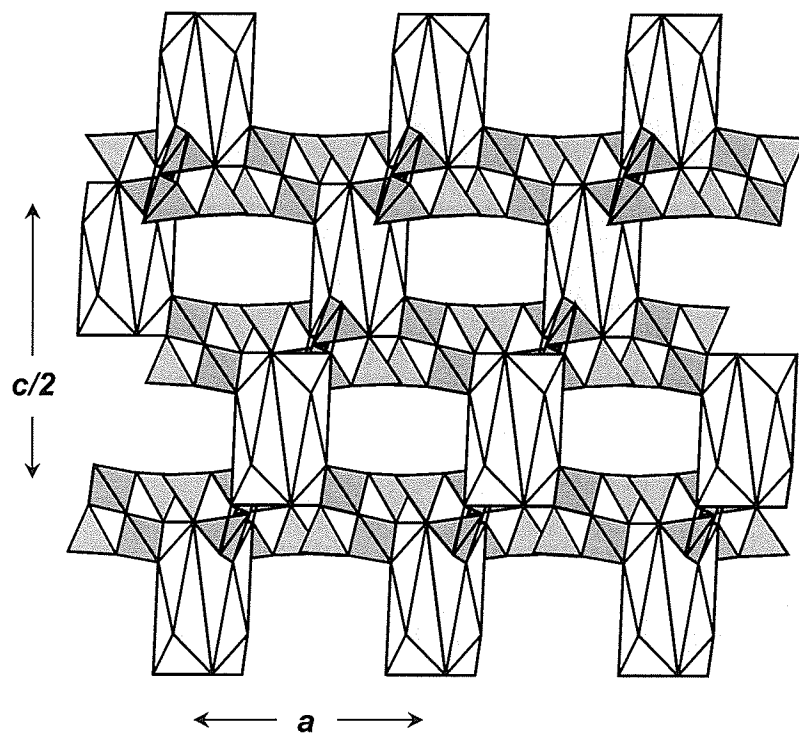
7.12
(c)
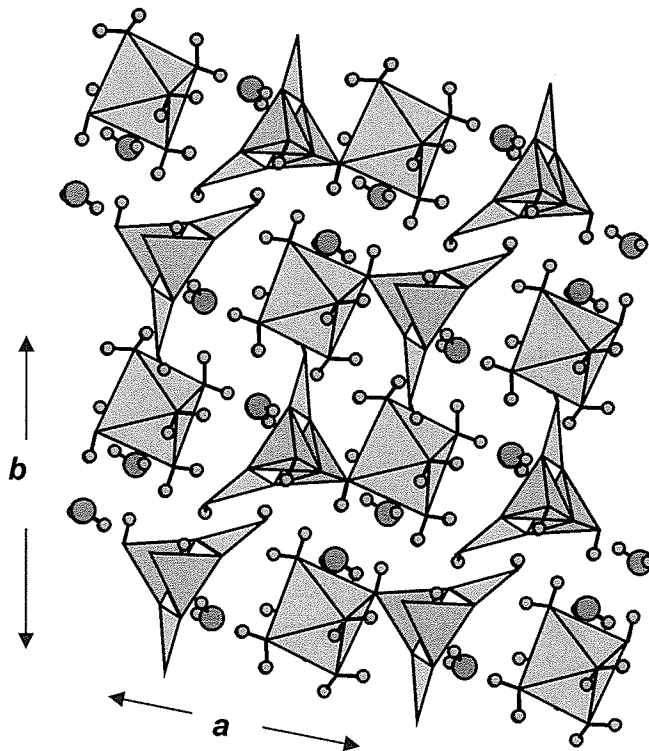
Figure 7.12. The crystal structures of (a) borax $Na_2[B_4O_5(OH)_4](H_2O)_8$, (b) tincalconite $Na_2[B_4O_5(OH)_4](H_2O)_3$ and (c) hungchaoite $Mg[B_4O_5(OH)_2](H_2O)_3$. In (a) B tetrahedra are dark blue and B triangles are green; in (b) and (c) B tetrahedra are green and B triangles are light blue. Na is yellow, Mg is pink. Hydrogen omitted from (a) and (b) for simplicity.
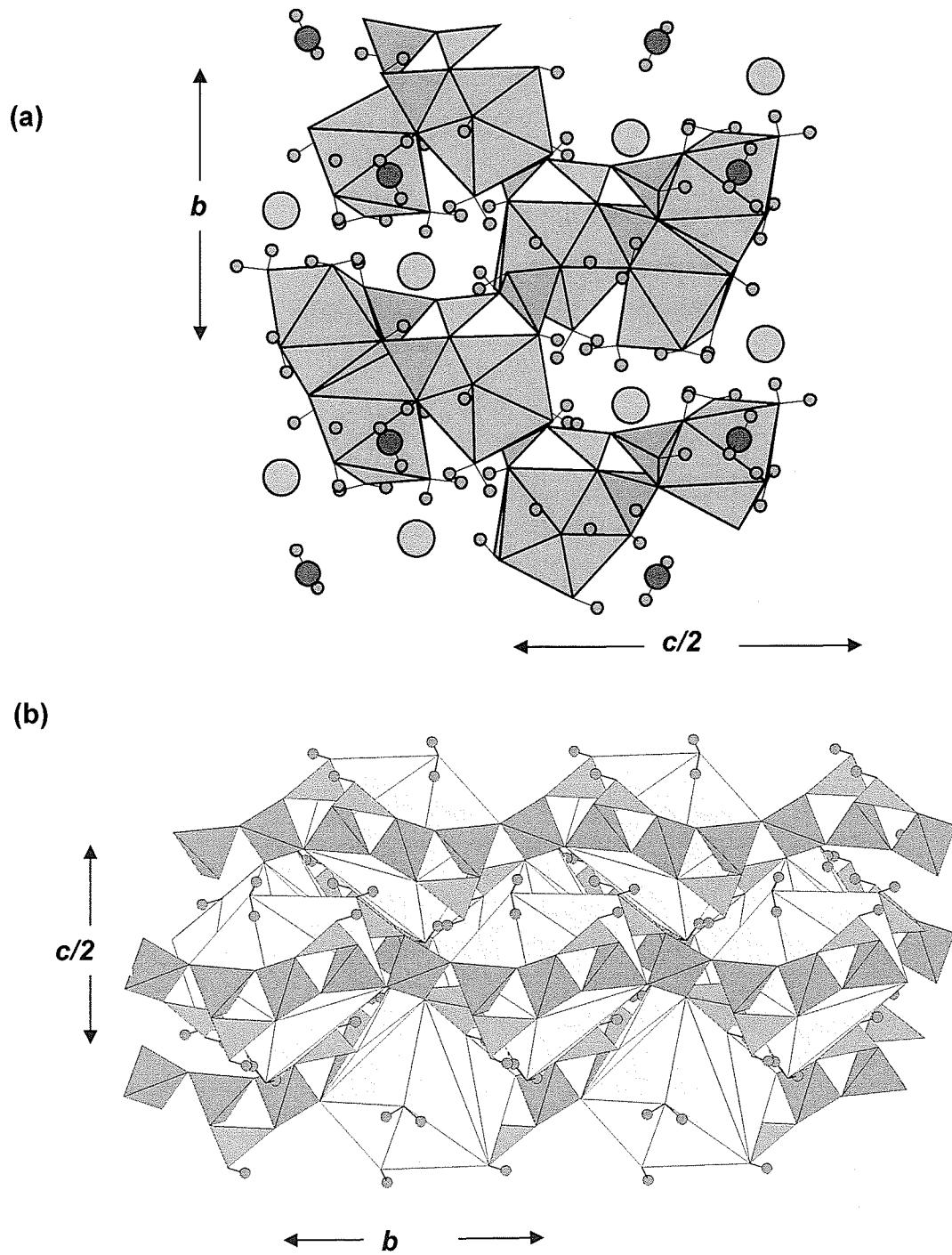
Figure 7.13. The crystal structures of (a) hydrochlorborite and (b) kernite.

7.9 Pentaborates

The pentaborate complex known to occur in aqueous solution is a cluster of five B polyhedra, composed of two three-membered rings with a common BO_4 group; both rings consist of two B triangles and one B tetrahedron, sharing the B tetrahedron (Figure 7.14). This cluster is not found as a structural unit in any known mineral.
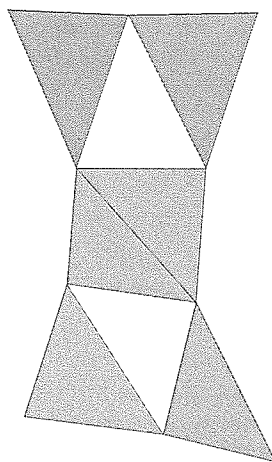
Figure 7.14. The structure of $[B_5O_6(OH)_4]^-$;terminal hydrogen atoms omitted.

In solution, this cluster occurs within a very narrow region of stability in the pH range of 5-7 that is strongly controlled by the activity of B in solution. It can be formed from the polymerization of aqueous complexes according to the following schemes:
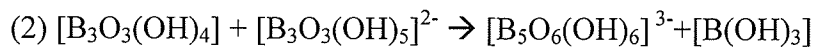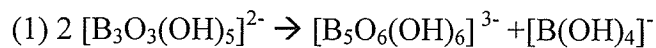
$$[B_3O_3(OH)_4] + 2[B(OH)_3] \rightarrow [B_5O_6(OH)_4]^- + 6\ H^+$$

$$2[B_3O_3(OH)_4] \rightarrow [B_5O_6(OH)_4]^- + [B(OH)_4]^-$$

$$2\ [B_3O_3(OH)_4]^-\ [B_5O_6(OH)_4]^- + [B(OH)_4]^-$$
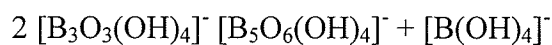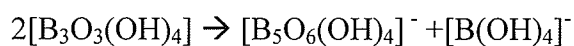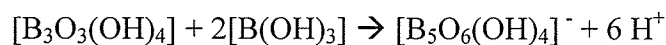
7.9.1 Pentaborate crystal structures with $[B_5O_6(OH)_6]^{3-}$ structural unit

$[B_5O_6(OH)_6]^{3-}$ is not found as a complex in borate solutions, however it is the fundamental building block of a number of minerals. It is a cluster of five B polyhedra; two three-membered rings consisting of one B triangle and two B tetrahedrons each sharing one of the B tetrahedra (Figure 7.15).
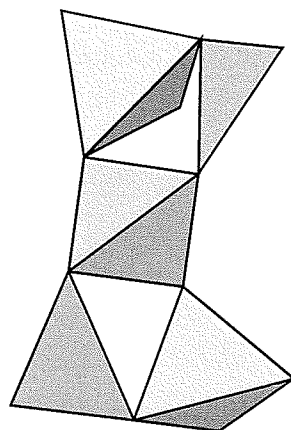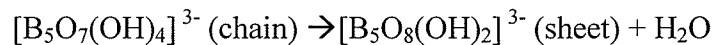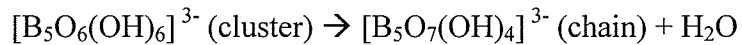

Figure 7.15. The structure of $[B_5O_6(OH)_6]^{3-}$; terminal H atoms omitted.

The cluster may be formed by the polymerization of various aqueous complexes according to the following schemes:

$$(1)\ 2\ [B_3O_3(OH)_5]^{2-} \rightarrow [B_5O_6(OH)_6]^{3-} + [B(OH)_4]^-$$

$$(2)\ [B_3O_3(OH)_4] + [B_3O_3(OH)_5]^{2-} \rightarrow [B_5O_6(OH)_6]^{3-} + [B(OH)_3]$$

$$(3)\ [B_3O_3(OH)_4]^- + 2[B(OH)_4]^- \rightarrow [B_5O_6(OH)_6]^{3-} + 3\ H_2O$$

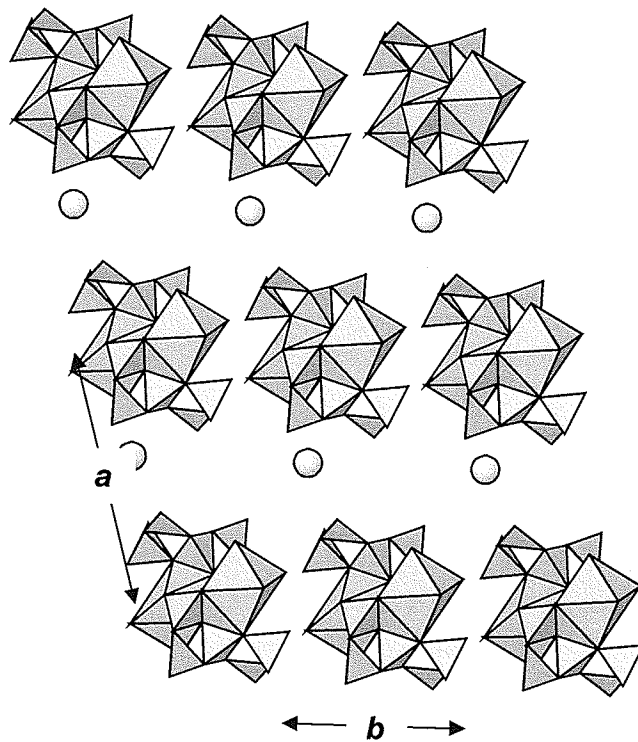$$(4)\ [B_3O_3(OH)_5]^{2-} + [B(OH)_4]^- + [B(OH)_3] \rightarrow [B_5O_6(OH)_6]^{3-} + 2\ H_2O + OH^-$$
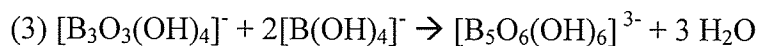
It seems more likely that two identical complexes would be utilized unless the solution composition was on or near the equilibrium boundary between the complex stability fields. However, we must also consider that the most likely reactions to occur would be the ones with the least degree of B − O bond breaking and reorganization of B polyhedra.
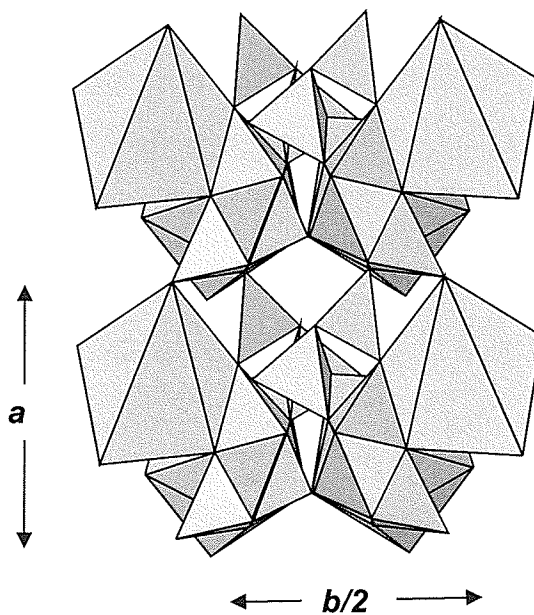
Ulexite $NaCa[B_5O_6(OH)_6](H_2O)_5$ contains this isolated pentaborate cluster which can be polymerized to form the infinite chains found in probertite $NaCa[B_5O_7(OH)_4](H_2O)_3$, the infinite sheets found in tuzlaite $NaCa[B_5O_8(OH)_2](H_2O)_3$ and the framework found in hilgardite (group) $Ca[B_5O_9]Cl(H_2O)$ (Figure 7.16) according to the following schemes:

$$[B_5O_6(OH)_6]^{3-} \text{ (cluster)} \rightarrow [B_5O_7(OH)_4]^{3-} \text{ (chain)} + H_2O$$

$$[B_5O_7(OH)_4]^{3-} \text{ (chain)} \rightarrow [B_5O_8(OH)_2]^{3-} \text{ (sheet)} + H_2O$$

$$[B_5O_8(OH)_2]^{3-} \text{ (sheet)} \rightarrow [B_5O_9]^{-} \text{ (framework)} + H_2O$$
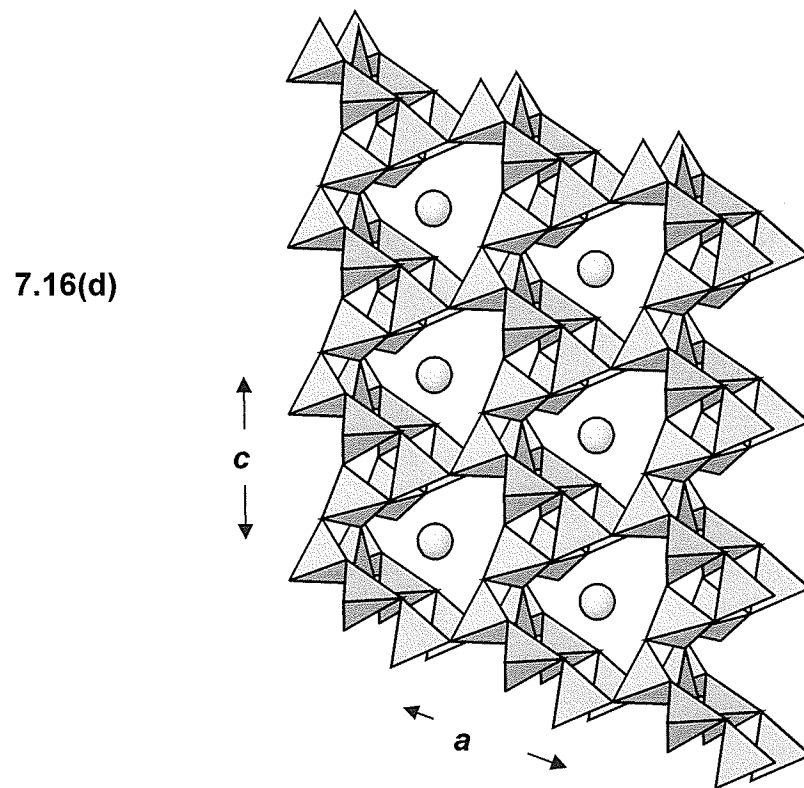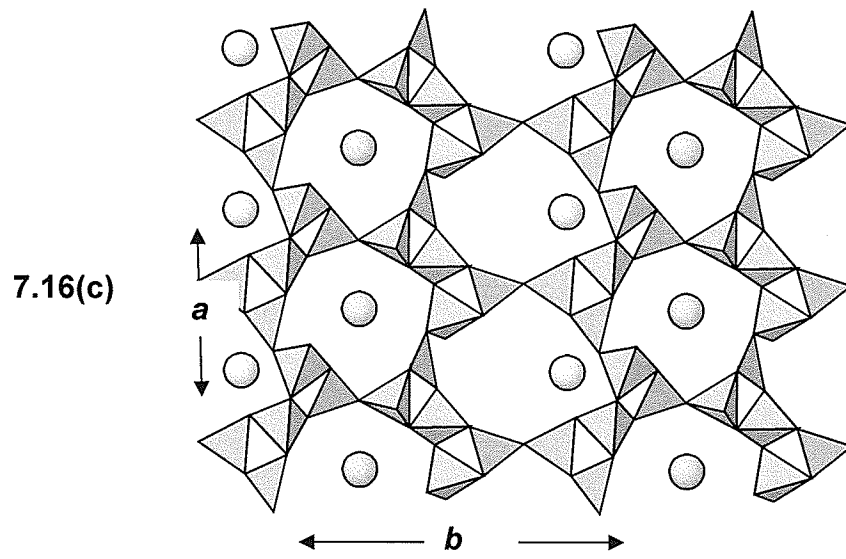
7.16(a)

a

b

7.16(b)

a

b/2

132

Figure 7.16. The crystal structures of (a) ulexite, (b) probertite, (c) tuzlaite, and (d) hilgardite 1-A.
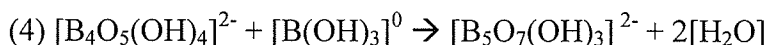
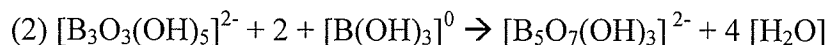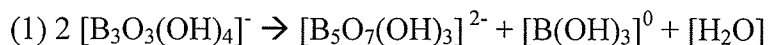## 7.9.2 Pentaborate crystal structures with the $[B_5O_7(OH)_3]^{2-}$ structural unit

$[B_5O_7(OH)_3]^{2-}$ is not found as a complex in borate solutions, however it is the fundamental building block of a number of minerals. It is a cluster of five B polyhedra; two three-membered rings with a common BO_4 group. One ring consists of two B triangles and one B tetrahedron and the other consists of two B tetrahedra and one tetrahedron. sharing one of the B tetrahedra (Figure 7.17).
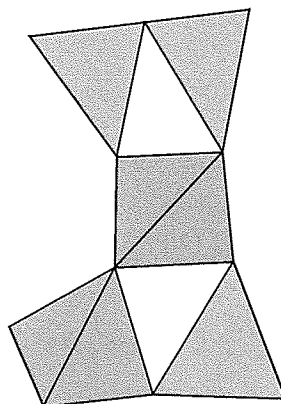

Figure 7.17. The structure of $[B_5O_7(OH)_3]^{2-}$ terminal hydrogen omitted.

The cluster (which, in its isolated form is not known in to occur in crystal structures) may be formed by the polymerization various complexes according to the following schemes:
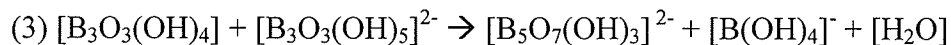
$$(1)\ 2\ [B_3O_3(OH)_4]^- \rightarrow [B_5O_7(OH)_3]^{2-} + [B(OH)_3]^0 + [H_2O]$$

$$(2)\ [B_3O_3(OH)_5]^{2-} + 2 + [B(OH)_3]^0 \rightarrow [B_5O_7(OH)_3]^{2-} + 4\ [H_2O]$$

$$(3)\ [B_3O_3(OH)_4] + [B_3O_3(OH)_5]^{2-} \rightarrow [B_5O_7(OH)_3]^{2-} + [B(OH)_4]^- + [H_2O]$$

$$(4)\ [B_4O_5(OH)_4]^{2-} + [B(OH)_3]^0 \rightarrow [B_5O_7(OH)_3]^{2-} + 2[H_2O]$$

It seems more likely that two identical complexes would be utilized unless the solution composition was on or near the equilibrium boundary between the complex stability fields. However, we must also consider that the most likely reactions to occur would be the ones with the least degree of B – O bond breaking and reorganization of B polyhedra.

There are no structures that contain this structural unit as an isolated cluster. Ezcurrite $Na_2[B_5O_7(OH)_3](H_2O)_2$ contains this pentaborate cluster as the structural unit forming chains (Figure 7.18). It can be polymerized to form the sheets found in biringuccite $Na_2[B_5O_8(OH)](H_2O)$ (Figure 7.19) and nasinite $Na_2[B_5O_8(OH)](H_2O)_2$. Gowerite $Ca[B_5O_8(OH)][B(OH)_3](H_2O)_3$ and the veatchite group $Sr[B_5O_8(OH)][B(OH)_3](H_2O)_3$ contains the structural unit polymerized to form sheets; however they also contain an additional isolated $[B(OH)_3]^0$ group (Figures 7.19, 7.20). Polymerization occurs according to the following scheme:

$$[B_5O_7(OH)_3]^{2-}\ (chain) \rightarrow [B_5O_8(OH)]^{2-}\ (sheet) + H_2O$$
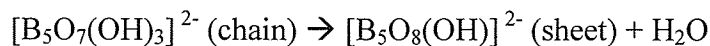
Because the structural units in gowerite and veatchite also contain isolated $[B(OH)_3]^0$

groups, one might speculate that they form via reaction (1) rather than in the sequence of
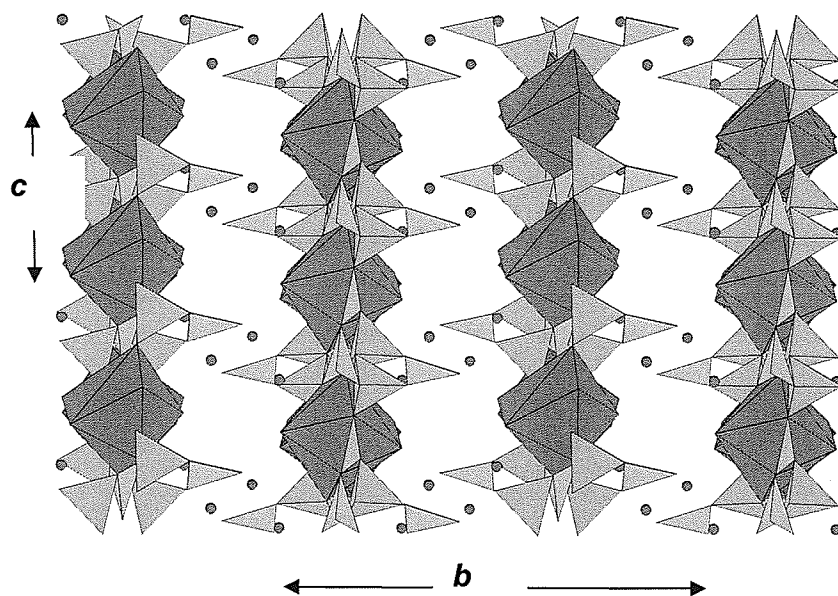
polymerization schemes.
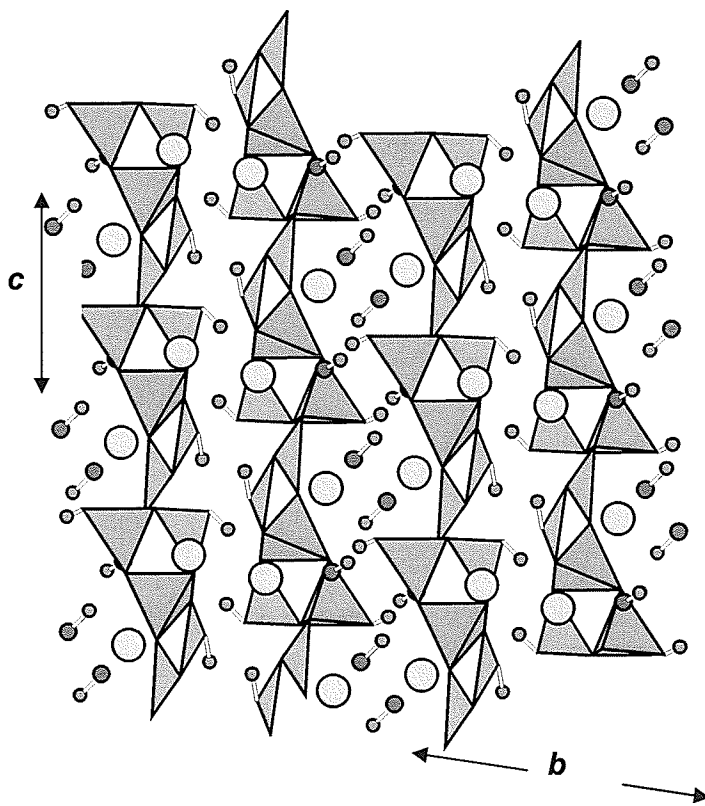
Figure 7.18. The crystal structure of ezcurrite $Na_2[B_5O_7(OH)_3](H_2O)_2$; Na is pink, [4]B is green, [3]B is light blue, H is grey, and O involved in H_2O groups is dark blue.
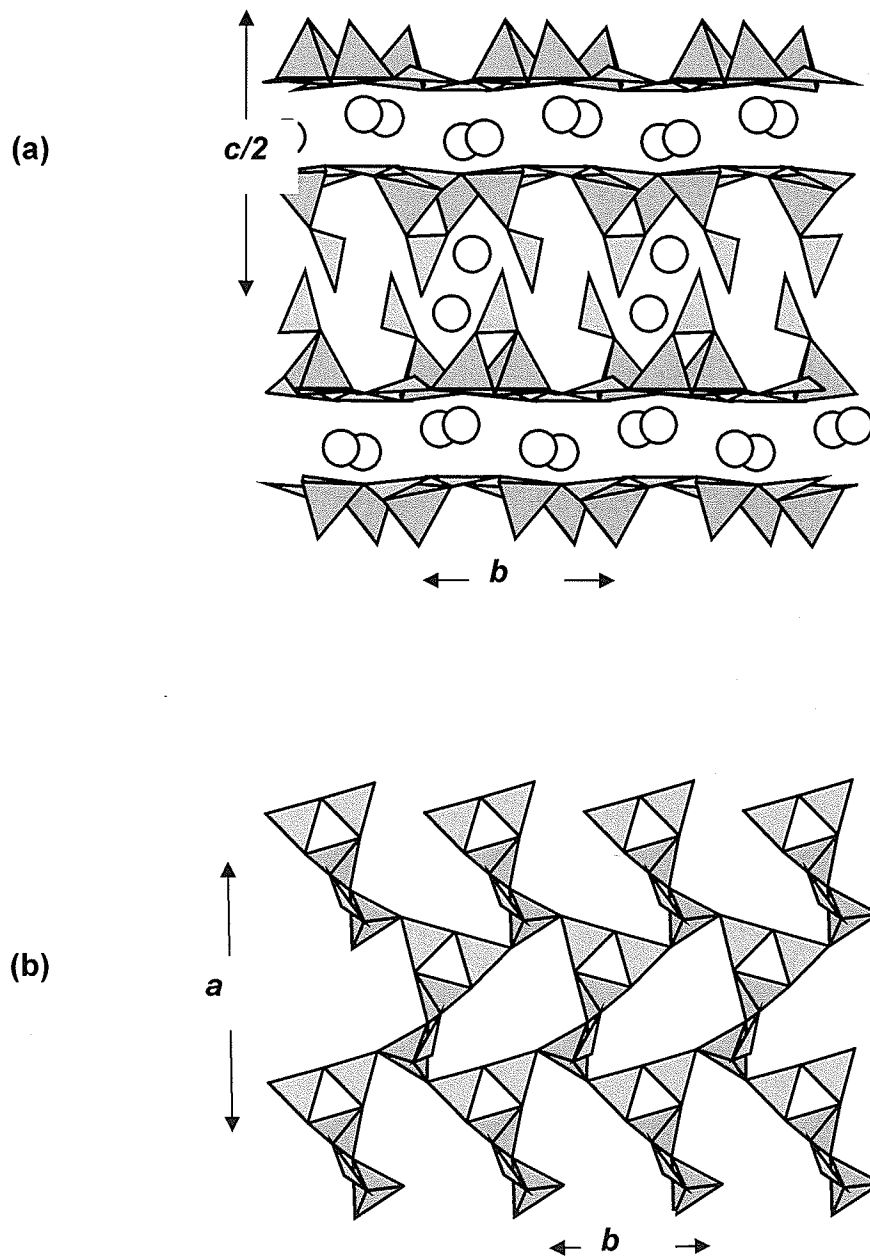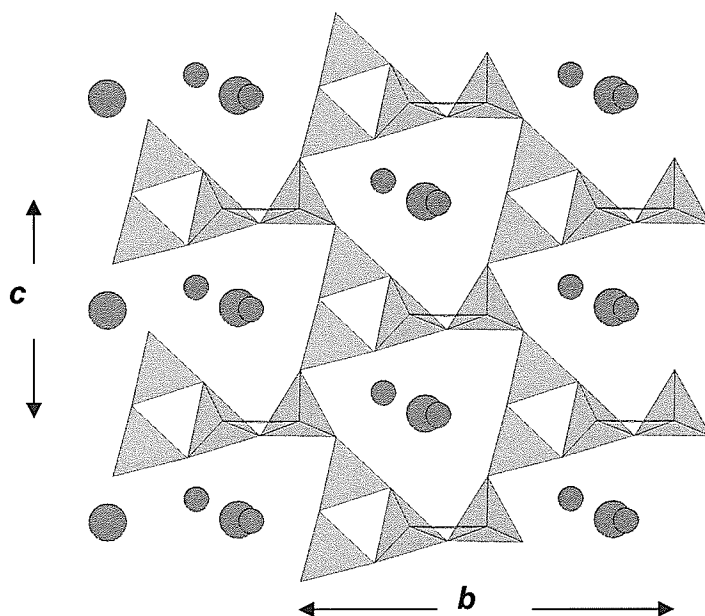
Figure 7.19. The crystal structure of biringuccite Na₂[B₅O₈(OH)](H₂O) (a), and the birunguccite borate sheet (b). Na is yellow, [4]B is blue, and [3]B is green.

Figure 7.20. The crystal structure of gowerite $Ca[B_5O_8(OH)][B(OH)_3](H_2O)_3$. Ca polyhedral are pink, [4]B is green, [3]B is light blue; dark blue dots represent interstitial H_2O.

Figure 7.21. The crystal structure of veatchite $Sr[B_5O_8(OH)][B(OH)_3](H_2O)_3$. Sr is pink, [4]B is green, [3]B is light blue; dark blue dots represent interstitial H_2O.

138

One exception is the pentaborate priceite $Ca_4[B_5O_7(OH)_5](H_2O)$ in which the structural unit is a cluster composed of 4 B tetrahedra and 1 B triangle. Its configuration is two three-membered rings (one with 3 tetrahedra and one with two tetrahedra and one triangle) that share a common tetrahedron; they are polymerized to form sheets held together by hydrogen bonds (Figure 7.22).

(a)

(b)
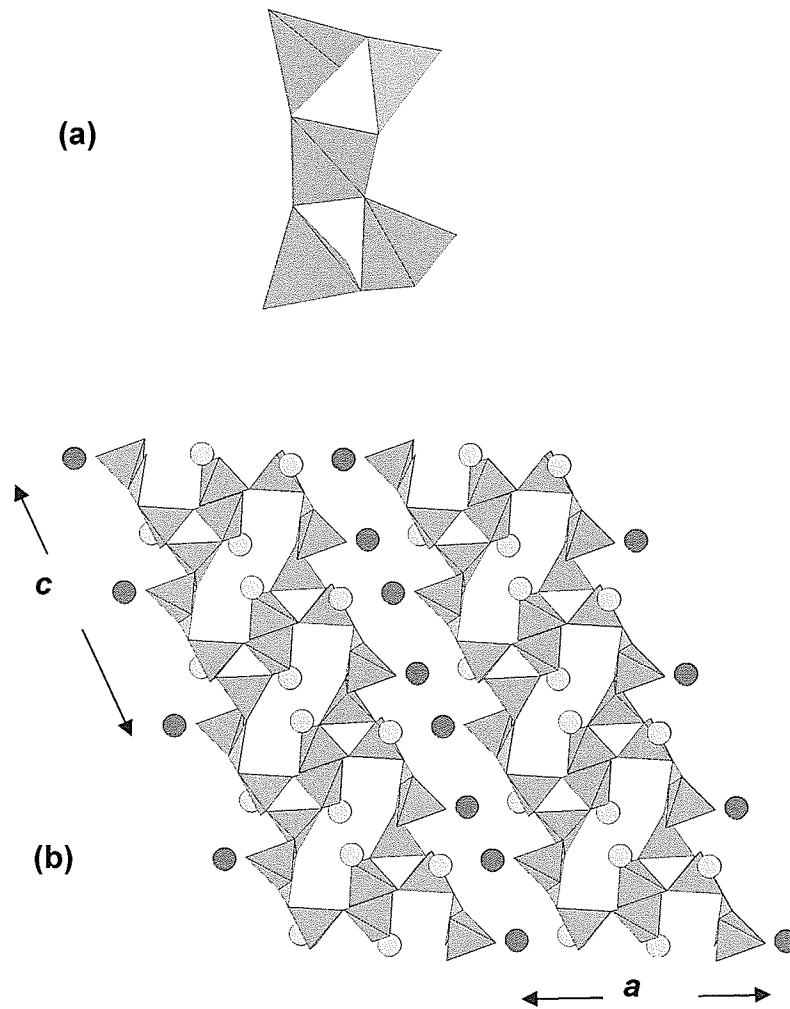
Figure 7.22. The crystal structure of priceite $Ca_4[B_5O_7(OH)_5](H_2O)$ (a) the structural unit and (b) the structural unit polymerized to form thick sheets. Ca is pink, [4] is blue, [3] is green, blue dots represent interstitial H_2O.

7.10 Hexaborate crystal structures

No hexaborate complexes are known in solution. All hexaborate structural units known in minerals are composed of 3 B tetrahedra and 3 B triangles and are arranged such that they form a cluster of 3 three-membered rings that share a common anion (Figure 7.23).
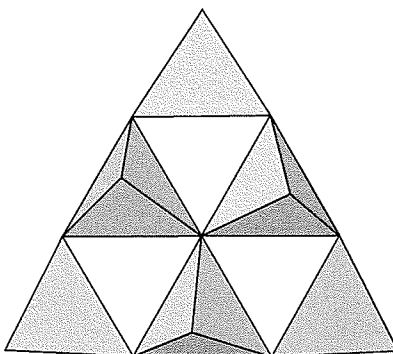
Figure 7.23. The structure of $[B_6O_7(OH)_6]^-$; terminal hydrogen atoms omitted.

It can be formed in aqueous solution by the polymerization of one of each of the three-membered ring clusters according to the following scheme:

$$[B_3O_3(OH)_4]^- + [B_3O_3(OH)_5]^{2-} \rightarrow [B_6O_7(OH)_6]^- + H_2O + OH^-$$
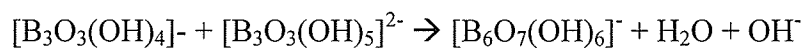
$[B_6O_7(OH)_6]^-$ is the finite cluster structural unit in the minerals mcallisterite

$Mg_2[B_6O_7(OH)_6]_2(H_2O)_9$, admontite $Mg_2[B_6O_7(OH)_6]_2(H_2O)_7$, aksaite
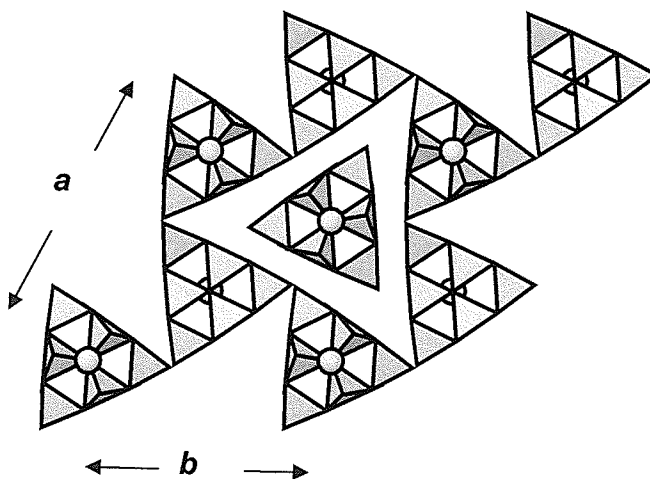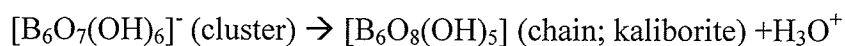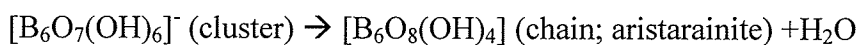
$Mg_2[B_6O_7(OH)_6]_2(H_2O)_2$ and rivadavite $Na_6Mg[B_6O_7(OH)_6]_4(H_2O)_{10}$ (Figures 7.24-7.27).

This cluster can be further polymerized into the chains found in aristarainite

$NaMg[B_6O_8)(OH)_4]_2(H_2O)_4$)Figure 7.28) (and kaliborite $KMg_2H[B_6O_8(OH)_5](H_2O)_4$,

which has a slightly different arrangement), and the sheets found in nobleite

$Ca[B_6O_9(OH)_2](H_2O)_3$ and tunellite $Sr[B_6O_9(OH)_2](H_2O)_3$(Figure 7.29).

$[B_6O_7(OH)_6]^-$ (cluster) → $[B_6O_8(OH)_4]$ (chain; aristarainite) +H_2O

$[B_6O_7(OH)_6]^-$ (cluster) → $[B_6O_8(OH)_5]$ (chain; kaliborite) +H_3O^+

$[B_6O_8(OH)_4]$ (chain; aristarainite)→ $[B_6O_9(OH)_2]^{2-}$ (sheet; tunellite) + H_2O

Figure 7.24. The crystal structure of mcallisterite $Mg_2[B_6O_7(OH)_6]_2(H_2O)_9$; Mg is pink, [4]B is green and [3]B is blue. Hydrogen omitted for simplicity.
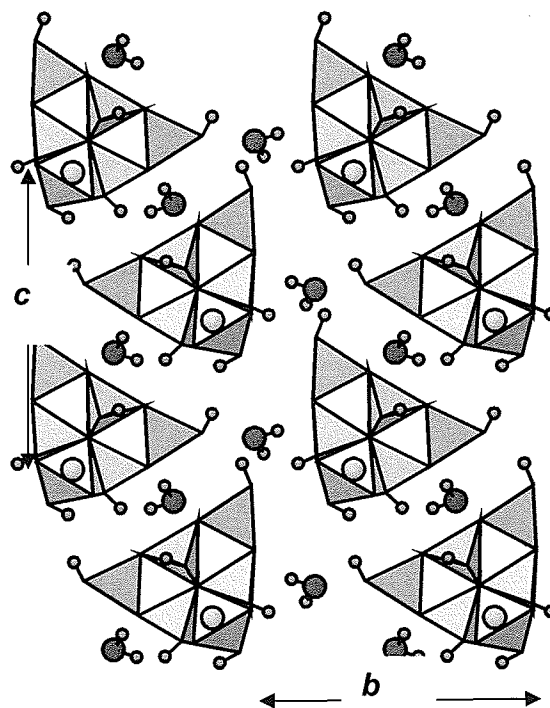
Figure 7.25. The crystal structure of admontite $Mg_2[B_6O_7(OH)_6]_2(H_2O)_7$; Mg is pink, [4]B is green, [3]B is blue, H_2O groups are red and grey.
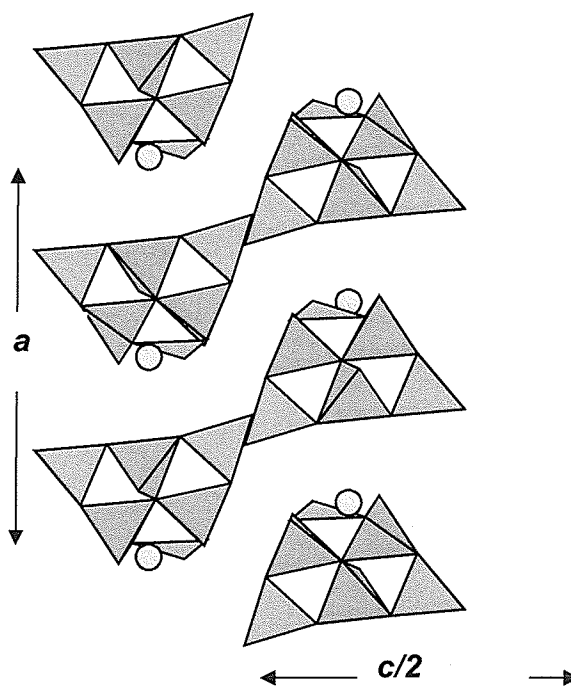
Figure 7.26. The crystal structure of aksaite $Mg_2[B_6O_7(OH)_6]_2(H_2O)_2$; Mg is pink, [4]B is green, [3]B is blue, H and H_2O omitted.

142
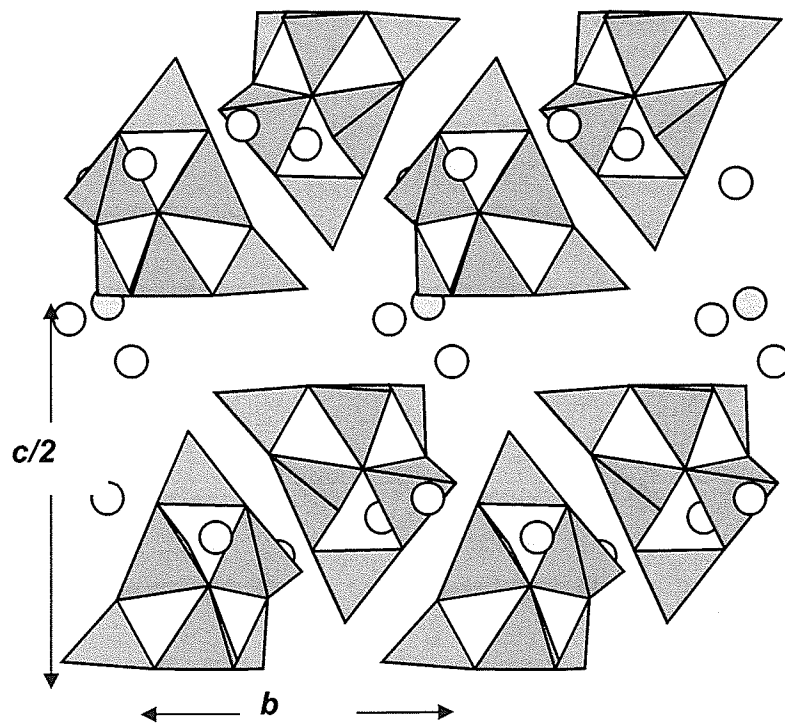
Figure 7.27. The crystal structure of rivadavite $Na_6Mg[B_6O_7(OH)_6]_4(H_2O)_{10}$; Mg is pink, Na is yellow, [4]B is green, [3]B is blue, H and H_2O omitted.
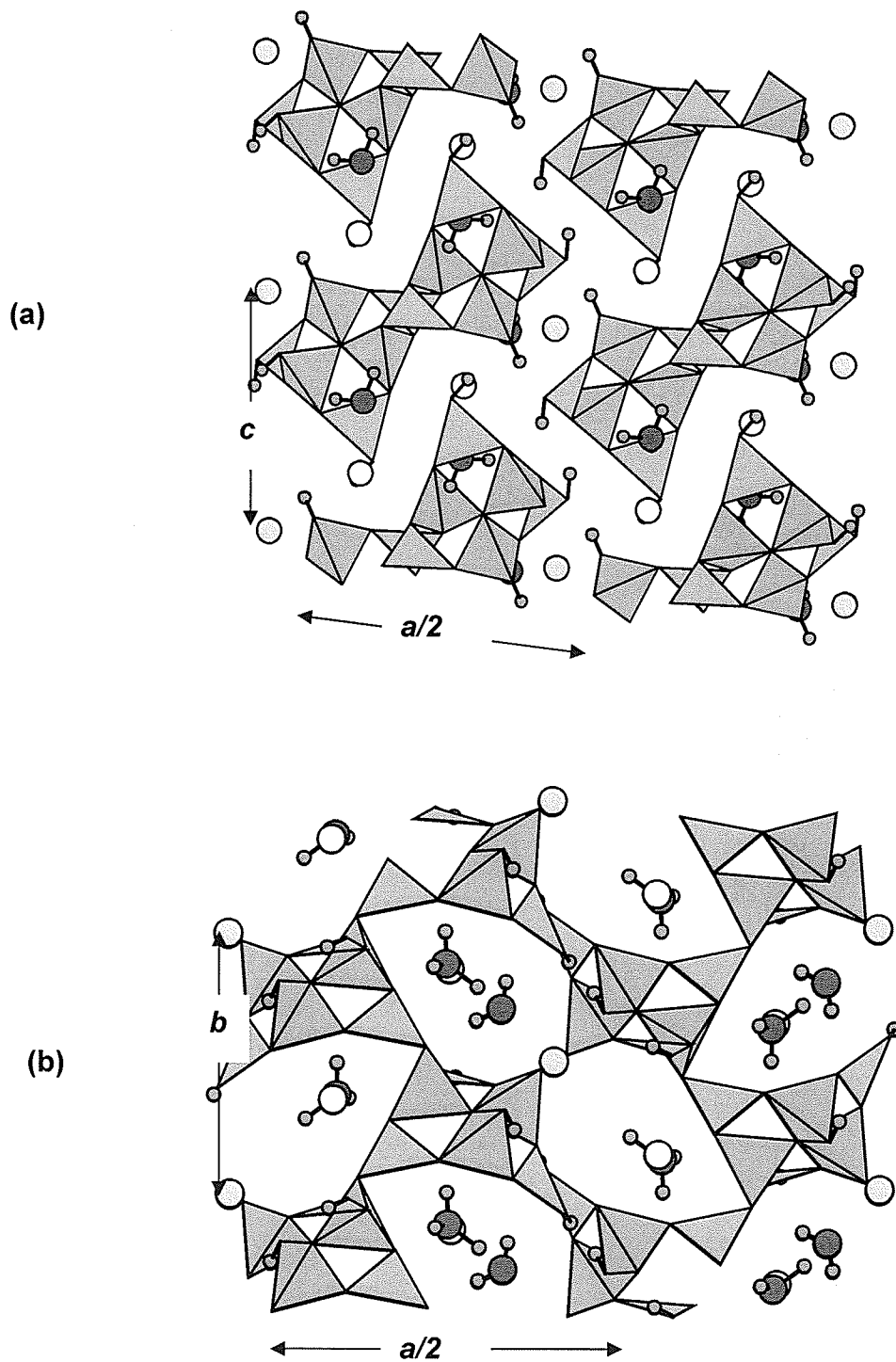
Figure 7.28. The crystal structure of aristarainite $NaMg[B_6O_8)(OH)_4]_2(H_2O)_4$ (a) viewed down b, showing the structural units, and (b) viewed down c, showing the linkage of the chains that extend in the b direction. Mg is pink, Na is yellow, [4]B is green, [3]B is blue, H is grey and O is red.

144
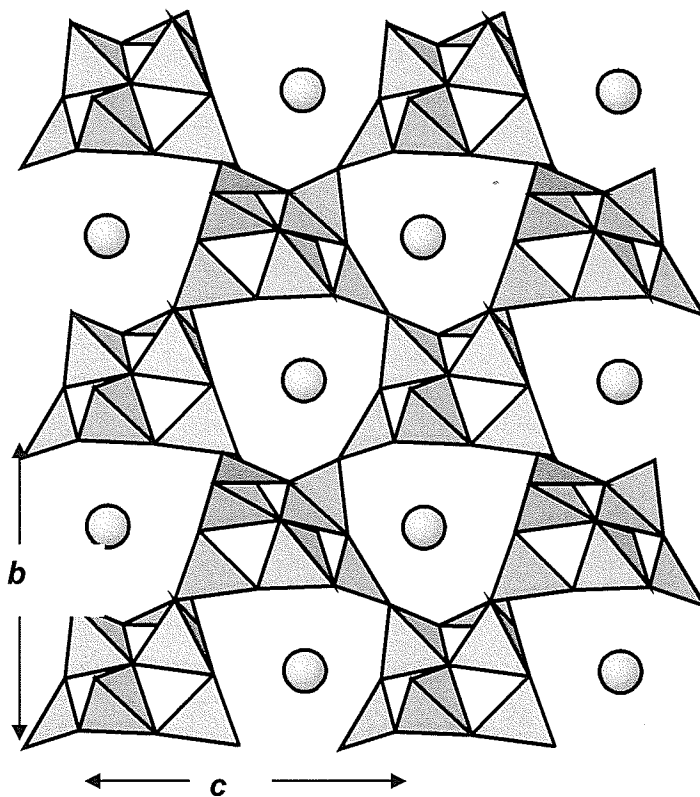
Figure 7.29. The crystal structure of tunellite $Sr[B_6O_9(OH)_2](H_2O)_3$; Sr is pink, [4]B is green, [3]B is blue, H and H_2O omitted.

7.11 Borates with structural units containing greater than six borate polyhedra

Most of the structural units contain six or less B polyhedra, however there are some exceptions. There are a number of borate sheet and framework structures with large and complex structural units which contain 8 to 26 boron atoms in both [3] and [4]-coordination. They have complex structures and chemistry, and many occurrences are low-temperature metamorphic, therefore they are difficult to relate to any paragenetic sequence.

The boracite-group M_3 [B_7O_{13}] Cl (M= Mg, Fe^{2+}, Mn^{2+}) have framework structures based on [B_7O_{13}]$^{5-}$ structural units. The structural unit is composed of six [4]-coordinated boron atoms and one [3]-coordinated boron atom, in the configuration of a hexaborate structural unit (but composed solely of [4]-coordinated boron) that is singly decorated by a boron triangle (Figure 7.30). The simplest way to form this structural unit from aqueous complexes is by combining isolated boron tetrahedra plus one triangle:

$$6 \ [B(OH)_4]^- + [B(OH)_3]^0 \rightarrow [B_7O_{13}]^{5-} + 13 \ H_2O + OH^-$$
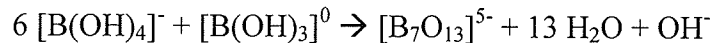
It could stoichiometrically be formed by other more complicated reactions involving various aqueous complexes, however this would require significant B-O bond breaking and polyhedra reorganization.
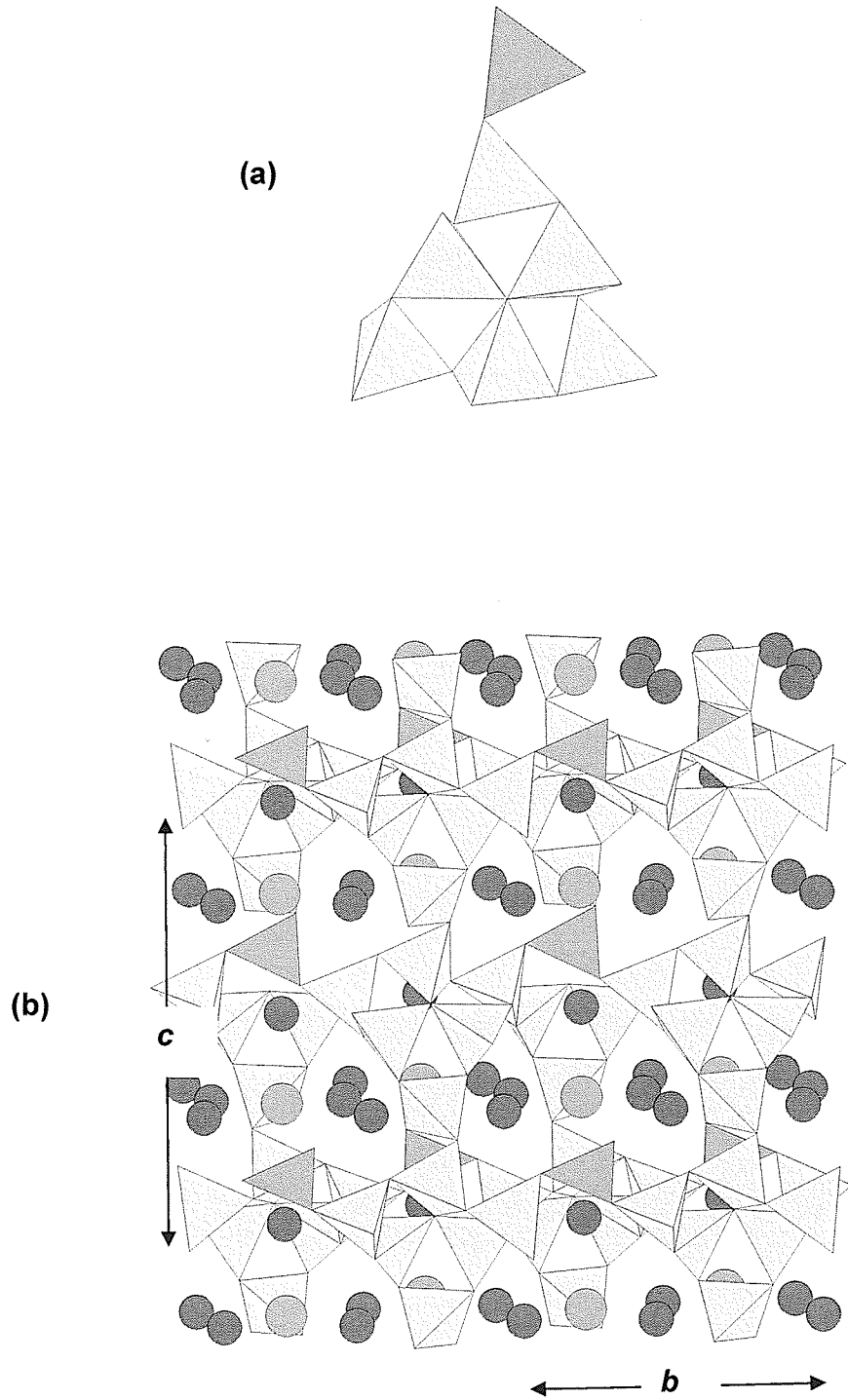
Figure 7.30 The boracite structural unit (a) and crystal structure (b); M^{2+} is pink, Cl is blue, [4]B isgreen and [3]B is blue.

Strontioborite $Sr[B_8O_{11}(OH)_4]$ has a sheet structure based on a $[B_8O_{11}(OH)_4]^{2-}$ structural unit(Figure 7.31). The structural unit is composed of five [3]-coordinated and three [4]-coordinated boron atoms, and is nearly identical to the hexaborate structural units which are composed of three [3]-coordinated and three [4]-coordinated boron atoms arranged such that they form a cluster of 3 three-membered rings that share a common anion, with the exception that one of the tetrahedrons links to a $[B_2O(OH)_4]^0$ dimer. It can be formed in a manner similar to the hexaborate structural unit, with the addition of two extra hydrated triangular groups:

$$[B_3O_3(OH)_4] + [B_3O_3(OH)_5]^{2-} + 2[B(OH)_3] \rightarrow [B_8O_7(OH)_{11}]^{2-} + 6\ H_2O + H^+$$
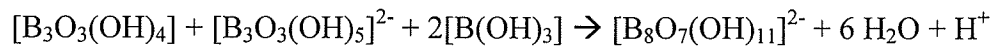
It seems likely that strontioborite $Sr[B_8O_{11}(OH)_4]$ and tunellite $Sr[B_6O_9(OH)_2](H_2O)_3$ are paragenetically related or strontioborite may be an alteration/dehydration product of tunellite; this is shown in the following reactions in terms of the chemistry of (a) the structural units only, and (b) the whole mineral compositions:

$$\text{(a)}\ [B_6O_9(OH)_2]^2 + 2[B(OH)_3] \rightarrow [B_8O_7(OH)_{11}]^{2-} + 2(H_2O)$$

$$\text{(b)}\ Sr[B_6O_9(OH)_2](H_2O)_3 + 2[B(OH)_3] \rightarrow Sr[B_8O_{11}(OH)_4] + 5\ (H_2O)$$
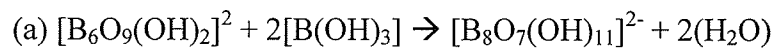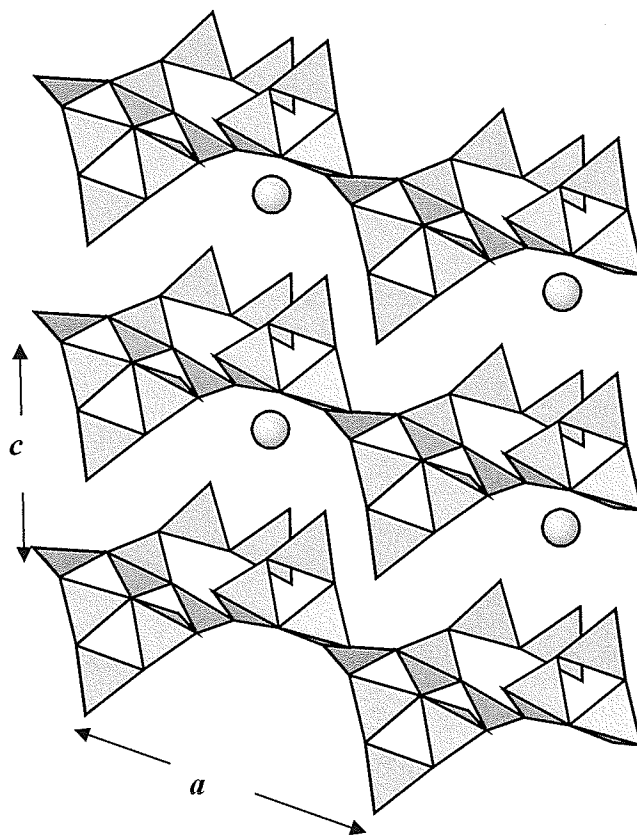
Figure 7.31 The crystal structure of strontioborite; Sr is pink, [4]B is green and [3]B is blue. Hydrogen omitted for clarity.

Penobsquisite $Ca_2Fe^{2+}[B_9O_{13}(OH)_6]Cl(H_2O)_4$ has a complicated framework structure based on a $[B_9O_{13}(OH)_6]$ structural unit (Figure 7.32). The fundamental building block is composed of fourteen [3]-coordinated and sixteen [4]-coordinated boron atoms and is produced by translations of the $[B_9O_{13}(OH)_6]$ unit (Figure 7.33). It can be formed by the polymerization of various aqueous complex as shown by the following scheme:

$$[B_3O_3(OH)_4] + 2[B_3O_3(OH)_5]^{2-} \rightarrow [B_9O_{13}(OH)_6] + 4\ H_2O$$
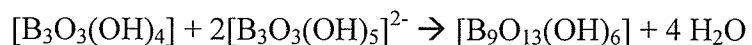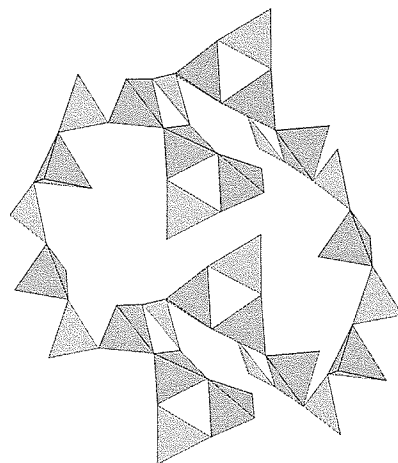
Figure 7.32 The structural unit in Penobsquisite $Ca_2Fe^{2+}[B_9O_{13}(OH)_6]Cl(H_2O)_4$; [4]B is blue and [3]B is green. Hydrogen omitted for clarity.
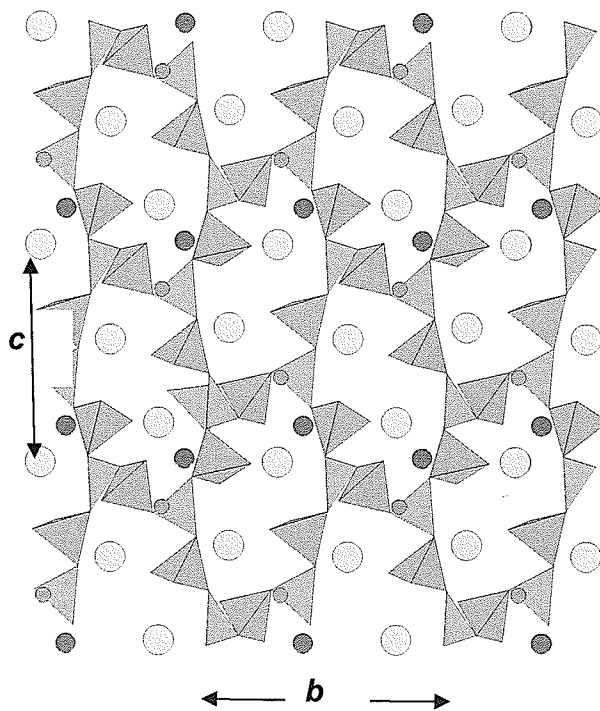
Figure 7.33 The crystal structure of Penobsquisite $Ca_2Fe^{2+}[B_9O_{13}(OH)_6]Cl(H_2O)_4$; Ca is pink, Fe is dark blue, Cl is green, [4]B is green and [3]B is blue. Hydrogen omitted for clarity.

Preobrazhenskite $Mg_3[B_{11}O_{15}(OH)_9]$ has a sheet structure based on a $[B_{11}O_{15}(OH)_9]^{6-}$ structural unit (Figure 7.34). The structural unit is composed of seven [4]-coordinated and five [3]-coordinated boron atoms (Figure 7.35). It can be formed by the polymerization of aqueous borate complexes as shown by the following scheme:

$$[B_3O_3(OH)_4] + 2[B_3O_3(OH)_5]^{2-} + 2[B(OH)_3] \rightarrow [B_{11}O_{15}(OH)_9]^{6-} + 6\ H_2O + H^+$$

This reaction is exactly the same as for the formation of the strontioborite structural unit but with one additional $[B_3O_3(OH)_5]^{2-}$ group. It is also very similar to the reaction forming the preobrazhenskite structural unit but without the two additional $B(OH)_3$ groups.
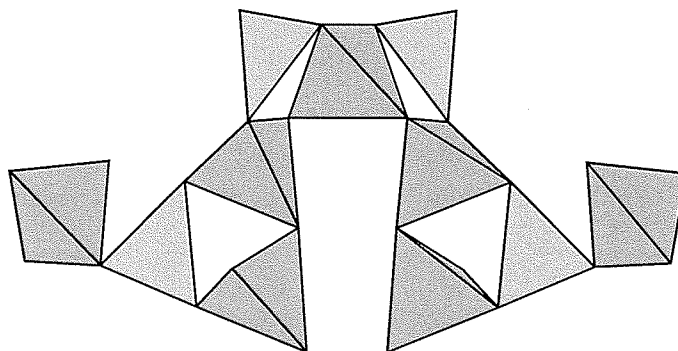
Figure 7.34 The $[B_{11}O_{15}(OH)_9]^{6-}$ structural unit in preobrazhenskite $Mg_3[B_{11}O_{15}(OH)_9]$; [4]B is blue and [3]B is green. Terminal and symmetric hydrogen bonds not shown.
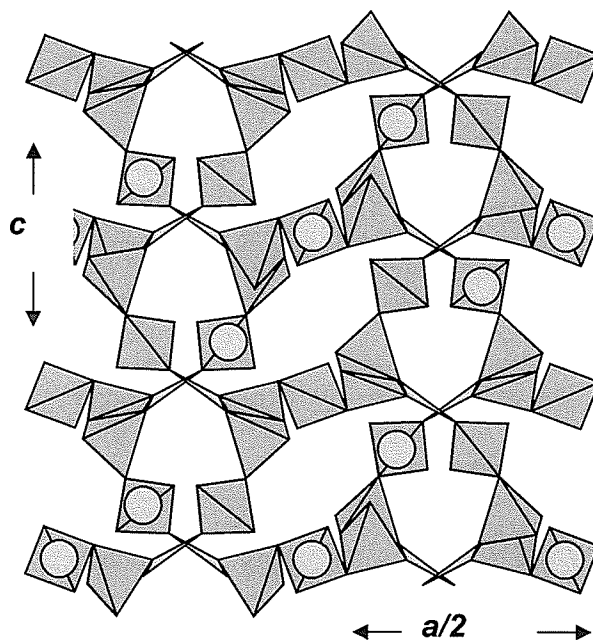
Figure 7.35 The (010) sheet in preobrazhenskite $Mg_3[B_{11}O_{15}(OH)_9]$; [4]B is blue and [3]B is green, Mg is pink. Hydrogen not shown.

Ginorite $Ca_2[B_{14}O_{20}(OH)_6](H_2O)_5$ and strontioginorite $SrCa[B_{14}O_{20}(OH)_6](H_2O)_5$ have sheet structures based on a $[B_{14}O_{20}(OH)_6]^{4-}$ structural unit. The structural unit is composed of six [4]-coordinated and eight [3]-coordinated boron atoms linked so that it is a dimerized $[B_6O_7(OH)_6]^-$ "mccallisterite-like" cluster decorated by a triangular pyroborate group (Figure 7.36 and 7.37). It can be formed in aqueous solution by the polymerization of two of each of the three-membered ring clusters and two $B(OH)_3$ groups according to the following scheme:

$$2[B_3O_3(OH)_4] + 2[B_3O_3(OH)_5]^{2-} + 2[B(OH)_3] \rightarrow [B_{14}O_{20}(OH)_6]^{4-} + 9H_2O + O^{2-}$$
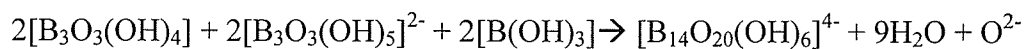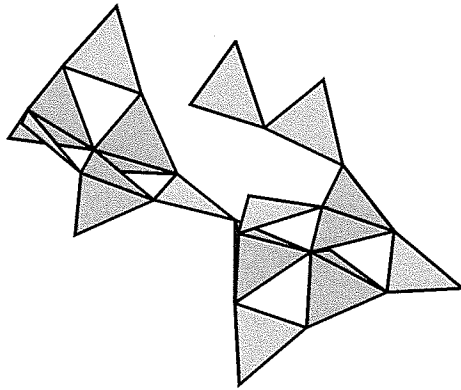
Figure 7.36 The $[B_{14}O_{20}(OH)_6]^{4-}$ structural unit in ginorite; [4]B is blue and [3]B is green.
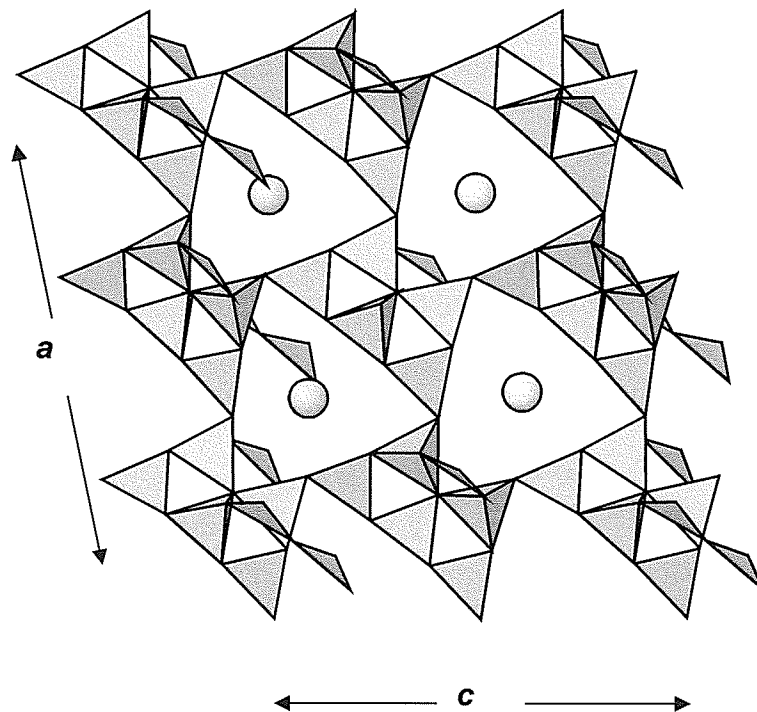
Figure 7.37 The (010) sheet in Ginorite $Ca_2[B_{14}O_{20}(OH)_6](H_2O)_5$; [4]B is green and [3]B is blue, Ca is pink. Hydrogen not shown.

It seems possible that ginorite and nobleite $Ca[B_6O_9(OH)_2](H_2O)_3$ are paragenetically related or ginorite may be an alteration/dehydration product of nobleite; this is shown in the following reactions in terms of the chemistry of (a) the structural units only, and (b) the whole mineral compositions:

(a) $2 [B_6O_9(OH)_2]^2 + 2[B(OH)_3] \rightarrow [B_{14}O_{20}(OH)_6]^{4-} + 2(H_2O)$

(b) $2 Ca[B_6O_9(OH)_2](H_2O)_3 + 2[B(OH)_3] \rightarrow Ca_2[B_{14}O_{20}(OH)_6](H_2O)_5 + 3 (H_2O)$

Strontioginorite may be an intermediate paragenetic step between the Ca and Sr borates based on the $[B_6O_7(OH)_6]^-$ unit:

nobleite $Ca[B_6O_9(OH)_2](H_2O)_3$ ginorite $Ca_2[B_{14}O_{20}(OH)_6](H_2O)_5$

strontioginorite $SrCa[B_{14}O_{20}(OH)_6](H_2O)_5$

tunellite $Sr[B_6O_9(OH)_2](H_2O)_3$ strontioborite $Sr[B_8O_{11}(OH)_4]$

strontioborite $Sr[B_8O_{11}(OH)_4] +$ nobleite $Ca[B_6O_9(OH)_2](H_2O)_3 + 2(H_2O) =$ strontioginorite $SrCa[B_{14}O_{20}(OH)_6](H_2O)_5$
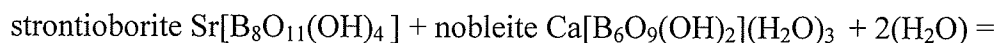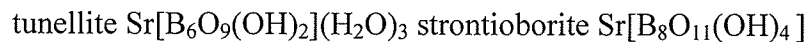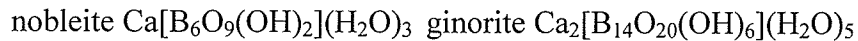
Some general observations are: 1) there are no known Mg or Na $[B_6O_7(OH)_6]^-$ borates (mcallisterite, admontite, aksaite, rivadavite) polymerized to > hexaborate structures as the Ca and Sr $[B_6O_7(OH)_6]^-$ borates are , and 2) all Ca and Sr minerals with structures based $[B_6O_7(OH)_6]^-$ structural units are sheet structures.

154

The polymorphs pringleite and ruitenbergite $Ca_9[B_{26}O_{34}(OH)_{24}]Cl_4(H_2O)_{13}$ are framework structures based on extremely large and complex structural units of the composition $[B_{26}O_{34}(OH)_{24}]^{14-}$.(Figure 7.39.). The structural units are composed of thirteen [4]-coordinated boron atoms and fourteen [3]-coordinated boron atoms that share corners in the configuration shown in Figure 7.38. These minerals are thought to have metamorphic origin and may not crystallize directly from solutions.
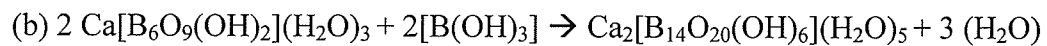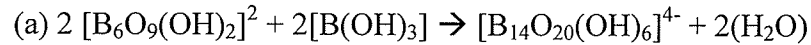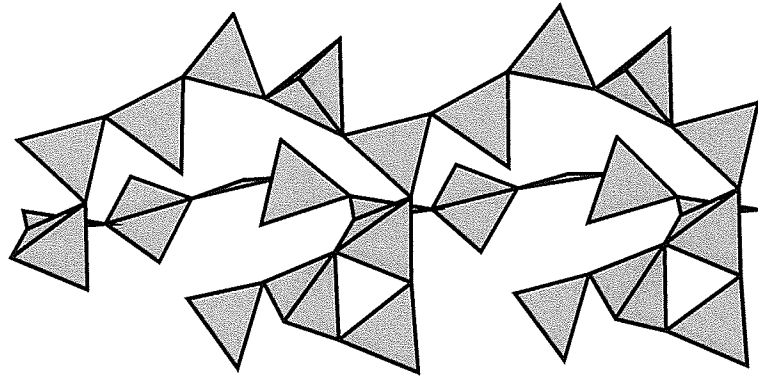

Figure 7.38. The $[B_{26}O_{34}(OH)_{24}]^{14-}$ structural unit in pringleite; [4]B is blue and [3]B is green. Hydrogen not shown.

155
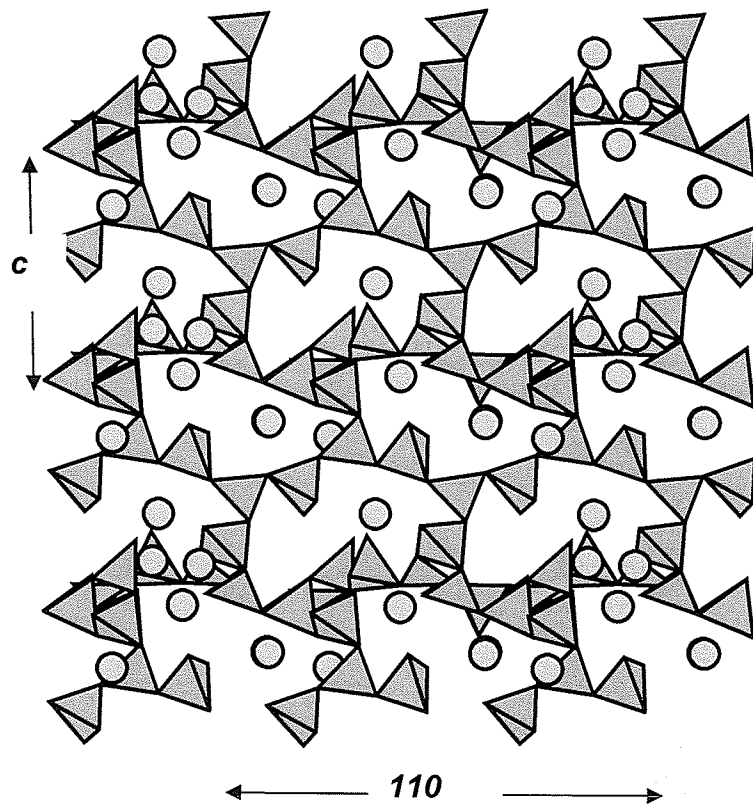
Figure 7.39. The crystal structure of pringleite $Ca_9[B_{26}O_{34}(OH)_{24}]Cl_4(H_2O)_{13}$[4]B is blue and [3]B is green, Ca is pink. Hydrogen not shown.

7.12 Toward the origin of the "megaborates"

In the previous section, possible paragenetic links were proposed for several of the minerals with structural units consisting of more than six borate polyhedra. Preobrazhenskite, penobsquisite, and the polymorphs pringleite and ruitenbergite have the most complex borate structures and may be of metamorphic origin; hence they are difficult to relate to any paragenetic sequence.

Using the data of Ingri (1963)(Figure 7.40), the percentage of each complex present at specific pH values was calculated. The degree of polymerization for each aqueous borate complex in solution was determined (the number of shared oxygens divided by the total number of oxygens), and then using the calculated percentages of each complex at specific pH values, a bulk polymerization degree was determined. Figure 7.41 shows the bulk polymerization degree of borate complexes in 0.4M $B(OH)_3$ solution as a function of pH. Maximum polymerization occurs at pH 8.8, which is in the pH range where maximum concentration of borate complexes exist. The area of maximum bulk polymerization corresponds almost exactly to the outer limit of the speciation fields of the aqueous borate complex (excluding isolated $[B(OH)_3]^0$ and $[B(OH)_4]^-$ fields (Figure 7.41)

Ingri, N. (1963): Equilibrium studies of polyanions containing B(III), Si(IV), Ge(IV) and V(V). *Svensk Kemisk Tidskrift*. **74**(4). 199-230.

Figure 7.40. Borate speciation in 0.4M B(OH)₃ solution (after Ingri, 1963)
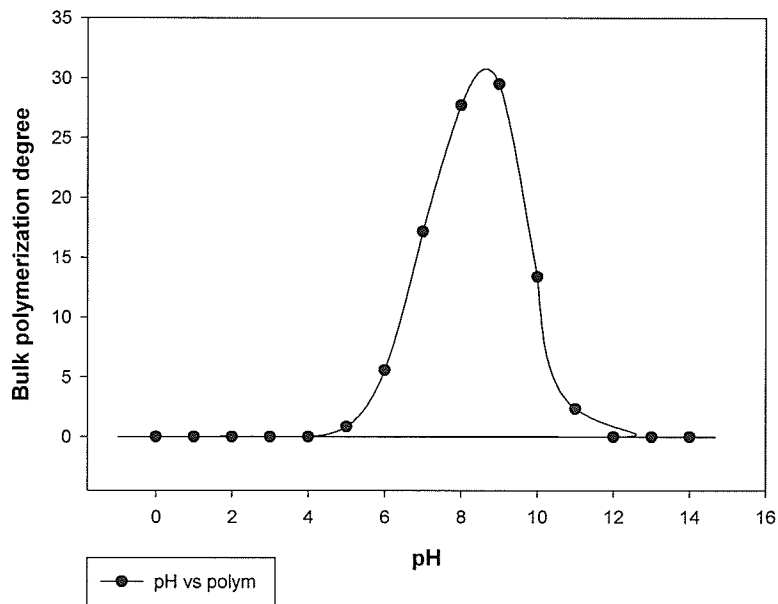
Figure 7.41. Bulk polymerization degree of borate complexes in 0.4M B(OH)₃ solution as a function of pH.

Figure 7.42 shows the bulk polymerization degree of borate complex in a 0.4M

B(OH)3 solution plotted as a function of bulk average basicity. Maximum polymerization

within solution corresponds to an average basicity of about 0.32 vu; it is noteworthy that

the complex borate structural units in the "megaborates" pringleite and ruitenbergite have

average basicitites of 0.32 vu. The two other largest borate structural units of

preobrazhenskite and penobsquisite have average basicities of 0.33 vu. These average

basicities correspond to a pH of about 8.8. Thus these borates with extremely large and

complex structural units may have crystallized from highly concentrated borate solutions

with a pH ~8.8.
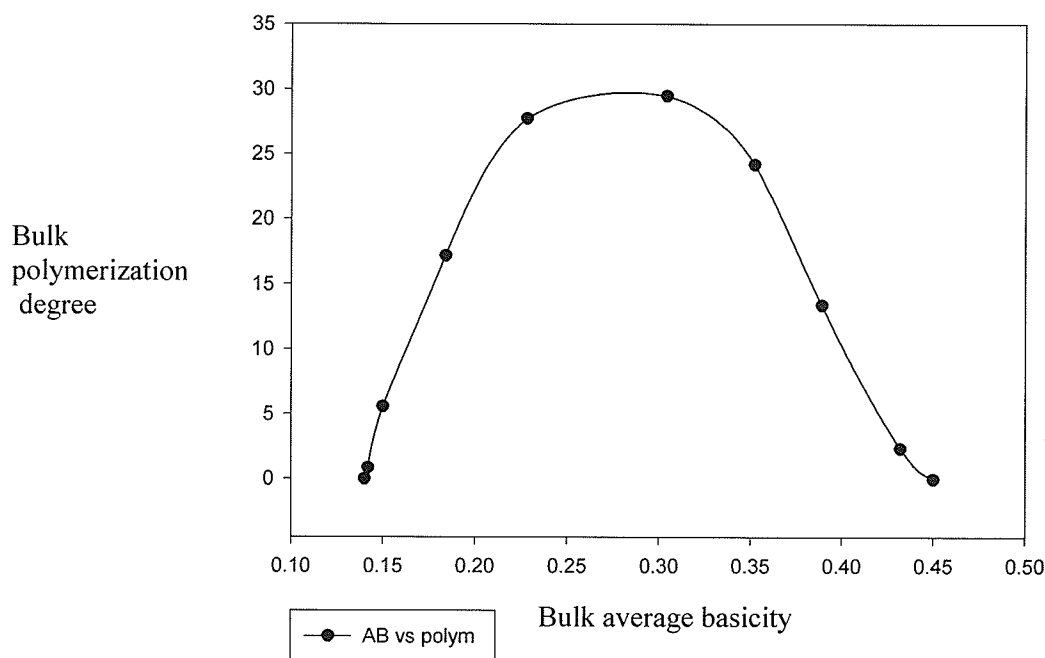
Figure 7.42. Bulk polymerization degree of borate complex in a 0.4M B(OH)3 solution plotted as a function of bulk average basicity

7.13 Number of hydrated borate minerals with respect to proportions of [3]- and [4]-coordinated boron

The most common borate structural units are those with the lowest [3]B : [4]B ratios i.e. $[B_3O_3(OH)_5]^{2-}$ and $[B_4O_5(OH)_4]^{2-}$, which have 1:2 and 1:1 ratios respectively. The bond-valence characteristics show that BO_4 groups are more amenable to polymerization; for $[B(OH)_4]$, each B –O bond has a strength of 0.75 vu, and each O – H bond has a strength of about 0.8 vu., leaving each oxygen of the $[B(OH)_4]^-$ group deficient in bond valence by ~0.45 vu. It must polymerize further to be satisfied. In $[B(OH)_3]$, each B – O bond has a strength of 1.0 vu., and each O – H bond has a strength of ~0.8 vu, leaving each oxygen of the $[B(OH)_3]$ group deficient in bond valence by only ~0.2 vu and is close to being completely satisfied. In order to break the O – H bonds of this group for further polymerization, it would require three incoming bonds from a divalent octahedrally coordinated cation ($[6]M^{2+}$), giving 0.33x3=0.99 vu – this would be sufficient to break an O–H bond as incoming strength of 0.99 vu exceeds the strength of the existing bond of 0.8 vu.

7.14 Borate crystallization and polymerization

As shown in the reactions in the previous sections, borate structural units may potentially form via a number of different reactions involving different aqueous complexes. However, the most likely reactions to occur are those with the least degree of B–O bond breaking and reorganization of B polyhedra because that is the simplest option. Kinetics will not be considered in this work but could be included in future research.

7.14.1 Accretion

In the case where a borate structural unit is the same as an observed aqueous complex, it seems likely that minerals with these structural units crystallize by direct condensation and accretion from aqueous solutions saturated with those complexes. In the process of accretion, an aqueous borate complex becomes a structural unit when it attaches to an aqueous hydrated cation which in turn becomes the interstitial complex. Like building blocks, these clusters continue to come together, linking to form the mineral structure. In this case, crystallization is not accompanied by topological change to the aqueous complex as it is incorporated into the mineral structure as the structural unit.

The composition of the mineral (aside from SU) can be determined by the other aqueous complex present; (Schindler & Hawthorne, 2001) prediction of IC compositions for SU's.

An example of crystallization by simple accretion is sassolite. The structure of sassolite, $[B(OH)_3]$ consists of layers of $B(OH)_3$ triangles that are hydrogen-bonded together to form sheets (Figure 7.43a). There is no interstitial complex involved and no hydrogen of any form is lost upon crystallization. Another example of crystallization by accretion, but involving a simple interstitial complex, is frolovite $Ca[B(OH)_4]_2$. Frolovite consists of edge-sharing Ca_2O_{14} dimers which are cross-linked into sheets by $[B(OH)_4]$ tetrahedra; the sheets are linked by hydrogen bonding (Figure 7.43b).
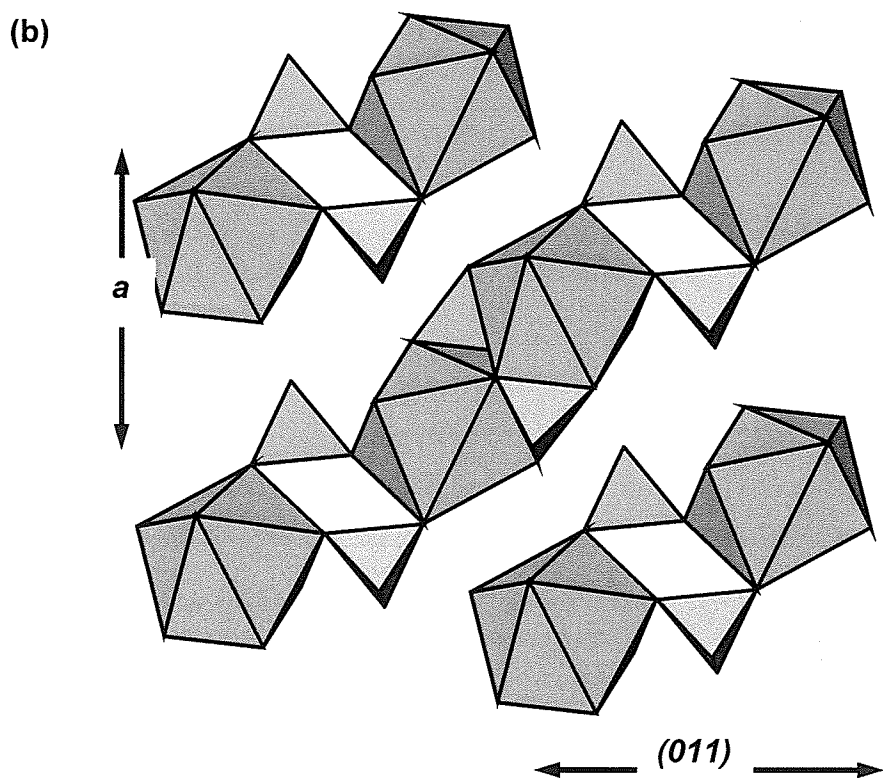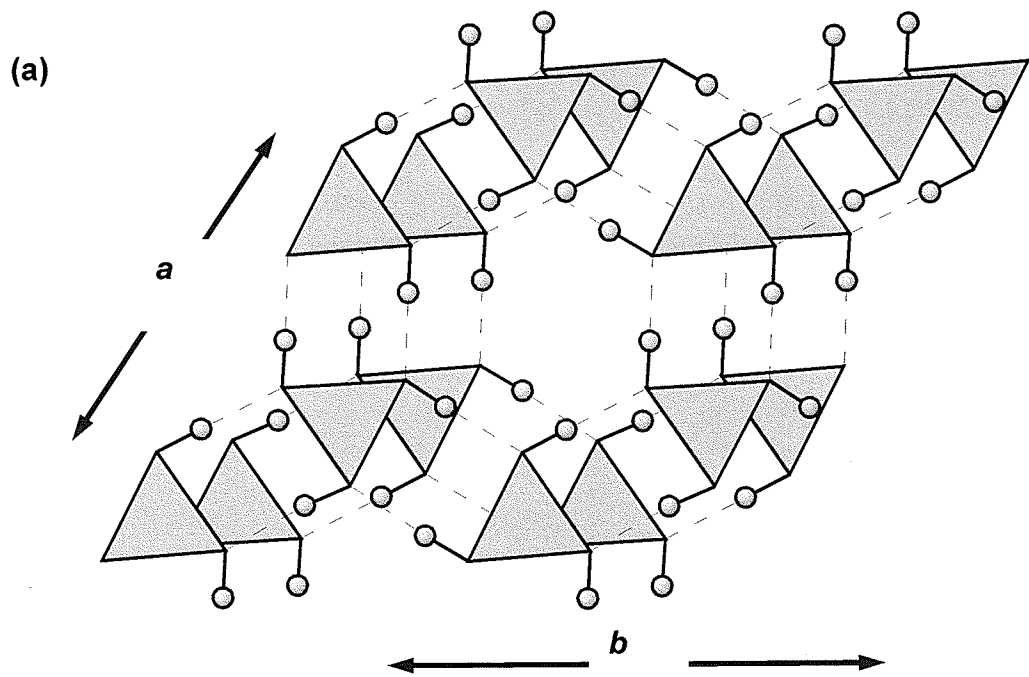
Figure 7.43. The crystal structures of (a) sassolite and (b) frolovite.

162

7.14.2 Polymerization: shared anion, shared polyhedron

In the process of polymerization, an aqueous borate complex builds the structural unit by linking to other aqueous borate complexes. This linking involves the loss of oxygen(s) and hydrogen through oxygen-sharing as linking occurs.

Polymerization may result in the loss of one oxygen atom whereby the remaining oxygen is shared by two boron atoms (eg. the shared oxygen in the dimer in pinnoite $Mg[B_2O(OH)_6]$ Figure 7.44a). It may also result in the loss of two oxygen atoms whereby the remaining oxygen is shared by three boron atoms (eg. the common anion in the hexaborate unit in aksaite $Mg[B_6O_7(OH)_6](H_2O)_2$ Figure 7.44b).

(a)

$$2[B(OH)_3] \rightarrow [B_2O(OH)_4] + H_2O$$

(b)

$$[B_3O_3(OH)_5]^{2-} + [B_3O_3(OH)_4]^- \rightarrow$$
$$[B_6O_7(OH)_6]^{2-} + H_2O + OH^-$$
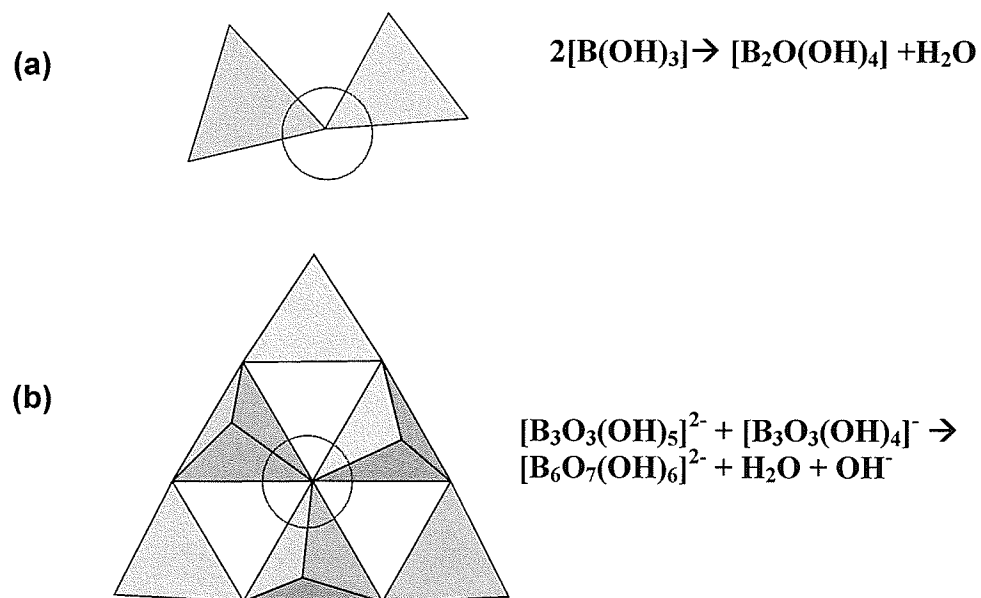
Figure 7.44. Polymerization via shared anion.

Polymerization may also result in a shared polyhedron which involves the loss of two oxygen atoms; there are two remaining oxygens, one of which is shared by two boron atoms and the other is shared by three boron atoms (e.g. the pentaborate unit in ulexite $NaCa[B_5O_6(OH)_6](H_2O)_5$ Figure 7.45). Once the pentaborate unit (finite cluster) is formed, it can polymerize into chains, sheets and frameworks by progressive oxygen sharing as the clusters link together.

$$[B_3O_3(OH)_4]^- + 2[B(OH)_4] \rightarrow [B_5O_6(OH)_6]^{3-} + 3 H_2O$$
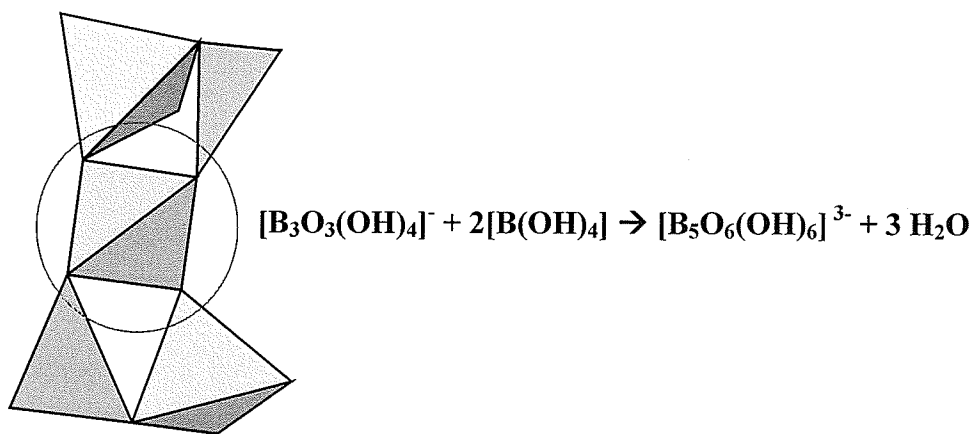
Figure 7.45. Polymerization via a shared polyhedron.

Consider the pentaborate structures based on the $[B_5O_6(OH)_6]^{3-}$ structural unit. Ulexite, $NaCa[B_5O_6(OH)_6](H_2O)_5$, contains this isolated pentaborate cluster which can polymerize to form the infinite chains in probertite $NaCa[B_5O_7(OH)_4](H_2O)_3$, the infinite sheets in tuzlaite $NaCa[B_5O_8(OH)_2](H_2O)_3$, and the framework in hilgardite (group) $Ca[B_5O_9]Cl(H_2O)$ by the "splitting off"of water. At each stage of polymerization there is a total loss of one oxygen atom. The total number of oxygens in the $[B_5O_6(OH)_6]$ finite cluster is 12. To form a chain, this cluster links to two other $[B_5O_6(OH)_6]$ clusters by

sharing two corners, one on each end of the cluster in a linear fashion. Each link results in a net loss of half an oxygen atom, and in this case there are two links forming to make a chain, resulting in a total loss of one oxygen atom. The structural unit building the chains in probertite is $[B_5O_7(OH)_4]$, which has 11 oxygen atoms, one less than ulexite. To form a sheet structure from the chain structure, an additional two links must be made (so that the original finite cluster is now linked to four other finite clusters in the same plane), since each link results in the loss of ½ an oxygen atom, a total of one oxygen atom is lost. The structural unit building the sheets in tuzlaite $[B_5O_8(OH)_2]$ has 10 oxygen atoms, one less than the structural unit of the chains in probertite. To form a framework structure from the sheet structure, an additional two links must be made (so that the original finite cluster is now linked all directions to six other finite clusters), since each link results in the loss of ½ an oxygen atom, a total of one oxygen atom is lost. The structural unit building the framework of hilgardite 1A $[B_5O_9]$ has 9 oxygen atoms, one less than the structural unit of the sheets in tuzlaite.

7.15 Chapter 7 summary

The structures of 49 low temperature borates were examined to determine the occurrence of borate aqueous complexes as structural units. Some structural units are composed of discrete borate complexes found in solution, while some are formed by a combination of different aqueous complexes, or by multiples of the same aqueous complex; the structural units may be polymerized to form clusters, chains, sheets and frameworks.

In the process of polymerization, an aqueous borate complex builds the structural unit by linking to other aqueous borate complexes which involves the loss of oxygen(s)

through oxygen-sharing as linking occurs; the type of linkage (shared anion shared polyhedron) determines the number of oxygens lost.

The m aximum degree of polymerization in solution corresponds to an average basicity of about 0.32 vu which corresponds to the average basicities of the complex borate structural units in the "megaborates" pringleite and ruitenbergite; an average basicity of 0.32 corresponds to a pH of 8.8, suggesting that these minerals may have crystallized from a solution of pH 8.8.

8.0 Overview and Conclusions

Hydrogen plays a significant role in contributing to the structural and chemical diversity of minerals, via the flexibility of the bonds it forms. Hydrogen bonding has a major influence on the stability of minerals, especially when hydrogen is a component of the interstitial complex of a crystal structure. These hydrogen bonds are much weaker than the bonds of the structural unit component of a crystal structure, and are more easily broken with changing environmental conditions. As part of the structural unit in minerals, OH and H_2O limit the polymerization of the structural unit. OH and H_2O groups can prevent other polyhedra from linking onto a structure, thereby exercising structural control. The activity of H_2O and pH affect polymerization of structural units. With increasing activity of H_2O, structural units trend from frameworks to sheets to chains to clusters to isolated polyhedra i.e., they become less polymerized.

In the kröhnkite, talmessite and fairfieldite groups, the interstitial hydrogen bonding arrangements introduce flexibility in the way that topologically identical structural units can link together, arising in different structure types. In fact, it introduces such great flexibility that alternative hydrogen bonding arrangements are possible, whether or not they occur in nature.

Minerals of the $MgSO_4(H_2O)_n$ series (n= 0-1, 4-7) can accommodate increasing amounts of H_2O by altering their crystal structures. With addition of H_2O, structural modifications involve depolymerization, which can be quantitatively described by adecrease in O-M^{2+}+T^{6+} linkages as they are replaced by O-M^{2+}+H+H and O-T^{6+} linkages. The linkages introduce flexibility such that alternative structural and hydrogen bonding arrangements are possible, whether or not they actually occur.

The structures of 49 hydrated borates were examined to determine the occurrence of borate aqueous complexes as structural units; some structural units are composed of discrete borate complexes found in solution, while some are formed by a combination of different aqueous complexes, or by multiples of the same aqueous complex. In some cases it appears that crystallization occurs via direct condensation and accretion. In the process of polymerization, an aqueous borate complex builds the structural unit by linking to other aqueous borate complexes. This linking involves the loss of oxygen(s) and hydrogen through oxygen-sharing as linking occurs. The type of linkage (e.g. shared anion or shared polyhedron) determines the number of hydrogen and oxygen lost during the process.

Because borate aqueous complexes are stable within distinct pH ranges, the complexes, or proportions of each complex making up the structural unit of a given borate mineral may indicate the pH at which the mineral formed.

REFERENCES

Balarew, Chr., Tepavitcharova, S., Rabadjieva, D., Voigt, W. (2001) Solubility and crystallization in the system $MgCl_2$-$MgSO_4$-H_2O at 50 and 75° C. *Journal of Solution Chemistry*, **30**(9): 815-823.

4. Baur, W.H. 1964. On the crystal chemistry of salt hydrates. II. A neutron diffraction study of $MgSO_4(H_2O)_4$. *Acta crystallographica*. **17**. 863-869.

5. Baur, W.H., Rolin, J.L. 1972. Salt hydrates. IX. The comparison of the crystal structure of magnesium sulfate pentahydrate and magnesium chromate pentahydrate. *Acta crystallographica B*. **28**. 1448-1455.

3. Berdesinski, W. (1952) Sanderit, leoohardtit, allenit und hexahydrit, neue mineralien der marinen Kalisalzlagerstatten. *Neues Jahrb. Mineral. Monatsh.* **1**: 28-29.

Bokii, G.B.&Kravchenko, V.B.(1966) Crystal-chemical classification of borates, Institute of Radio Engineering and Electronics. Translated from Zhurnal Strukturnoi Khimii, Vol. 7, No. 6, pp. 920–937.

Brotherton, P.D., Maslen, E.N., Pryce, M.W., White, A.H. 1974: Crystal Structure of collinsite. *Aust. J. Chem.* **27**, 653-656.

Brown, I.D. (1976): On the geometry of $O - H...O$ hydrogen bonds. *Acta Crystallographica*. **A32**, 24-31.

Brown, I.D. (2002): *The Chemical Bond in Inorganic Chemistry*. The Bond Valence Model. IUCr Monographs on Crystallography. **12**. Oxford University Press. 273pp.

Brown, I.D.(1981): The bond-valence method: an empirical approach to chemical structure and bonding. *In* Structure and Bonding in Crystals II (M. O'Keefe and A. Navrotsky, eds.) Academic Press, New York.(1-30).

Brown, I.D. and Shannon, R.D.(1973): Empirical bond-strength bond-length curves for oxides. *Acta Crystallographica*. **A29**. 266-282.

Brown, ID., Altermatt, D.(1985): Bond-valence parameters obtained from a systematic analysis of the inorganic crystal structure database. *Acta Crystallographica*. **B41**. 244-247.

Burns, P.C. 1999: The crystal chemistry of uranium. In, Uranium: Mineralogy, Geochemistry and the Environment. Eds. Burns & Finch. *Rev. Mineral.* **38**, 23-90.

Burns, P.C., Miller, M.L., and Ewing, R.C. 1996: U6+ minerals and inorganic phases: a comparison and hierarchy of structure. *Can Mineral*.**34**, 845-880.

7. Calleri, M., Gavetti, A., Ivaldi, G., Rubbo, M. 1984: Synthetic epsomite, $MgSO_4(H_2O)_7$: Absolute configuration and surface features of the complementary (111) forms. *Acta crystallographica B*. **40**. 218-222.

Catti, M. Ferraris, G., Ivaldi, G. 1977: Hydrogen bonding in the crystalline state. Structure of talmessite, Ca2(Mg,Co)(AsO4)2-2 H2O, and crystal chemistry of related minerals. *Bull.Soc. Fr.Mineral.Crystallogr*.**100**, 230-236.

Chipera, S. J., Vaniman, D.T., Bish, D.L., Carey, J.W., Feldman, W.C. (2005) Experimental stability and transformation kinetics of magnesium sulfate hydrates that may be present on Mars. Lunar and Planetary Science Conference, **XXXVI**, March 2005, Abstract number 1497.

Chou, I.M. & Seal, R.R.II. (2003) Evaporites, water, and life, Part 1: Determination of epsomite-hexahydrite equilibria by the humidity-buffer technique at 0.1 MPa with implications for phase equilibria in the system $MgSO_4$-H_2O. *Astrobiology*, **3**(3): 619-630.

Christ, C.L.(1960): Crystal chemistry and systematic classification of hydrated borate minerals. *American Mineralogist.***45**. 334-340.

Christ, C.L. and Clark, J.R. (1977): A crystal-chemical classification of borate structures with emphasis on hydrated borates. *Physics and Chemistry of Minerals*. **2**, 59-87.

Dahlman, B. (1951): The crystal structures of kröhnkite, $CuNa_2(SO_4)_2 2H_2O$ and brandtite, $MnCa_2(AsO_4)_2 2H_2O$. *Arkiv Mineral. Geol.* **1,** 339-366.

10.Dahmen, T., Glaum, R., Gruehn, R. (1990) Zur Darstellung und Kristallstruktur von $CrSO_4(H_2O)_3$. *Zeitschrift fuer Anorganische und Allgemeine Chemie*, **586**: 141-148.

16. Dunn, P.J., Sturman, D.B., & Nelen, J.A. (1987a): Wendwilsonite, the Mg analogue of roselite, from Morocco, New Jersey, and Mexico, and new data on roselite. *Am. Mineral.* **72,** 217-221.

22. Dunn, P.J., Peacor, D.R., Su, Shu-Chun, Wicks, F.J. & Parker, F.J.(1987b) Parabrandtite, the Mg analogue of talmessite, from Sterling Hill, Ogdensburg, New Jersey. *Neues.Jahrb.Mineral., Abh.* **157,** 113-119.

24. Fanfani, L., Nunzi, A. & Zanazzi, P.F. (1970): The crystal structure of fairfieldite. *Acta Crystallogr.* **B26,** 640-645

FIZ Karlsruhe Information Services http://www.fiz-Karlsruhe.de/ecid/Internet/en/DB/icsd/

Fleck, M. & Kolitsch, U. (2003): Natural and synthetic compounds with kröhnkite-type chains. An update. *Z. Kristallogr.* **218**, 553-567.

Fleck, M , Hertweck, B., Kolitsch, U., Giester, G., Wildner, M., Prem, M. & Wohlschläger, A. (2002a): Crystal structures of the double salt dihydrates $K_2Cd(SeO_4)_2$-$2H_2O$, $K_2Mn(SO_4)_2$-$2H_2O$, $(NH_4)_2Cu(SeO_4)_2$-$2H_2O$ and $KFeH(SO_4)_2$-$2H_2O$. *Z. Kristallogr.* **217**, 242-248.

Fleck, M., Kolitsch, U. & Hertweck, B. (2002b): Natural and synthetic compounds with kröhnkite-type chains: review and classification. *Z. Kristallogr.* **217**, 435-443.

21. Frondel, C. (1955): Neomesselite and beta-roselite: two new members of the fairfieldite group. *Am. Mineral.* **40**, 828-833.

8. Gunter, J.R. & Dubler, E. (1986) Crystal structure and topotactic dehydration of magnesium tungstate dihydrate. *Journal of Solid State Chemistry,* **65**: 118-126.

12. Hawthorne, F.C & Ferguson, R.B. (1975): Refinement of the crystal structure of kröhnkite. *Acta Crystallogr.* **B31,** 1753-1755.

14. Hawthorne, F.C & Ferguson, R.B (1977): The crystal structure of roselite. *Can. Mineral.* **15,** 36-42.

Hawthorne, F.C. (1983): Graphical enumeration of polyhedral clusters. *Acta Crystallogr.* **A39,** 724-736.

Hawthorne, F.C (1984): The crystal structure of stenonite and the classification of the alumino-fluoride minerals. *Can. Mineral.* **22**, 245-251.

Hawthorne, F.C (1985): Towards a structural classification of minerals: The $^{VI}M^{IV}T_2\varphi_n$ minerals. *Am. Mineral.* **70**, 455-473.

Hawthorne, F.C (1986): Structural hierarchy in $^{VI}M_x^{III}T_y\varphi_z$ minerals. *Can. Mineral.* **24**, 625-642.

2. Hawthorne, F.C., Groat, L.A., Raudsepp, M. (1987) Kieserite, $Mg(SO_4)(H_2O)$, a Titanite-group mineral. *Neues Jahrbuch Miner. Abh.* **157**(2): 121-132.

Hawthorne, F.C (1990): Structural hierarchy in $^{[6]}M^{[4]}T\varphi_n$ minerals. *Z. Kristallogr.* **192**, 1-52.

Hawthorne, F.C (1992): Bond Topology, Bond-Valence and Structure Stability. *In* The Stability of Minerals (G.D. Price & N.L. Ross, eds.). Chapman & Hall, London, 25-87.

171

Hawthorne, F.C. (1992): The role of OH and H_2O in oxide and oxysalt minerals. *Zeitschrift fur Kristallographie.* **201**, 183-206.

Hawthorne, F.C (1994): Structural aspects of oxides and oxysalt crystals. Acta. Crystallogr. **B50**, 481-510.

Hawthorne, F.C., Burns, P.C., Grice, J.D. (1996): The crystal chemistry of boron. *In* Boron: Mineralogy, Petrology and Geochemistry (E.S.Grew & M. Anovitz eds.). *Reviews in Mineralogy.* **33**. (41-115).

Hawthorne, F.C (1997): Structural aspects of oxide and oxysalt minerals. *In*: European Mineralogical Union Notes in Mineralogy, Vol.1, Modular Aspects of Minerals (S. Merlino, ed.). Eötvös University Press, 373-429.

Hawthorne, F.C, Krivovichev, S.V. & Burns, P.C. (2000): The crystal chemistry of sulfate minerals. *Rev. Mineral.* **40**, 1-112.

Hawthorne, F.C & Huminicki, D.M.C. (2002): The crystal chemistry of beryllium. *Rev. Mineral.* **50**, 333-403.

Hawthorne, F.C, Ungaretti, L. & Oberti, R. (1995): Site populations in minerals: terminology and presentation of results of crystal-structure refinement. *Can. Mineral.* **33**, 907-911.

Heller, G., Janda. R., Mathieu, J. 1980. Investigation of the Polyborate Equilibria in Aqueous solutions by 11B-NMR and Raman Spectroscopy. Inorganica Chimica Acta, v40. 107-108.

Hodenberg, R.F., Kuhn, R. (1967) Zur Kenntnis der Magnesiumsulfathydrate und der Effloreszenzen des Kieserits von Hartsalzen. *Kali und. Steinhalz.* 4(10): 326-340.

Ingri, N. (1963): Equilibrium studies of polyanions containing B(III), Si(IV), Ge(IV) and V(V). *Svensk Kemisk Tidskrift.* **74**(4). 199-230.

Janda, R., Heller, G. 1979: 11B NMR Spectroscopic Studies on Aqueous Polyborate Solutions. Z.Naturforsch. 34b, 1078-1083.

Jeffrey, G.A.(1997) An Introduction to Hydrogen Bonding. Oxford University Press. 320pp.

25. Joswig, W., Paulus, E.F. & Liebscher, B. (2004): Crystal structure of dicalcium (cobalt, magnesium)diarsenate dehydrate, $Ca_2(Co_{0.532}Mg_{0.468})[AsO_4]_2(H_2O)_2$, hydrogen bonding in talmessite. *Z.Kristallogr.* **219**, 341-342.

17. Keller, P., Innes, J., Dunn, P.J. (1986): Zincroselite, $Ca_2Zn(AsO_4)_2(H_2O)_2$, a new mineral from Tsumeb, Namibia. *Neues Jahrb. Mineral. Mh*, 523-527.

17. Keller, P, Lissner, F. & Schleid, T. (2002): Zinkroselith und Gaitit, zwei Modifikationen von $Ca_2Zn(AsO_4)_2-2H_2O$, aus Tsumeb (Namibia). *Z. Kristallogr. Suppl.* **19**, 87.

17. Keller, P, Lissner, F. & Schleid, T. (2004): The crystal structures of zincroselite and gaitite: two natural polymorphs of $Ca_2Zn[AsO_4]_2-2H_2O$ from Tsumeb, Namibia. *Eur. J. Mineral.* **16**, 353-359.

Kolitsch, U. & Fleck, M. (2005): Second update on compounds with kröhnkite-type chains. *Z. Kristallogr.* **220**, 31-41.

Kotz, J.C. & Treichel,P (1996) Chemistry & Chemical Reactivity, 3rd Edition, by published by Saunders College Publishing, Fort Worth.

Liferovich, R.P., Pakhomovsky, Y.A., Bogdanova, A.N., Balaganskaya, E.G., Laajoki, K.V.O., Gehor, S. & Chukanov, N.V. (2001): Collinsite in hydrothermal assemblages related to carbonatites in the Kovdor complex, northwestern Russia. *Can. Mineral.* **39**, 1081-1094.

Maya, L. 1976. Identification of Polyborate and Fluoropolyborate Ions in Solution by Raman Spectroscopy. Inorganic Chemistry, v.15, no.9: 2179-2184

O'Keefe, M. (1989): The Prediction and Interpretation of Bond Lengths in Crystals. In *Structure and Bonding*. **71**. 161-191.

O'Keefe, M.(1990): A method for calculating bond valences in crystals. *Acta Crystallographica.* **A46**. 138-142.

1.Rentzeperis, P.J., Soldatos, C.T. 1958: The crystal structure of the anhydrous magnesium sulfate. Acta crystallographica. 11. 686-688.

Richens, D.T. (1997) *The Chemistry of Aqua Ions*. John Wiley & Sons Ltd., Baffin Lane, Chichester, West Sussex PO19UD, England.

Salentine, C. 1983: High-Field 11B NMR of alkali borates. Aqueous polyborate equilibria. Inorganic Chemistry. V.22: 3290-3294

11. Schindler, M., Hawthorne,F.C., D.M.C. Huminicki, P. Haynes, J.D. Grice & H.T. Evans (2003) Bobjonesite, $V^{4+}O(SO_4)(H_2O)_3$, a new mineral species from Temple Mountain, Emery County, Utah, U.S.A. *Canadian Mineralogist*, **41**:83-90.

Schindler, M, Hawthorne, F.C., 2001: A bond-valence approach to the structure, chemistry and paragenesis of the hydroxyl-hydrated oxysalt minerals. III. Paragenesis of borate minerals. The Canadian Mineralogist, v39, 1257-1274.

Schindler, M, Hawthorne, F.C., 2001: A bond-valence approach to the structure, chemistry and paragenesis of the hydroxyl-hydrated oxysalt minerals. II. Crystal structure and chemical composition of borate minerals. The Canadian Mineralogist, v39, 1243-1256..

Schindler, M, Hawthorne, F.C., 2001: A bond-valence approach to the structure, chemistry and paragenesis of the hydroxyl-hydrated oxysalt minerals. I.Theory. The Canadian Mineralogist, v39, 1225-1242

Shape Software http://www.shapesoftware.com

Strunz, H. (1997) Classification of borate minerals. *European Journal of Mineralogy,* v. 9; no. 1; p. 225-232

Sheldrick, G.L.(1997) SHEL XL Version 5.1.

Vaniman, D.T., Bish, D.L., Chipera, S.J., Fialips, C.I., Carey, J.W., Feldman, W.C. (2004) Magnesium sulfate salts and the history of water on Mars. *Nature,* **431**(7 October): 663-665.

23. Yakubovich, O.V., Massa, W., Liferovich, R.P., Gavrilenko, P.G., Bogdanova, A.N. & Tuisku, P. (2003): Hillite: a new member of the fairfieldite group: it's description and crystal structure. *Can. Mineral.* **41**, 981-988.

Yuan, G. & Xue, D.(2007) Crystal chemistry of borates: the classification and algebraic description by topological type of fundamental building blocks *Acta Cryst.* (2007). B63, 353-362.

6. Zalkin, A., Ruben, H., Templeton, D.H. 1964: The crystal structure and hydrogen bonding of magnesium sulfate hexahydrate. Acta crystallographica. 17. 235-240.

9. Zahrobsky, R.F. & Baur, W.H. (1968) On the crystal chemistry of salt hydrates. V. The determination of the crystal structure of $CuSO_4(H_2O)_3$ (Bonattite). *Acta crystallographica B,* 24: 508-513.

Zhihong, L., Bo, G., Shuni, L. Mancheng, H., Shuping, H. 2004: Raman spectroscopic analysis of supersaturated aqueous solution of MgO-B2O3-32%MgCl2-H2O during acidification and dilution. Spectrochimica Acta Part A. v.60, 3125-3128.